

UNIVERSITY OF BOLOGNA

DEPARTMENT OF ELECTRICAL, ELECTRONIC, AND INFORMATION
ENGINEERING “GUGLIELMO MARCONI”

XXV PhD. Course in Electronics Engineering, Telecommunications and
Information Technology

ING-INF/03, 09/F2

Cognitive radio applications for enhanced spectrum efficiency

Candidate:

Valeria Petrini

Coordinator:

Prof. Alessandro Vanelli-Coralli

Supervisors:

Prof. Giovanni Emanuele Corazza

Dr. Guido Riva

March 2013

To my family

In the middle of difficulty lies opportunity
Albert Einstein

Contents

1	Cognitive Radio Communication	7
1.1	What is Cognitive Radio?	8
1.2	Cognitive Radio Capabilities	10
1.3	Cognitive Radio Network	14
1.3.1	Cognitive Network Components	14
1.3.2	Cognitive Network Access	15
1.3.3	Spectrum Sharing Techniques	17
1.4	Spectrum Sensing and Geo-location Database	18
2	White Spaces Identification	23
2.1	Spectrum Sensing	24
2.1.1	Spectrum Sensing Techniques	25
2.1.1.1	Energy detector	26
2.1.1.2	Cyclostationarity feature detection	27
2.1.1.3	Matched filter detection	28
2.1.2	Hidden Node Problem and Cooperative Spectrum Sensing	29
2.2	White Space Database	30
2.2.1	Threshold-based approach	31
2.2.2	Location Probability approach	32
2.3	Combined White Space Database and Sensing Techniques	34
2.4	Simulation and Measurements Results	35
2.4.1	Threshold-based Approach: West Piedmont	35
2.4.2	Location Probability-based Approach	38
2.4.3	Combined Geo-location and Sensing Approach	40
2.4.3.1	Geo-location Database	40
2.4.3.2	Measurements for Spectrum Sensing	43
2.4.3.3	Combined Approach	45

3	White Space Device Emission Limits	47
3.1	TV White Space Database for WSD Emission Levels	48
3.1.1	DTT Location Probability	49
3.1.1.1	Definition of location probability	50
3.1.1.2	Common approach for calculation of location probability	51
3.1.1.3	A new approach for derivation of q_1	53
3.1.1.4	Numerical Results	54
3.1.2	Calculation of the Maximum Permitted WSD EIRP	55
3.1.2.1	Problem formulation	57
3.1.2.2	Monte Carlo simulations	59
3.1.2.3	New approach	59
3.1.3	Database Calculations	61
3.1.3.1	Interferer-victim geometries	63
3.1.3.2	Statistics of coupling gains between white space devices and TV receivers within a pixel	66
3.1.3.3	Statistics of coupling gains between white space devices and TV receivers that are some pixels apart	67
3.1.4	Numerical Results of Maximum Permitted Emission Levels	70
3.2	Numerical Examples and Further Considerations on White Space Device Emission Limits	77
3.2.1	Fixed Δq analysis	77
3.2.2	Δq variations analysis	80
3.2.3	Co-channel analysis, $\Delta q = 1\%$	85
3.2.4	Co-channel analysis, Δq varying	90
3.2.5	DTT self-interference variation analysis, $\Delta q = 1\%$	94
3.3	WSD operating in MFN and SFN	96
3.3.1	Methodology to derive EIRP limits over all DTT channels	98
3.3.2	WSDs operating in a SFN	99
3.3.3	WSDs operating in a MFN with non-overlapped coverage areas	104
3.3.4	WSDs operating in a k-SFN with non-overlapped coverage areas	108
3.3.5	WSDs operating in a MFN with overlapped coverage areas	111
3.3.6	Comparison between MFN, SFN and k-SFN planning strategies	114
4	Applications of Cognitive Radios	117
4.1	CR in Emergency Management Scenario	118

4.1.1	ICT Emergency Management Requirements	121
4.1.2	Communication Infrastructure	125
4.1.3	Distributed Computing Infrastructure	127
4.1.4	Cognitive and Autonomic Approach to Emergency Management	132
4.2	CR in Hybrid Satellite-Terrestrial System	138
4.2.1	Hybrid Cognitive Terrestrial-Satellite Scenarios	139
4.2.2	The stochastic geometry interference model	140
4.2.3	Numerical Results	143
Conclusions		147
Appendices		153
A Energy Efficiency in Mobile Systems		155
A.1	Single Cell Layout	157
A.2	Regular Manhattan Layout	158
A.3	Simulation Results	159
B Methods for the Summation of Log-normal Distributions		163
B.1	Schwartz and Yeh Method	163
B.2	k-LNM Method	166
C Property of Log-Normal Distribution		169
D Computation of Carrier to Interference-plus-Noise Ratio		171
Bibliography		174

List of Figures

1.1	The spectrum bands between 30 MHz and 3GHz utilization [1].	9
1.2	Dynamic spectrum access concept.	11
1.3	The cognitive radio learning loop.	13
1.4	Cognitive Network Architecture [2].	16
1.5	Cognitive Network on licensed spectrum bands.	17
1.6	Cognitive Network on unlicensed spectrum bands.	18
1.7	Geo-location database translation process architecture.	21
2.1	Multi-dimensional spectrum awareness.	25
2.2	Hidden node problem.	29
2.3	Geo-location database: approaches to compute the potentially available pixels.	33
2.4	West Piedmont map.	35
2.5	Pontentially available channels, $h = 10$ m	36
2.6	Pontentially available channels, $h = 1.5$ m	36
2.7	CCDF of the amount of white space per pixel	37
2.8	CCDF of the amount of white space per population	37
2.9	DTT coverage area	39
2.10	Percentage of population living in potential white space areas	39
2.11	Database: example of received DTT signal strength	41
2.12	Database: comparison for different field strength thresholds	41
2.13	Sensing: measurement locations	42
2.14	Measured data: comparison for different field strength thresholds	44
2.15	Database: contiguous channels	45
2.16	Measured data: contiguous channels	46
3.1	Location Probability: powers distribution	53

3.2	DTT location probability. Noise-limited environment.	55
3.3	DTT location probability. $m_V = -96$ dBm, $\sigma_V = 3.2$ dB.	56
3.4	DTT location probability. $m_V = -70$ dBm, $\sigma_V = 4.9$ dB.	56
3.5	DTT location probability. $m_V = -60$ dBm, $\sigma_V = 5$ dB.	57
3.7	Reference and non-reference geometries	65
3.8	Reference geometry	67
3.9	Two-ray path gain	69
3.10	Non-reference geometry	69
3.11	Maximum permitted WSD EIRP. Noise-limited DTT coverage. $m_V = -\infty$	71
3.12	Maximum permitted WSD EIRP. Interference-limited DTT coverage, $m_V = -96$ dBm, $\sigma_V = 3.2$ dB.	71
3.13	Maximum permitted WSD EIRP. Interference-limited DTT coverage, $m_V = -70$ dBm, $\sigma_V = 4.9$ dB.	72
3.14	Maximum permitted WSD EIRP. Interference-limited DTT coverage, $m_V = -60$ dBm, $\sigma_V = 5$ dB.	72
3.15	P_{IB} trend explanation. Low DTT coverage condition	73
3.16	P_{IB} trend explanation. Mean DTT coverage condition.	74
3.17	P_{IB} trend explanation. High DTT coverage condition.	74
3.18	Fixed Δq variations. Noise-limited DTT coverage. $m_V = -\infty$	78
3.19	Fixed Δq variations. $m_V = -70$ dBm, $\sigma_V = 4.9$ dB.	78
3.20	Fixed Δq variations. $m_V = -60$ dBm, $\sigma_V = 5$ dB.	79
3.21	Location probability degradation function, Δq_A	82
3.22	Location probability degradation function, Δq_B	82
3.23	Maximum permitted WSD EIRP for three different Δq functions. Noise-limited DTT coverage. $m_V = -\infty$	83
3.24	Maximum permitted WSD EIRP for three different Δq functions. $m_V = -70$ dBm, $\sigma_V = 4.9$ dB.	84
3.25	Maximum permitted WSD EIRP for three different Δq functions. $m_V = -60$ dBm, $\sigma_V = 5$ dB.	84
3.26	Maximum permitted WSD EIRP. Co-channel usage, reference geometry, $\Delta q = 1\%$. $m_V = -70$ dBm, $\sigma_V = 4.9$ dB.	85

3.27	WSD interferer - DTT receiver distance for different WSD EIRP values. Co-channel usage, actual distance between WSD and DTT receiver, free-space propagation, $\Delta q = 1\%$. Noise-limited DTT coverage. $m_V = -\infty$	86
3.28	WSD interferer - DTT receiver distance for different WSD EIRP values. Co-channel usage, actual distance between WSD and DTT receiver, free-space propagation, $\Delta q = 1\%$. $m_V = -70$ dBm, $\sigma_V = 4.9$ dB.	86
3.29	WSD interferer - DTT receiver distance for different WSD EIRP values. Co-channel usage, actual distance between WSD and DTT receiver, free-space propagation, $\Delta q = 1\%$. $m_V = -60$ dBm, $\sigma_V = 5$ dB.	87
3.30	WSD interferer - DTT receiver distance for different WSD EIRP values. Co-channel usage, non-reference geometry, dual-slope propagation, $\Delta q = 1\%$. Noise-limited DTT coverage. $m_V = -\infty$	88
3.31	WSD interferer - DTT receiver distance for different WSD EIRP values. Co-channel usage, non-reference geometry, dual-slope propagation, $\Delta q = 1\%$. $m_V = -70$ dBm, $\sigma_V = 4.9$ dB.	89
3.32	WSD interferer - DTT receiver distance for different WSD EIRP values. Co-channel usage, non-reference geometry, dual-slope propagation, $\Delta q = 1\%$. $m_V = -60$ dBm, $\sigma_V = 5$ dB.	89
3.33	WSD interferer - DTT receiver distance for three different Δq functions. Co-channel usage, non-reference geometry, dual-slope propagation, WSD EIRP = 10 dBm, $m_V = -70$ dBm, $\sigma_V = 4.9$ dB.	90
3.34	WSD interferer - DTT receiver distance for three different Δq functions. Co-channel usage, non-reference geometry, dual-slope propagation, WSD EIRP = 15 dBm, $m_V = -70$ dBm, $\sigma_V = 4.9$ dB.	91
3.35	WSD interferer - DTT receiver distance for three different Δq functions. Co-channel usage, non-reference geometry, dual-slope propagation, WSD EIRP = 20 dBm, $m_V = -70$ dBm, $\sigma_V = 4.9$ dB.	92
3.36	WSD interferer - DTT receiver distance for three different Δq functions. Co-channel usage, non-reference geometry, dual-slope propagation, WSD EIRP = 30 dBm, $m_V = -70$ dBm, $\sigma_V = 4.9$ dB.	93
3.37	DTT location probability for different values of m_S . $\sigma_S = 5.5$ dB, adjacent-channel usage, reference geometry, $\Delta q = 1\%$	95

3.38	Maximum permitted WSD EIRP for different values of m_S . $\sigma_S = 5.5$ dB, adjacent-channel usage, reference geometry, $\Delta q = 1\%$	95
3.39	Covered pixel: Spatial pattern of the usage of three DTT channels	98
3.40	Non-covered pixel: Spatial pattern of the usage of three DTT channels	101
3.41	Example of a SFN in Friuli-Venezia Giulia: Location Probability of covered pixels ($q_1 \geq 0.7$).	102
3.42	SFN in Friuli-Venezia Giulia: maximum WSD EIRP	103
3.43	DTT installations MFN.	105
3.44	Example of a MFN with non-overlapped coverage areas in Friuli-Venezia Giulia: Location Probability of covered pixels ($q_1 \geq 0.7$).	107
3.45	MFN in Friuli-Venezia Giulia: maximum WSD EIRP	108
3.46	DTT installations k-SFN.	109
3.47	Example of a k-SFN with non-overlapped coverage areas in Friuli-Venezia Giulia: Location Probability of covered pixels ($q_1 \geq 0.7$).	110
3.48	k-SFN in Friuli-Venezia Giulia: maximum WSD EIRP	112
3.49	MFN with overlapped coverage areas in Friuli-Venezia Giulia: maximum WSD EIRP	113
3.50	Comparison: CCDF of q_1 for different planning strategies	114
3.51	Comparison: CDF of P_{IB} for different planning strategies	115
4.1	Communication Infrastructure.	126
4.2	The cognitive and autonomic approaches interdependency.	129
4.3	The automic learning loop.	131
4.4	Emergency Management learning loop.	133
4.5	The relaying cognitive scenario.	137
4.6	Example of cognitive satellite system.	139
4.7	Cognitive terrestrial system.	141
4.8	Outage probability with $\lambda_{int} = 10^{-2} \text{ m}^{-2}$	144
4.9	Outage probability with $\lambda_{int} = 10^{-4} \text{ m}^{-2}$	144
4.10	Outage probability with $\lambda_{int} = 10^{-6} \text{ m}^{-2}$	145
A.1	Manhattan cellular layout.	158
A.2	Single cell BS transmitted power density as a function of the cell radius.	159

List of Tables

2.1	DTT reference planning configurations	34
2.2	WS POTENTIALLY AVAILABLE FROM GEO-LOCATION DATABASE . . .	42
2.3	MEASUREMENT LOCATIONS	45
2.4	DOUBLE GREEN PERCENTAGE	46
3.1	MONTE CARLO SIMULATIONS FOR THE CALCULATIONS OF THE MAX- IMUM PERMITTED WSD EIRP	59
3.2	NEW METHODOLOGY FOR THE CALCULATION OF THE MAXIMUM PERMITTED WSD EIRP	61
3.3	PARAMETER VALUES USED IN THE NUMERICAL EXAMPLES OF THIS SECTION	76
3.4	ILLUSTRATIVE EMISSION LIMITS FOR WSD OPERATING AT FRE- QUENCY f_1	100
3.5	ILLUSTRATIVE EMISSION LIMITS FOR WSD OPERATING AT FRE- QUENCY f_3	100
3.6	WSD EMISSION LIMITS	100
3.7	EXAMPLE OF PERCENTAGE OF POPULATION RELATED TO LOCATION PROBABILITY IN MFN	106
3.8	EXAMPLE OF PERCENTAGE OF POPULATION RELATED TO LOCATION PROBABILITY IN K-SFN	111
A.1	SINGLE CELL LAYOUT PARAMETERS	158
A.2	POWER DENSITY AND PERCENTAGE OF COVERED LOCATIONS	160
A.3	INDOOR COVERAGE PERCENTAGE	161
A.4	OUTDOOR COVERAGE PERCENTAGE	161

List of Acronyms

ACLR Adjacent-Channel Leakage Ratio

ACS Adjacent-Channel Selectivity

ANS Autonomic Nervous System

ARNS Aeronautical Radio Navigation Service

ARPU Average Revenue Per Unit

BTS Base Transceiver Station

BS Base Station Coded Orthogonal Frequency-Division Multiplexing

CCDF Complementary Cumulative Distribution Function

CDF Cumulative Distribution Function

CEPT European Conference of Postal and Telecommunications Administrations

COFDM Coded Orthogonal Frequency-Division Multiplexing

CP Cyclic Prefix

CPU Central Processing Unit

CR Cognitive Radio

DT Detection Threshold

DTT Digital Terrestrial Television

DVB-T Digital Video Broadcasting Terrestrial

EC European Commission

- ECC** Electronic Communications Committee
- Ecc** Emergency communications car
- EIRP** Equivalent Isotropically Radiated Power
- ERP** Equivalent Radiated Power
- EU** European Union
- FCC** Federal Communications Commission
- FDMA** Frequency Division Multiple Access
- GEO-06** Geneva 2006 Agreement
- GPS** Global Position System
- GSM** Global System for Mobile Communications
- GS** Ground Station
- ICT** Information and Communication Technology
- IMT** International Mobile Telecommunications
- ISM** Industrial Scientific and Medical
- LNM** Log-Normal Method
- LOS** Line Of Sight
- LP** Location Probability
- MANET** Mobile Ad hoc Network
- MFN** Multi-Frequency Network
- MGF** Moment Generating Function
- MIMO** Multiple Input Multiple Output
- MT** Mobile Terminal
- NLOS** Non Line Of Sight
- NPRM** Notice of Proposed Rulemaking

Ofcom	Office of Communications
OFDM	Orthogonal Frequency Division Multiplexing
OPEX	OPERating EXpenditure
PDA	Personal Digital Assistant
PDF	Probability Density Function
PMSE	Program Making and Special Event
PSD	Power Spectral Density
PU	Primary User
QoS	Quality of Service
RAN	Radio Access Network
RAS	Radio Astronomy Service
RPC	Reference Planning Configuration
RSPP	Radio Spectrum Policy Programme
SFN	Single Frequency Network
SINR	Signal to Interference plus Noise Ratio
SNR	Signal to Noise Ratio
SRTM	Shuttle Radar Topography Mission
SU	Secondary User
SY	Schwartz and Yeh
TDSC	Time-Domain Symbol Cross-Correlation
TDMA	Time Division Multiple Access
TETRA	TERrestrial TRunked RAdio
TPC	Transmit Power Control
TV	Television

UK United Kingdom

UMTS Universal Mobile Telecommunications System

WMAN Wireless Metropolitan Area Network

WiMAX Worldwide Interoperability for Microwave Access

WS White Space

WSD White Space Device

WSDB White Space Database

WSN Wireless Sensor Network

WSS Wide Sense Stationary

3G 3rd Generation

4G 4th Generation

Introduction

Motivation and Goals

This thesis is the outcome of the work performed during my PhD research activities. The focus of my research has been on the study of techniques for an efficient management and use of the spectrum based on cognitive radio (CR).

The growth of wireless data traffic and the scarcity of radio frequency spectrum have led many countries to highlight the need of additional spectrum band for mobile broadband services in the next decade. A higher efficiency of the overall spectrum use can be obtained by a most flexible spectrum usage, allowing the widest possible ranges of uses and technologies. In this context, there has been a great deal of interest from both academia and the communications industry in the use of interleaved spectrum ("white space" - WS -) in UHF digital terrestrial television (DTT) frequencies by so-called cognitive radios or white-space devices (WSDs) [3]. The new devices are able to adapt dynamically its operating transmission parameters to exploit the available spectrum resources. The use of this technology creates a complex sharing situation where novel approaches are required to ensure that WSDs use frequencies in a manner that does not cause interference to nearby broadcast users.

The white space spectrum might help to face the scarcity of the spectrum, encouraging the development of new wireless technologies. White spaces in UHF band between 470 MHz and 790 MHz offer a significant amount of untapped spectrum in an attractive band because it has excellent propagation characteristics that allow signals to cover farther distances and penetrate walls and other structures.

The use of cognitive radio technology has been considered by European Union (EU) within the program to optimize the use of the spectrum, enhancing the efficiency and flexibility (European Conference of Postal and Telecommunications Administrations (CEPT) Report 24 [4]).

In particular, the radio spectrum scarcity due to rapid growth of wireless com-

munication systems and inefficient utilization of licensed spectrum, has motivated the European Commission (EC) to draw up the Radio Spectrum Policy Programme (RSPP) guidelines [5] to promote the harmonization of use of radio frequencies across the EU, consistent with the need to ensure effective and efficient use thereof.

Cognitive radio technology has been envisaged in the RSPP in order to enhance the flexibility and efficiency in spectrum usage.

The adoption of the RSPP will also help to reduce the digital divide, make Europe a connected and competitive continent and introduce more wireless broadband choices. According to the deal, the 800 MHz band (spectrum band between 790 MHz and 862 MHz) that has been released after the switch-over from analogue to DTT, should be made available for wireless broadband service in all EU countries by January 2013. This so-called *Digital Dividend* provides an unique opportunity to meet the demand for spectrum by next generation mobile communications services. This opens the possibility for operators to bring 4G technologies to a large portion of the population, and even to reach those areas where people still do not have broadband access (digital dividend areas).

The potential growth of mobile services, on the other hand, has led to pay more attention on the aspects related to the power consumptions of cellular networks. The RSPP also supports the Europe 2020 Strategy [6] that sets environmental objectives for a sustainable, energy-efficient and competitive economy, for example by improving energy efficiency by 20% by 2020. Efficient use of spectrum technologies could also help reduce energy consumption by radio equipment and limit the environmental impact.

During my PhD I have dealt with these issues. In particular I focused my research on CR technologies to identify spectrum opportunities in order to better exploit the spectrum resource. I performed also studies on planning criteria to improve energy efficiency in mobile radio systems and some propagation analysis on band 3.5 GHz. Some of the obtained results have been presented at European framework meetings [7, 8, 9].

Thesis Outline

This thesis is organized in four chapters. The first chapter deals with the main issues of cognitive radio and introduces the concepts of spectrum sensing and geo-location database in order to obtain information on the electromagnetic environment. Chap-

ter two focuses on the techniques to identify the white spaces. The third chapter analyses the WSD emission levels in different scenarios considering a novel methodology developed to evaluate those limits. Chapter four describes the applications of cognitive radio technology in two different scenarios, i.e. emergency management and satellite-terrestrial systems.

This thesis includes also four annexes. Annex A deals with a study on the energy efficiency problem in mobile radio systems, while the other annexes are related to mathematical derivations of some concepts useful to better understand some issues that rise in the thesis.

The ability of cognitive radio technologies to adapt to the real-time conditions of its operating environment, offers the potential for more flexible and efficient use of available spectrum while reducing the risk of harmful interference. The first chapter deals with the main aspects related to cognitive radio providing an overview of the cognitive radio technology and introducing the techniques to identify the spectral resources. These concepts are then better explained in the second chapter which is focused on white spaces identification.

In particular in this thesis three methodologies have been considered in order to investigate spectral resources potentially available for white space devices in the TV band. The adopted methodologies are based on the geo-location database approach used either in autonomous operation or in combination with sensing techniques.

The calculations which a geo-location database would need to perform in order to derive location-specific maximum permitted WSD emission levels are then analysed in chapter three. These levels are calculated in such a way to afford protection to the digital terrestrial TV service in terms of maximum permitted degradation in DTT location probability. In this chapter an approach for the calculation of DTT location probability which improves considerably on the accuracy of the technique commonly used for this purpose is presented. A novel methodology for the calculation of maximum permitted WSD EIRP is proposed. It is shown that the methodology generates results which compare favourably with those generated via Monte Carlo simulations. Both presented techniques are suitable for implementation in TV white space database. Then considerations, supported by numerical examples, on degradation of coverage location probability for the determination of the maximum WSD EIRP limits are provided. Finally the permitted transmit power as well as the location probability distribution in a real Italian scenario is illustrated. A real DTT network is considered and three different planning strategies, i.e. SFN,

MFN and k-SFN, are analysed.

The forth chapter deals with two different applications of cognitive radio technology. The first considered application is the emergency management. The attention is focused on the consideration of both cognitive and autonomic networking approaches when deploying an emergency management system. The cognitive approach was initially considered specifically for wireless communications, while the autonomic approach was initially introduced for managing complex computing systems; however, they share several similarities in dealing with fully reconfigurable systems. It has been shown how the future trend could be to expand their influence toward the global optimization of the Information and Communication Technology (ICT) infrastructure for the specific case of emergency management systems. The cognitive radio technology is then considered in applications related to satellite systems. In particular hybrid cognitive satellite-terrestrial system is introduced. Analysis of coexistence between terrestrial and satellite networks by considering a cognitive approach is performed. A statistical interference model that aims at evaluating the mutual interference among the two systems is presented.

The study performed on energy efficiency in mobile radio systems is presented in Annex A. The cellular layout of a mobile radio system has an impact on its performance (in terms of both coverage and capacity) as well as on its economical and environmental sustainability in terms of power consumption and of exposure of population to electromagnetic field. In this annex different cellular coverage strategies to identify which solutions better meet the constraints on the above mentioned parameters are studied. Both an idealized, 2D case and a more detailed urban layout case are considered in the work: in the latter case a 3D ray tracing tool is used as propagation model. Generally, a trade-off is required to reach the best performance in terms of radio coverage, system throughput and energy efficiency.

Original Contributions

The activities performed during the three years of this doctorate led me to obtain original scientific contributions in several fields. Regarding cognitive radios and white space devices, the main contributions are the following:

- Introduction of novel methodology for the calculation of the maximum permitted emission levels for WSD operating in DTT band [10]. This work has been performed during six months I worked in Ofcom (Office of communications),

UK. The related project was on the characterization of the digital terrestrial television signal quality necessary for studying the impact of the interference due to white space devices on television services.

- Analysis of different methodologies to estimate the amount of spectrum potentially available as white space in UHF band [11].
- Evaluation of the coexistence of terrestrial and satellite networks considering a cognitive approach [12].
- Study of a fully reconfigurable approach to emergency management system [13].

Regarding the energy efficiency techniques in mobile networks the main contributions are:

- Study of different cellular coverage strategies to identify which solutions better meet the constraints in terms of power consumption [14].
- Study of factors that have to be considered to study the power consumption of an entire cellular network [15].

During my PhD I had the opportunity to collaborate with Instituto de Telecomunicações - DEM of University of Beira Interior, Portugal on matters concerning studies on 3.5 GHz propagation. In particular we performed an intensive measurements campaign that led us to characterise the propagation phenomena at 3.5 GHz in different environments [16].

Chapter 1

Cognitive Radio Communication

The studies on cognitive radios are relatively new. In Europe the discussion on this kind of technology started in the scope of implementing the so-called digital dividend in the band 790-862 MHz. In this framework the CEPT aims at high efficiency of the overall spectrum use and the most flexible spectrum usage while allowing the widest possible ranges of uses and technologies. Therefore CEPT Report 24 [4] indicates that cognitive radio devices may be allowed to use the interleaved spectrum of the remaining TV spectrum ("white spaces" and thus the designation white space devices - WSDs) subject to the restriction that they will not cause harmful interference to incumbent services to which the band is allocated. A cognitive radio will therefore have to obtain information about the available channels before being allowed to transmit on locally unused channels [17].

In this chapter the main characteristics and the key elements related to cognitive radio technology are presented. The needed capabilities that can be incorporated into cognitive radios in order to operate correctly without interfering the primary system are investigated and an example of cognitive radio network is shown. Then two cognitive techniques, i.e. sensing and geo-location database, are introduced in order to identify potentially available unoccupied channels. With spectrum sensing, WSDs try to detect autonomously the presence of the protected incumbent services in each of the potentially available channels. These aspects will be then dealt in details in chapter 2.

1.1 What is Cognitive Radio?

Nowadays a significant problem for the rise of next generation communication systems is the lack of available frequencies. Cognitive networks are motivated by the apparent lack of spectrum under the current management policies. The right to use the wireless spectrum and regulation of radio emissions are coordinated by national bodies. The national regulatory bodies assign spectrum to holders, also known *primary users* (PU). Most of the frequency bands useful to wireless communication have already been licensed. Few bands have however been designed to be unlicensed bands, most notably the Industrial Scientific and Medical bands (ISM bands), over which the immensely popular WiFi device transmits. These model for assigning spectrum usage rights are known as "command-and-control" model and "commons" or "open access" model.

As most of the bands have been licensed out, and the unlicensed bands are also rapidly filling up, it is becoming difficult to find spectrum that can be made available either for new services or to expand existing ones.

According to measurements carried out by Federal Communications Commission (FCC), temporal and geographical variations in the utilization of assigned spectrum range from 15% to 85%. As confirmed by figure 1.1, where the measured spectrum band occupancy in Vienna (VA, USA) [1] is shown and according to [18], where some radio spectrum utilization measurements have been carried out in different European regions, the spectrum usage is concentrated on certain portions of the spectrum while a significant amount of spectrum remains under used or unused.

As licensed bands are difficult to reclaim and re-lease, the FCC has considered *dynamic* and *secondary* spectrum licensing [19, 20] as an alternative to reduce the amount of unused spectrum. Bands licensed to primary users could, under certain negotiable conditions, be shared with non-primary users without having the primary licensee release its own license.

Cognitive radios (CRs), wireless devices with reconfigurable hardware and software (including transmission parameters and protocols), are capable of delivering what these secondary market devices would need: the ability to intelligently sense and adapt to their spectral environment. The concept of CR has been firstly introduced by Joseph Mitola in 1999 [21].

The definition of cognitive radio adopted by FCC is:

Cognitive radio: A radio or system that senses its operational electro-

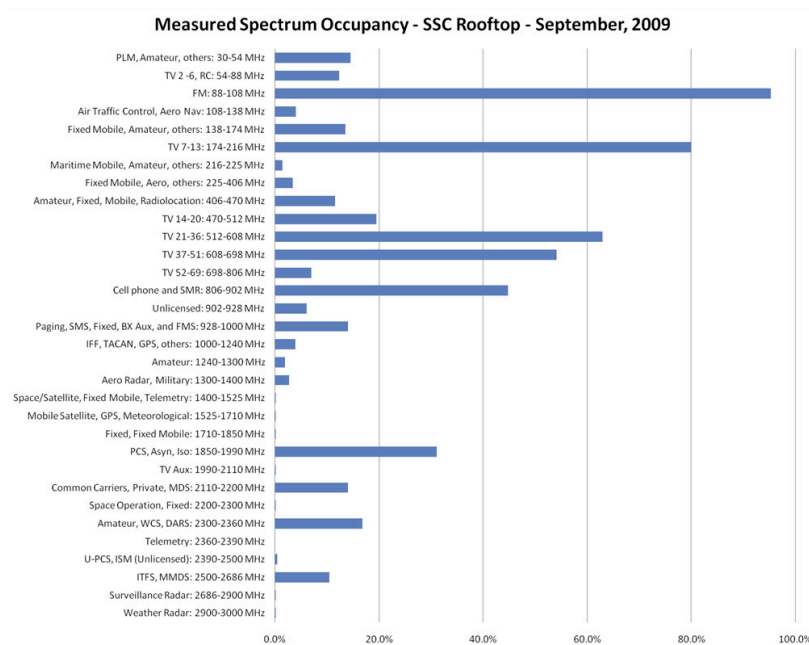


Figure 1.1: The spectrum bands between 30 MHz and 3GHz utilization [1].

magnetic environment and can dynamically and autonomously adjust its radio operating parameters to modify system operation, such as maximize throughput, mitigate interference, facilitate interoperability, access secondary markets.

The worldwide interest in the last years has been focusing on the use of CR technology in television (TV) bands. In [22], FCC adopts final rules to allow unlicensed radio transmitters to operate in the broadcast television spectrum at locations where that spectrum is not being used by licensed services (this unused TV spectrum is often termed *white spaces* - WSs). The official document was released in September 2010. This action allows the use a significant amount of spectrum with very desirable propagation characteristics. This was the culmination of many years of deliberations on the subject, starting with the first NPRM in May 2004 and followed by laboratory and field testing of sensing devices through 2007 and 2008 and the second report and order in 2008 [23].

In Europe the major regulatory agencies involved in developing rules for unlicensed use of TV white spaces are the Office of Communications (Ofcom) in the United Kingdom (UK) and the Electronic Communications Committee (ECC) of the Conference of European Post and Telecommunications (CEPT).

In particular the Working Group on Spectrum Engineering of the ECC tasked the project team SE43 [24] to define technical and operational requirements for the operation of cognitive radio systems (CRs) in the white spaces of the UHF broadcasting band (470-790 MHz) [4, 17].

Following this interest, the IEEE has formed a working group (IEEE 802.22 [25]) to develop an air interface for opportunistic secondary access to TV spectrum [26].

In the next subsections the main technical characteristics of cognitive radio technology are explored. More specifically, in section 1.2, the technical capabilities that could be incorporated into cognitive radio system are considered. A reference cognitive radio architecture on licensed and unlicensed band and spectrum sharing techniques are presented in section 1.3. Finally, in section 1.4, the concept of spectrum sensing is considered. Its related challenges are highlighted and the geo-location database technique as a more reliable way to assist the white space devices in finding unoccupied channels is introduced.

1.2 Cognitive Radio Capabilities

Cognitive radio technologies have the potential to provide a number of benefits that would result in increased access to spectrum and also make new and improved communication services available to the public. As the primary users have the priority in using the spectrum, a paramount capability of a CR is to work without interfering the existing users. New emerging cognitive radio paradigm allows radios to opportunistically transmit in the vacant portions of spectrum, already assigned to licensed users, without interfering with them.

As shown in figure 1.2, an unlicensed user that intends to transmit, before transmitting has to sense which portions of spectrum are available, select the best available channel, coordinate spectrum access with other users, manage and vacate the channel when a primary user reclaims the usage right [27].

Cognitive radio technology could also be used to facilitate interoperability between or among communication system in which frequency bands and/or transmission formats differ. For example, cognitive radio could select the appropriate operating frequency and transmission format, or it could act as a "bridge" between two systems by receiving signals at one frequency and format and retransmitting them at a different frequency and format [20]. As it will be highlighted in chapter 4 this characteristic is very useful in public safety conditions where the interoperability

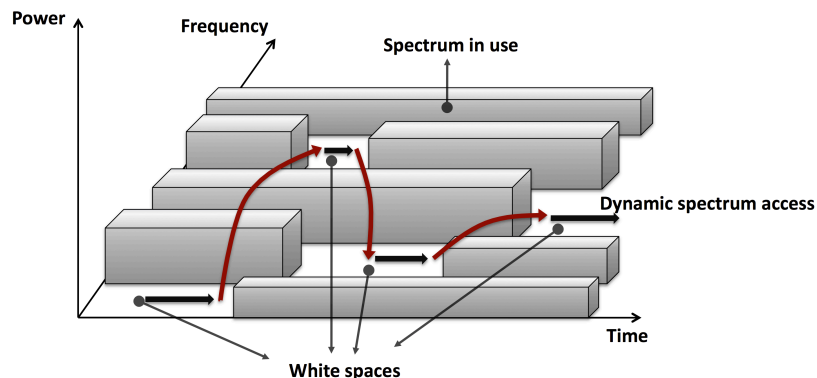


Figure 1.2: Dynamic spectrum access concept.

between different technologies is needed [13].

There are a number of capabilities that can be incorporated into cognitive radios. Five main characteristics can be defined [20]:

- *Frequency agility*: Frequency agility refers to the ability of a radio to change its operating frequency, combined with a method to dynamically select the appropriate operating frequency based on the sensing of signals from other transmitters or on some specific condition. The conditions could include, for example: the location of the device, its proximity to other devices or an operating requirement to adjust power to minimum needed to establish a reliable communication link. The methods that a device could use to decide when to change frequency could include spectrum sensing, geographic location monitoring, or an instruction from a network or another device.
- *Adaptive modulation*: Adaptive modulation techniques can modify transmission characteristics and waveforms to provide opportunities for improved spectrum access and more intensive use of spectrum while "working around" other signals that are present. A CR could select the appropriate modulation type for use with a particular transmission system to permit interoperability between systems. Other possible uses of adaptive modulation include dynamically selecting the transmission bandwidth based on availability of spectrum and the desired transmission data rate. In addition, new types of modulation may be possible in a cognitive radio, such as splitting a signal to use multiple non-contiguous frequency bands simultaneously.
- *Transmit power control*: Transmit power control (TPC) is a feature that en-

ables a device to dynamically switch between several transmission power levels in the data transmission process. The term TPC can be used broadly to refer to a mechanism that switches the output power of a device based upon specific conditions. The conditions could include the proximity to other devices, the maximum power permitted at a geographic location, or an operating requirement to adjust power to minimum needed to establish a reliable communication link.

- *Geo-localization*: A cognitive radio could incorporate the capability to determine its location and the location of other transmitters, and then select the appropriate operating parameters such as the power and frequency allowed at its location. This could be done by using geo-location techniques such as Global Position System (GPS) to determine the geographic location, and then accessing a database over a network.
- *Negotiation*: A cognitive radio could incorporate a mechanism that would enable sharing of spectrum under terms of an agreement between a licensee and a third party. Parties may eventually be able to negotiate for spectrum use on an ad hoc or real-time basis, without the need for prior agreements between all parties [19, 28].

The tasks required for adaptive operation can be summarized in a cognitive cycle referred as *cognitive radio learning loop* (see figure 1.3).

The CR learning loop includes four main steps:

1. *Spectrum sensing* and possible interaction with a *geo-location database*;
2. *Analysis* of available resources;
3. *Reasoning* to determine the best frequency band;
4. *Reconfigurability*.

Through spectrum sensing, a CR can detect the spectrum holes at a specific time instant, or, in general, monitor the surrounding radio environment. The spectrum sensing task can be associated with the interaction of a CR device with a geo-location database that provides information on channels availability [17]. After recognizing the spectrum holes by sensing, a spectrum analysis is performed so that their characteristics are estimated. Then the spectrum management function

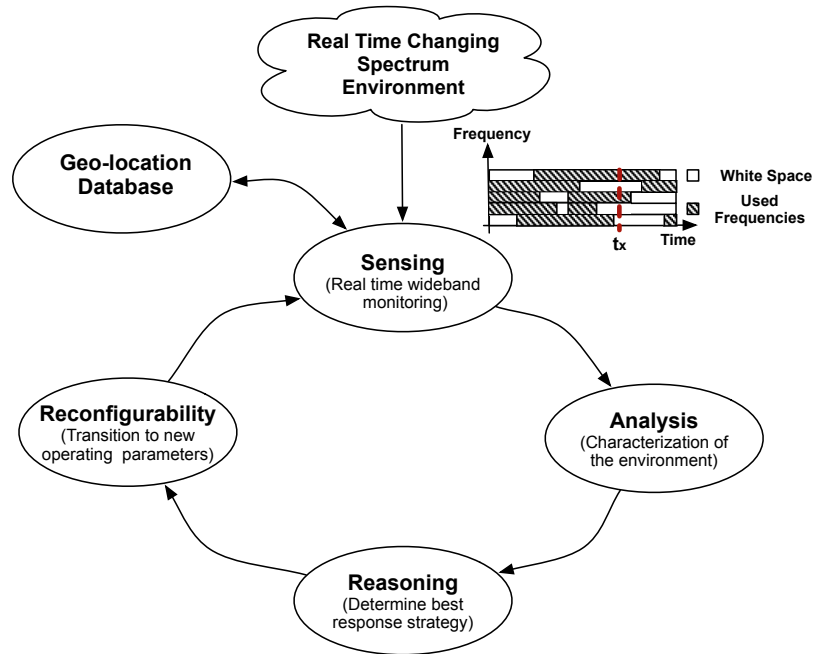


Figure 1.3: The cognitive radio learning loop.

of a CR enables to select the best frequency band and possibly hops among multiple bands according to time varying channel/traffic characteristics to meet various quality of service (QoS) requirements [27]. Finally, reconfigurability is the capability of adjusting operating parameters for transmission on fly, as well as of releasing the selected spectrum portion whenever a primary user activates. This capability enables the CR to adapt easily to dynamic radio environment. The reconfigurable parameters that can be incorporated into a CR include frequency, coding, modulation and transmission power [2].

Thanks to their flexibility, CRs can be used in many applications such as to enhance public safety and homeland security. A natural disaster or terrorist attack can destroy existing communication infrastructure, so that an emergency network becomes necessary to aid the search and rescue phase. As a CR can recognize spectrum availability and reconfigure itself for much more efficient communication, this provides public safety personnel with dynamic spectrum selectivity and reliable broadband communication to minimize information delay [13]. This aspect will be handled in chapter 2.

Moreover, CR can facilitate interoperability between various communication system. Through adapting to the requirements and conditions of another network, the

CR devices can support multiple service types, such as voice, data and video [27].

1.3 Cognitive Radio Network

1.3.1 Cognitive Network Components

Cognitive radio networks can be deployed in network-centric, distributed, ad hoc [29, 30], and mesh architectures [31], and serve the needs of both licensed and unlicensed applications.

A cognitive radio is by definition a device capable of using any of the heterogeneous wireless communication technologies on a given bandwidth provided it does not generate harmful interference to an incumbent user (i.e. a licensed user for that bandwidth). Such a bandwidth can either be a *spectrum hole* (i.e. a licensed band which is temporary or locally unused) or an *unlicensed band*. With reference to figure 1.4, the components of the cognitive network can thus be classified in two groups [2]:

- **Primary Network:** a network infrastructure which has an exclusive right to use a certain spectrum band, composed by:
 - *Primary Base Station (BS):* a fixed component responsible for licensed users' access to the spectrum. A typical BS is not necessarily equipped with cognitive capabilities, but it might be requested to be able to communicate with unlicensed users SUs too. It is worthwhile noting that the term BS is not referred to mobile base station transceiver only, but to access point or TV broadcasting transmitters as well. Basically BS refers to any possible fixed component that provides access to a specific service to the users.
 - *Primary Users:* devices accessing the spectrum subject to the primary BS control. These wireless devices are the primary licence-holders of the spectrum band of interest. In general, they have priority access to the spectrum, and subject to certain QoS constraints which must be guaranteed. They should not be affected by any of the operations of the secondary market networks.

It has to be highlighted that the all system to which the band is allocated are primary systems. This means that, for example, in frequency band 470-790

MHz both TV broadcast services, that are primary services in this band, and PMSE, RAS and ARNS systems [17], that are secondary services of this band but with regulatory priority, are primary systems and have to be protected by transmissions of unlicensed users.

- **Secondary Network:** a network which has not right on using a licensed band and manages the opportunistic access to the desired bands. This network either be an infrastructure network or an ad hoc network. Its components are:
 - *Secondary* or *CR Base Station*: a fixed component with cognitive capabilities providing single hop connections to its users.
 - *Secondary* or *CR User*: these users may access the spectrum which is licensed to the primary users. These cognitive users employ their "cognitive" abilities to communicate while ensuring the communication of the primary users is kept at an acceptable level. They can communicate either with other SUs (single-hop or multi-hop connections) or with secondary BSs on the licensed and unlicensed spectrum bands.
 - *Spectrum Broker*: a fixed component responsible for fair spectrum sharing among different secondary networks. In case this component is not used in the secondary network, secondary BSs should be able to communicate among them in order to share the available spectrum bands.

1.3.2 Cognitive Network Access

In [2] a reference cognitive network architecture is presented and the main aspects are briefly outlined in the following. Figure 1.4 shows the architecture. It consists of three different types of sub-networks: a primary network, an infrastructure based CR network, and an ad hoc CR network. CR networks can operate under the mixed spectrum environment that consists of both licensed and unlicensed bands. Also, CR users can either communicate with each other in multi-hop manner or access the BS. Thus, in CR networks, there are three different access types [2]:

- **CR Network Access:** SUs can access the secondary BS on both licensed and unlicensed spectrum bands.
- **CR Ad hoc Access:** SUs can communicate among them without a network infrastructure, through ad hoc connections on both licensed and unlicensed spectrum bands.

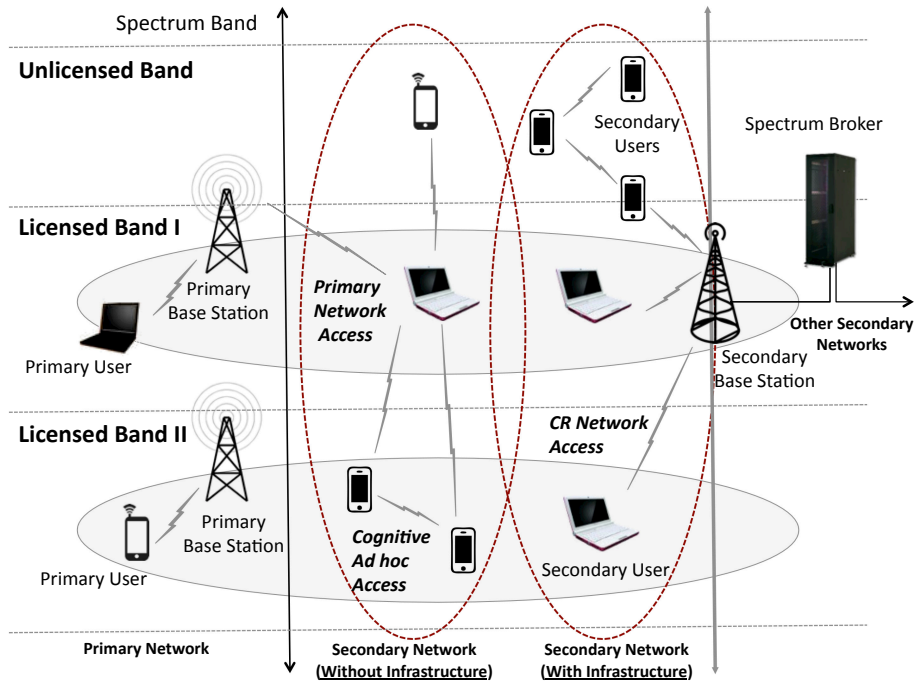


Figure 1.4: Cognitive Network Architecture [2].

- **Primary Network Access:** SUs can access the primary BS on licensed band, provided it has the capabilities to use cognitive functionalities.

Depending on the type of spectrum where the cognitive network intends to operate on, different functionalities are required for the network components. Accordingly, the CR network operations can be classified as *CR network on licensed band* and *CR network on unlicensed band*.

Figure 1.5 shows an example of *CR network on licensed band* [2]. It coexists with the primary network, i.e. in TV spectrum, at the same location (or an adjacent location) and on partially/fully overlapping spectrum bands. In this case the CR network operates on temporally unused spectrum holes in TV spectrum bands. Although the main purpose is to determinate the best available spectrum, cognitive functionalities should be mainly aimed at detection of PUs, as no harmful interference should occur. Furthermore, if a PU appears in the spectrum band occupied by SUs, they should immediately operate a *spectrum hand-off*, i.e. SUs must vacate the current channel and move to new available spectrum hole.

CR network can also be designed for operation on unlicensed bands like ISM band. The *CR network on unlicensed band* architecture is illustrated in figure 1.6

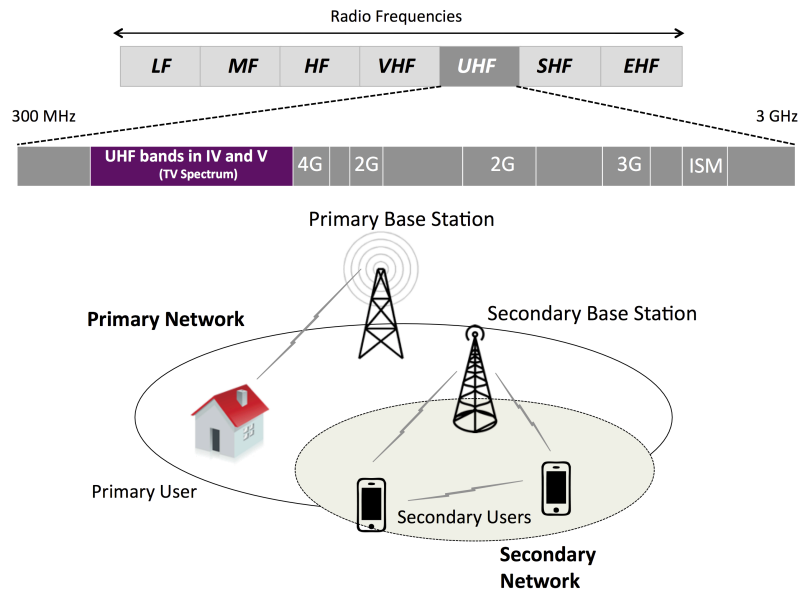


Figure 1.5: Cognitive Network on licensed spectrum bands.

[2]. Since there are no license holders, all network entities have the same right to access the spectrum bands. Multiple CR networks can coexist in the same area and communicate using the same portion of spectrum. As for the operations on licensed bands, SUs have to detect other users but in this scenario the spectrum hand-off is not triggered by appearance of PUs.

1.3.3 Spectrum Sharing Techniques

Networks which contain cognitive radios should intuitively be able to achieve better performance than networks in which they are absent. This because they are able to (1) exploit their cognitive abilities, i.e. sensing and adapting to their wireless environment, and (2) often (but not necessarily) exploit new policies in secondary spectrum licensing scenarios in which the agile cognitive radios are permitted to share the spectrum with primary users. Cognitive behaviour, or how the secondary cognitive users employ the primary spectrum, may be grouped into three categories, each of which exploits varying degrees of knowledge of the wireless environment at secondary users [3]:

- **Interference avoiding behaviour (spectrum overlay):** the secondary users employ the primary spectrum without interfering with the primary users. The primary and secondary signals may be thought of as being orthogonal to

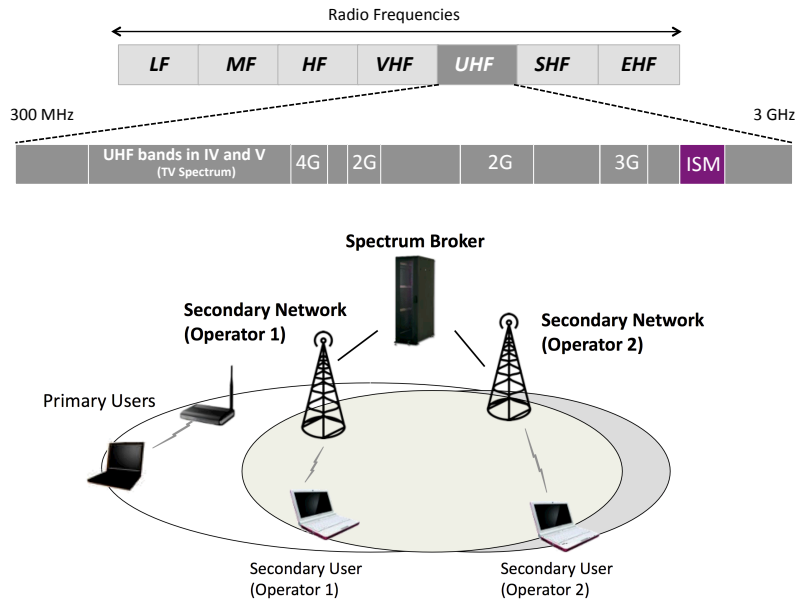


Figure 1.6: Cognitive Network on unlicensed spectrum bands.

each other: they may access the spectrum in Time Division Multiple Access (TDMA) fashion, in Frequency Division Multiple Access (FDMA) fashion, or in any fashion that ensure that the primary and secondary signals do not interfere with each other. The cognition required by the secondary users to accomplish this is knowledge of the spectral gaps (in for example time, frequency) of primary system. The secondary users may then fill in these spectral gaps.

- **Interference controlling behaviour (spectrum underlay):** the secondary users transmit over the same spectrum as the primary users, but do so in a way that the interference seen by the primary users from the cognitive users is controlled to an acceptable level. This acceptable level is captured by primary QoS constraints. The cognition required is knowledge of "acceptable levels" of interference at primary users in a cognitive user's transmission range as well as knowledge of the effect of the cognitive transmission at primary receiver.

1.4 Spectrum Sensing and Geo-location Database

As highlighted in previous paragraphs, an important requirement of the cognitive radio is to identify spectrum opportunities, i.e. white spaces. In particular in this work, the attention was focused on the white spaces in 470-790 MHz band. As stated

in [17], concerning the European scenario, the incumbent radio services/systems on this frequency band that have to be protected are:

- Terrestrial Broadcasting Service including DVB-T in particular.
- Program Making and Special Event (PMSE) Systems including radio microphones in particular.
- Radio Astronomy Service (RAS) in the 608-614 MHz band.
- Aeronautical Radio Navigation Service (ARNS) in the 645-790 MHz band.
- Mobile Service below 470 MHz and above 790 MHz.

In particular in the following analysis, only the protection of the TV broadcasting service in 470-790 MHz has been considered.

Two distinct technologies can support the white space devices in finding unoccupied channels: *spectrum sensing* and *geo-location database* (also known as *white space database*).

Spectrum sensing enables the cognitive users to adapt to environment by detecting the presence of the protected incumbent service in each of the potentially available channels. It is the task of obtaining awareness about the spectrum usage and existence of primary users in a geographical area. The main requirements for spectrum sensing are fast, robust and reliable signal detection in a low signal to noise (SNR) regime. An increasingly array of techniques is being applied to spectrum sensing to enhance the sensing performance, including energy detectors, matched filter detectors, wavelet detection and cyclostationary feature detectors [32]. Most of these traditional sensing algorithms are suffered from noise variations in the received signal data [33, 34].

In [17] the sensing thresholds were derived for different scenarios and taking into account a range of potential DTT receiver configurations. Depending on the DTT planning scenario, the values obtained vary in the range of -91 dBm and -155 dBm. It is extremely challenging to implement devices with such sensitivity using current technologies. Moreover, in some scenarios, even these low values for the detection threshold do not guarantee a reliable detection of the presence/absence of broadcasting signal.

For this reason, the sensing technique, if employed by a stand-alone WSD (autonomous operation), is not reliable enough to guarantee protection of the nearby

DTT receivers using the same channel. This led to consider a more feasible option to avoid possible interference to DTT receivers based on the use of a geo-location. Basically, the cognitive technique of geo-location is an approach, where the WSDs determine their location and make use of a geo-location database in order to get information on which frequencies they can use at their location [17]. In addition to the information on available frequencies, the geo-location database provides the WSD the information on the maximum permitted emission power levels on each available frequency.

The steps for the population of the geo-location database are generally referred as "translation process", [17], whose logical architecture is shown in figure 1.7.

The first step of the translation process is the analysis on how each DTT channel is employed over the territory, in order to estimate spectral occupancy. Therefore, propagation analysis represents the basis to determinate resources potentially available for WSDs, according to the specific criteria defined by the Administration to protect DTT against nuisance interference. Site-specific evaluations are generally performed tessellating the national territory in regular pixels (e.g. square pixels). In each pixel the field strength level received on each DTT channel has to be computed taking into account all DTT transmitters operating in that specific channel. The determination of the maximum permitted Equivalent Isotropically Radiated Power (EIRP) represents the last step of the algorithm to fill the look-up tables of the geo-location database and depends on the several factors, such as the DTT protection criteria and the WSD characteristics.

Spectrum sensing could be used to support the detection of incumbent radio services conducted using the geo-location database [11]. More details on spectrum sensing techniques, the use of geo-location database and the algorithm developed to calculate the maximum permitted EIRP will be presented in next sections.

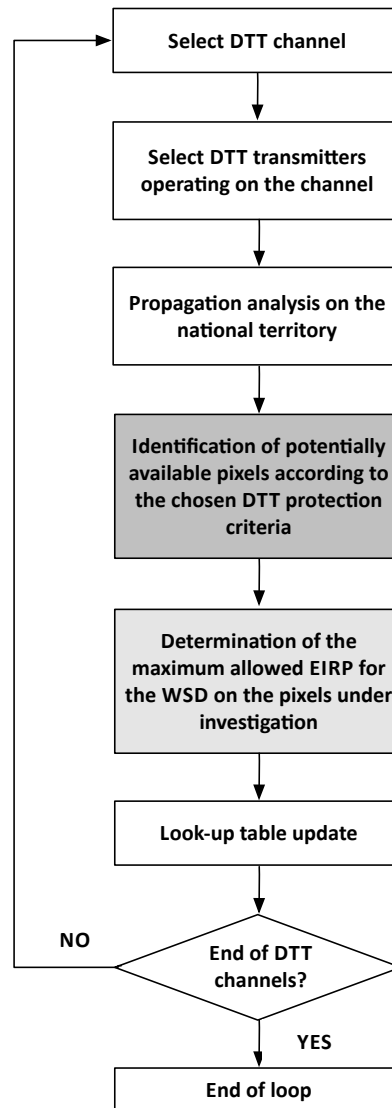


Figure 1.7: Geo-location database translation process architecture.

Chapter 2

White Spaces Identification

The estimation of the amount of spectrum potentially available as white space depends on several factors, as the WSD characteristics, the topology of the area, the national rules governing the use of spectrum, the applications or services using the adjacent bands, and many others: these factors still have to be fully defined by national or international regulators.

In [17] technical requirements for CRs operation in the "white spaces" of the frequency band 470-790 MHz have been investigated. As introduced in section 1.4 different methodologies have been identified to develop protection criteria for each possible incumbent service in the 470-790 MHz band: geo-location database approach shall provide the WSD with a list of allowed frequencies and their associated maximum transmit powers; an alternative approach is based on spectrum sensing techniques, used either in autonomous operation or in combination with the geo-location database. In [17], in order to assist the white space devices in finding unoccupied channels, also the use of techniques that exploit beacon signals are considered.

A number of different methods are proposed to identify the presence of primary signal transmissions based on spectrum sensing. Sensing methods can be mainly divided into two categories: energy detection and feature detection.

A relevant issue in spectrum sensing is the sensing periodicity: while utilizing a white space, the secondary system should continue to periodically sense the band in case primary user starts to transmit. The sensing period determines the maximum time during which the secondary user will be unaware of a reappearing primary user and hence may harmfully interference with it. In general the sensing period depends on the type of the primary service. For instance, one expects the sensing period to

be very small for public safety spectrum, while less frequent sensing may be allowed for TV spectrum where the spectrum usage varies over a much large timescale [35].

Detection performance of single user sensing, while scanning for primary users' transmissions, can be pretty limited by many factors like noise uncertainty, shadowing and multipath effect. To overcome this problem, a cooperative sensing has been considered effective in improving detection accuracy by taking advantage of spatial and multi-user diversity.

In section 2.1 the three most common spectrum sensing techniques proposed in the cognitive radio literature are presented and challenges associated with spectrum sensing are highlighted.

Moreover in section 2.2, three different methodologies mainly based on the geo-location database approach are investigated to estimate the amount of white space in different Italian regions in the UHF band [11].

A first simple methodology to identify spectrum available as white space is based on a threshold approach: in a specific location the received signal power on each channel is evaluated and if the estimated power on a channel is below a certain threshold it can be deduced that there are no licensed users for that channel in the proximity of the investigated location. In the second approach, the usage of a specific channel is prevented within the coverage area of each DTT transmitter employing that channel, in order to guarantee a wanted Location Probability related to proper field strength threshold. Finally a combined geo-location and sensing approach is considered in section 2.3. In section 2.4, simulations and measurements results are reported for different real Italian scenarios considering the different approaches.

2.1 Spectrum Sensing

In this section, the main aspects related to spectrum sensing are discussed. Three detection techniques are compared and the cooperative sensing is presented.

Multi-dimensional spectrum awareness refers to the possibility for a secondary user to exploit more spectrum opportunities to transmit than the traditional ones that always are considered, i.e. frequency, time and space. Traditional spectrum sensing algorithms are related to these dimensions. Other dimensions like code and angle dimensions can be exploited to use more efficiently the spectrum resources. The spectrum over a wideband might be used at a given time through spread spectrum or frequency hopping. This does not mean that there is no availability over

this band. Simultaneous transmission without interfering with primary users would be possible in code domain with an orthogonal code with respect to codes that primary users are using [36, 37]. Concerning the angle dimension, with the recent development of beamforming technology, multiple users can utilize the same channel/frequency at the same time in the same geographical location. Figure 2.1 represents time and frequency dimensions, geographical space dimension, code dimension and angle dimension [36].

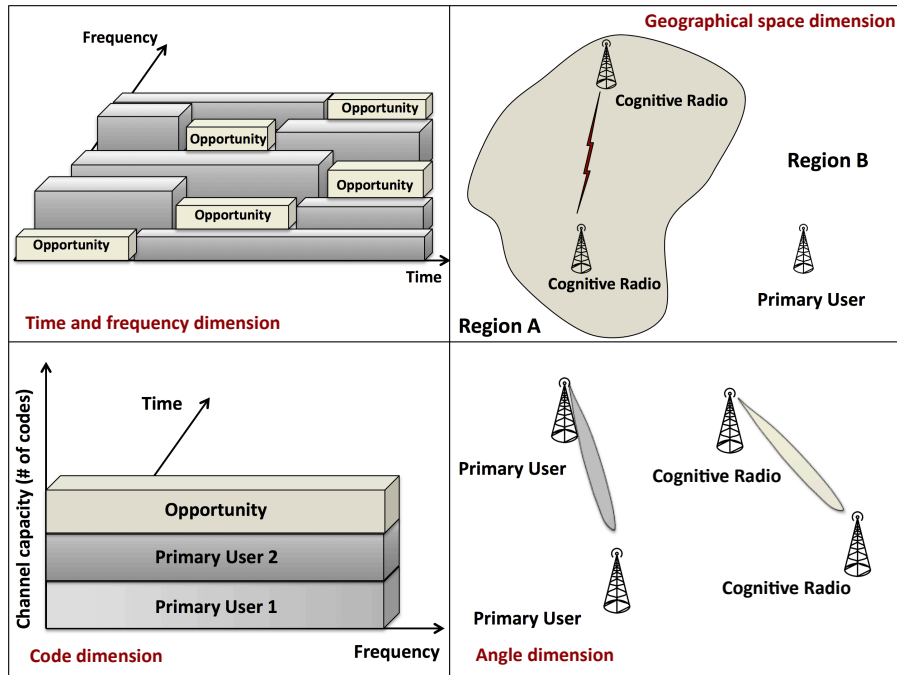


Figure 2.1: Multi-dimensional spectrum awareness.

2.1.1 Spectrum Sensing Techniques

In the literature a lot of spectrum sensing techniques are proposed for identifying the presence of the primary signal transmissions. Some approaches are very efficient but they need *a priori* information about the primary user signal that makes it complex to implement, while others are simple to implement but they are not very robust.

In this section, the most common spectrum sensing techniques are presented: *energy detection*, *cyclostationary feature detection* and *matched filter detection*.

2.1.1.1 Energy detector

Energy detection is the most common type of spectrum sensing because it is computational easy to implement and requires no prior knowledge about the primary signal.

The main idea of energy detector is to detect the presence of a primary user using a specific band by comparing the received signal with a threshold which depends on the noise floor. The basic model for transmitter detection is:

$$\begin{aligned} H_0 : y(t) &= n(t), \\ H_1 : y(t) &= hx(t) + n(t) \end{aligned}$$

where $y(t)$ is the received signal, $x(t)$ is the primary users' signal, $n(t)$ is the additive Gaussian noise and h is the channel gain from the primary user's transmitter to the secondary user's receiver.

H_0 is a null hypothesis, which means that there is no licensed user signal in a certain spectrum band, while H_1 indicates that there exist some licensed user transmission.

The detection statistics of the energy detector can be defined as the average (or total) energy of N observed samples [27].

$$T = \frac{1}{N} \sum_{t=1}^N |y(t)|^2 \quad (2.1)$$

The decision on whether the spectrum is free or it is being occupied by the primary user is made by comparing the detection statistics T with a predetermined threshold λ . The choice of λ is an important challenge in energy detector based sensing.

The performance of the detection algorithm can be summarized with two probabilities: the probability of false alarm, P_F and the probability of correct detection, P_D .

P_F is the probability that a primary user is detected but the spectrum resource is free, i.e. the probability that the hypothesis test decides H_1 while it is actually H_0 :

$$P_F = P_r(T > \lambda/H_0) \quad (2.2)$$

Instead, P_D is the probability of detecting correctly a signal on the considered frequency:

$$P_D = P_r(T > \lambda/H_1) \quad (2.3)$$

A good detector should ensure a high detection probability P_D and a low false alarm P_F or it should optimize the spectrum usage efficiency while guaranteeing a certain level of primary user protection. Since the detection performance is very sensitive to the noise power estimate error [33], it is very important to estimate the noise floor. A constant false alarm rate threshold is further computed to study the spectrum occupancy and its statistics. As mentioned before, an important challenge in designing a good energy detector is to select a decision threshold for finding an optimum balance between P_D and P_F . Indeed, the detection threshold depends on the noise power, which may change over time and hence it is difficult to measure precisely in real time. A well chosen detection threshold can minimize spectrum sensing error, provide the primary user with enough protection, and fully enhance spectrum utilization. In [38], the detection threshold is optimized iteratively to satisfy the requirement on false alarm probability. Furthermore, in low SNR conditions, reliable identification of primary user is even impossible due to the uncertainty in background noise power.

Another drawback is that the energy detector cannot differentiate signal types but can only determinate the presence of the signal. For this reason, the energy detector is prone to the false alarm detection triggered by the unintended signal.

2.1.1.2 Cyclostationarity feature detection

Feature detectors are a more sophisticated class of spectrum sensing algorithms that exploit some known features of the primary signal. This detector allows a cognitive radio to detect a specific primary user buried in noise and interference at the cost of increased complexity.

Cyclostationarity features are caused by the periodicity in the signal or in its statistic as the average and the autocorrelation. Exploiting these characteristics a detector can distinguish cyclostationary signals from stationary noise. This is a result of the fact that noise is wide-sense stationary (WSS) with no correlation while modulated signals are cyclostationary with spectral correlation due to the re-

dundancy of signal periodicity. Therefore, a cyclostationary feature detector can perform better than the energy detector in discriminating against noise due to its robustness to the uncertainty in noise power. Furthermore, it can be used for distinguishing among different types of transmissions and primary users. As drawback, this kind of detectors are computationally complex and require significantly long observation time.

Many of the modern radio frequency systems and emerging standards, adopt a more efficient transmission technique such as Orthogonal Frequency-Division Multiplexing (OFDM). Most of the existing OFDM spectrum sensing methods make use of the cyclostationarity of OFDM signals [39, 40, 41]. There are different ways for introducing cyclostationarity in OFDM signals, e.g., by the use of Cyclic Prefix (CP), or by the use of different transmit power on the subcarriers.

Obviously, the sensing performance of CP-based spectrum sensing methods highly depends on the length of CP that is inserted. When the CP length is short, a long sensing time is needed to obtain a good sensing performance. For this reason, more efficient algorithms for OFDM modulated signals are present in the literature exploiting other proprieties like a non-zero constant term embedded in the Time-Domain Symbol Cross-Correlation (TDSC) if two OFDM symbols have the same frequency-domain pilot symbols [40]. In [40], it is shown that the TDSC of two OFDM symbols having the same pilot tone pattern, consists of a constant and a noise term. Considering that the mean value of the noise term is zero, the mean value of TDSC function results to be not zero. This property allow to differentiate the signal from the noise. This is a very interesting method to identify OFDM modulated signals like DVB-T signals.

Compared with energy detectors, that are prone to high false alarm probability due to noise uncertainty and cannot detect weak signals in noise, cyclostationary detectors become good alternatives because they can differentiate noise from primary users' signal and have better detection robustness in low SNR regime.

2.1.1.3 Matched filter detection

If the structure of the primary signal is known, the optimal detector in stationary Gaussian noise is a matched filter followed by a threshold test.

The matched filter correlates the already known primary signal with the received

signal to detect the presence of the primary user and thus maximize the SNR in the presence of additive stochastic noise.

This type of coherent detection is very useful for the short time it requires to achieve a certain detection performance where the secondary system is limited to operate in a few primary bands. However, with more primary bands scanned for opportunistic access, the implementation cost and complexity associated with this approach will increase quickly [35].

Other drawbacks of this kind of spectrum sensing are its implementation complexity and its high power consumption. In fact it needs receivers for all types of signal and corresponding receiver algorithms to be executed.

Furthermore, matched filtering requires perfect knowledge of primary users' signal, such as the operating frequency, bandwidth, modulation type and order, pulse shape, packet format etc. If wrong information is used for matched filtering, the detection performance will be degraded a lot.

2.1.2 Hidden Node Problem and Cooperative Spectrum Sensing

Spectrum sensing as a cognitive technique needs to account for so called hidden node problem. Figure 2.2 illustrates this issue.

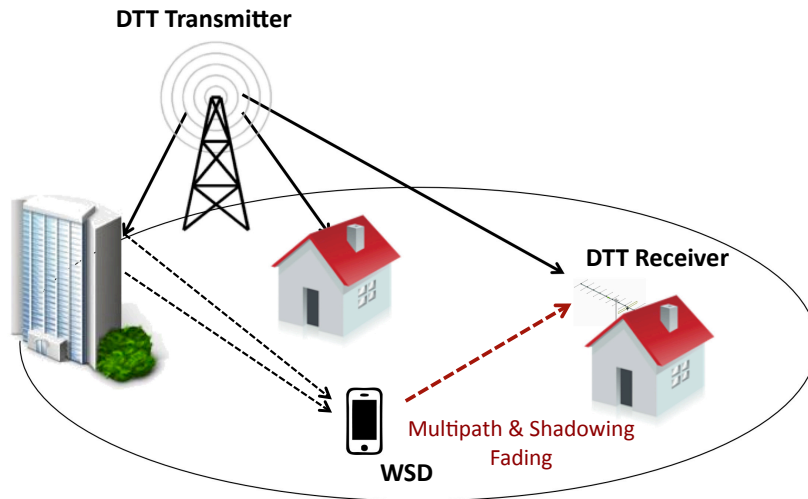


Figure 2.2: Hidden node problem.

As shown in the figure, the DTT receiver, that has to be protected, is better able to receive the DTT signal than the WSD in a low height scenario can. In fact, due to multiple attenuated copies of DTT signal and the blocking of a house, the WSD

experiences multipath and shadow fading such that the signal of the incumbent service may not be correctly detected. As a result, the transmission from the WSD may interfere with the reception at DTT receiver.

Cooperative sensing is used as a solution to problems that arise in spectrum sensing due to noise uncertainty, fading, and shadowing. By taking advantage of independent fading channels (i.e. spatial diversity) and multiuser diversity, cooperative spectrum sensing is exploited to improve the reliability of spectrum sensing, increase the detection probability to better protect a primary user, and reduce false alarm to utilize the idle spectrum more efficiently [42].

Cooperation can be implemented in two fashions: centralized or distributed. In centralized cooperative spectrum sensing, a central unit collect sensing information from cognitive devices, identifies the available spectrum, and broadcast this information to other cognitive radios or directly controls the cognitive radio traffic. To limit the overhead of the network, binary sensing results are gathered at a central place. Furthermore, only the cognitive radios with reliable information are allowed to report their decision to the central unit.

In distributed cooperative sensing, cognitive nodes share information among each other but they make their own decisions as to which part of the spectrum they can use. Distributed sensing is more advantageous than centralized sensing because it does not need a backbone infrastructure and reduce the cost. Both centralized and distributed cooperative sensing can consider the use of relay-assisted cooperative sensing [43]. In [43] the state-of-the-art survey of cooperative sensing is provided to address the issues of cooperation method, cooperative gain, and cooperation overhead.

2.2 White Space Database

In the context of identifying spectrum resources, much of the research, mainly by academia, has been directed toward the operation of autonomous WSDs. In previous section, main spectrum sensing techniques and algorithms have been presented. It is inevitable that the specification of the regulatory emission limits for the operations of such autonomous WSDs in DTT bands has to be based on worst-case geometry relating to the interfering and victim and worst-case sensing (i.e. hidden node) environments. Consequently, adequate protection of the DTT service can result in very stringent WSD sensing levels, applied uniformly at all locations.

The above issue can be resolved if the WSDs operate with assistance from geo-location database.

The most proper methodologies (e.g. algorithms and parameters and criteria) to be adopted in order to identify available resources for the WSD, whilst granting the most adequate level of protection to incumbent services, should be established by the Administrations, which intend to adopt the geo-location database approach to authorise WSDs. In the following, the protection of incumbent DTT service is taken as an example, even though a similar approach can be adopted also for other services [11]. A WSD, which intends to operate in a specific location, sends its information to the geo-location database and receives information on the available frequencies with associated values of maximum permitted EIRP. As explained in section 1.4 (see figure 1.7), the steps for population of the geo-location database are referred as "translation process". In this section the focus is on the first step of the translation process, that is the identification of spectral resources not used by incumbent services and thus potentially available as white spaces [11].

In the following, different methodologies to determine the amount of spectrum potentially available as white space are described. The proposed methodologies have been applied in Italy in order to fill the geo-location database with the information on the available frequencies.

2.2.1 Threshold-based approach for the population of the geo-location database

This is a simple methodology to identify spectrum available as white space: in a specific location the received signal power on each channel is evaluated by means of a proper propagation model [44], and if the estimated power on a channel is below a certain threshold it can be deduced that there are no licensed users for that channel in the proximity of the investigated location. Therefore a WSD is allowed to transmit its signal, provided that the specific emission requirements are met [17, 45, 10]. The threshold can be determined as a function of different parameters such as the incumbent service to be protected (e.g. DTT, PMSE) or the level of protection to be granted.

In particular, the WS estimation based on the threshold approach is performed as follows:

1. compute the power received on a given channel and in a given pixel (e.g. 600 m x 600 m) by a receiving antenna (e.g. omnidirectional with 0 dBi gain)

- assumed at a specific above ground level;
2. compare the received power against a specific threshold;
 3. if the received power is below the threshold, the channel is considered as vacant;
 4. iterate steps 1- 3 for all the channels from 21 to 60 and for all the pixels of the considered area.

Figure 2.3 (on the right) shows the flowchart of the threshold-based approach in order to fill the geo-location with information on the potentially available pixels.

2.2.2 Location Probability approach for the population of the geo-location database

This approach is particularly focused on the protection of the DTT service which is the one of paramount interest for Italian scenario. According to this approach, the usage of a specific channel is prevented within the coverage area of each DTT transmitter employing that channel, in order to guarantee a wanted Location Probability related to proper field strength threshold [46]. DTT field strength levels are evaluated using accurate propagation models, which take into account also diffraction phenomena. Predicted values are then employed to identify the DTT protection area and the paired zone outside the coverage area where the channel is potentially available for WSDs.

According to this approach, protection of DTT service is guaranteed evaluating a-priori the service area contour of each DTT transmitter. Potentially available white spaces can be located only outside the computed contour, which is estimated by means of propagation analysis, considering the Reference Planning Configurations (RPCs) specified in [46].

In table 2.1 the minimum median received field strength levels of the GEO-06 RPC at 650 MHz frequency are shown for fixed reception with respect to different location probabilities values.

The potentially available white spaces are calculated based on the following approach:

1. for each pixel and for each channel, the field strength level E_{rx} (dB μ V/m) considering all possible DTT transmitters is evaluated with a suitable propagation model;

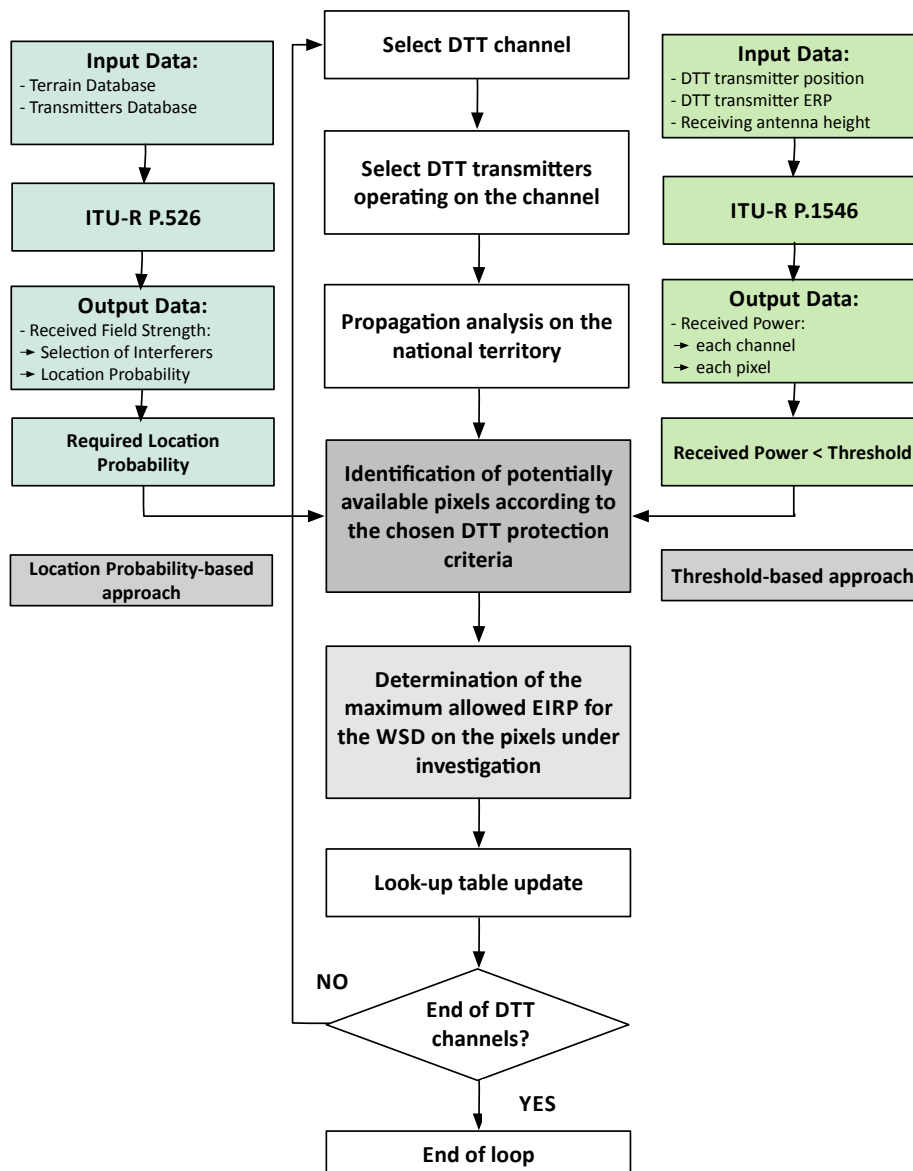


Figure 2.3: Geo-location database: approaches to compute the potentially available pixels.

Table 2.1: DTT REFERENCE PLANNING CONFIGURATIONS

Location Probability	$F_{k,min}$ dB μ V/m at 10 m
99 %	60
95 %	56
50 %	48
1 %	34

2. the calculated field strength E_{rx} is compared with the selected planning configuration threshold $F_{k,min}$ (table 2.1);
3. if E_{rx} is $\geq F_{k,min}$ the pixel is within the protected service contour, hence the channel is occupied ($D_G = 1$); if E_{rx} is $< F_{k,min}$ the pixel is outside the protected service contour, hence the channel is vacant ($D_G = 0$).

The logical architecture of the Location Probability- approach is shown in figure 2.3 (on the left).

2.3 Combined White Space Database and Sensing Techniques

In this approach geo-location database and sensing methodologies are combined to determine white spaces potentially available. In particular the combined geo-location and sensing approach is considered based on the latter methodology associated to some channel measurements performed in specific locations. Vacant and occupied channels are evaluated based on the following algorithm:

1. apply the methodology described in section 2.2.2 to identify white spaces (pixels and frequencies) potentially available based on the geo-location approach;
2. implement field strength measurements in different pixels and channels and compare the results with proper sensing threshold to identify occupied and un-occupied channels;
3. only when "un-occupied channels" are obtained from both steps 1 & 2 the considered pixel and frequency are potentially available for the WSD otherwise the channel is occupied.

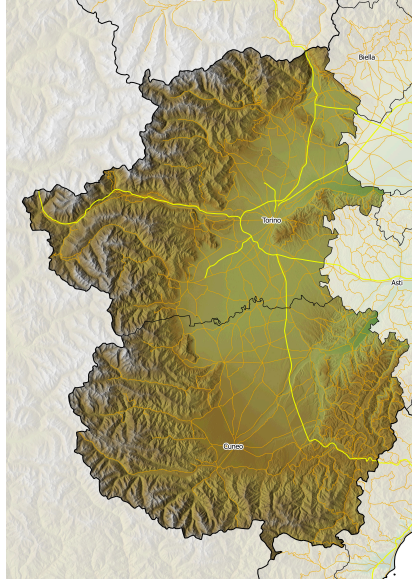


Figure 2.4: West Piedmont map.

2.4 Simulation and Measurements Results

2.4.1 Threshold-based Approach: West Piedmont

In this section, the estimation procedure described in section 2.2.1 section is applied to the case of West Piedmont [11]. Using public information on ERP values and positions of each DTT transmitter, the power received in each channel and location by means of the Recommendation ITU-R P.1546-3 [44] have been assessed, assuming the receiving antenna height at 1.5 m and 10 m. Two different thresholds set to -114 dBm and -120 dBm have been considered. Figure 2.5 and 2.6 show the West Piedmont area with the number of channels available for each pixel in different configurations of detection threshold (DT) and antenna height (h).

With reference to figure 2.4 which shows the West Piedmont map, it can be easily noted that areas where the WSDs actually could have channels available to operate on are mainly rural, in correspondence of mountains and valleys. Densely populated areas have little or no spectrum available as white space.

The amount of spectrum available as white space strongly depends on the chosen threshold. For instance, assuming a threshold equal to -120 dBm and an antenna height of 1.5 m, the percentage of pixels where there is at least 1 available channel is 47.19%, while raising the detection threshold to -114 dBm this percentage becomes 56.99%.

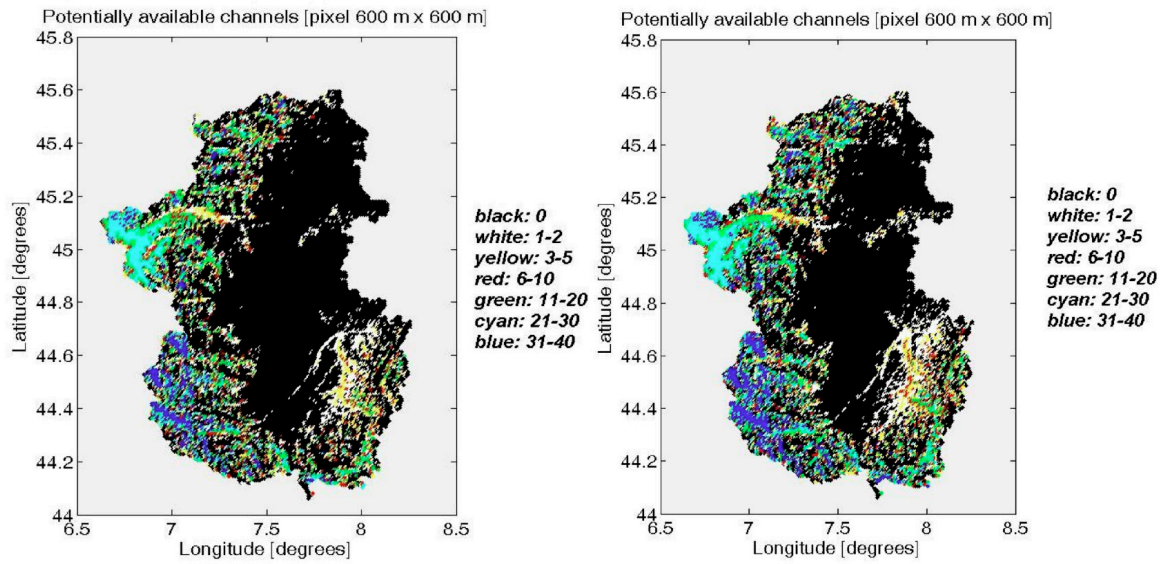


Figure 2.5: $h=10$ m, $DT=-120$ dBm (left) and $DT=-114$ dBm (right).

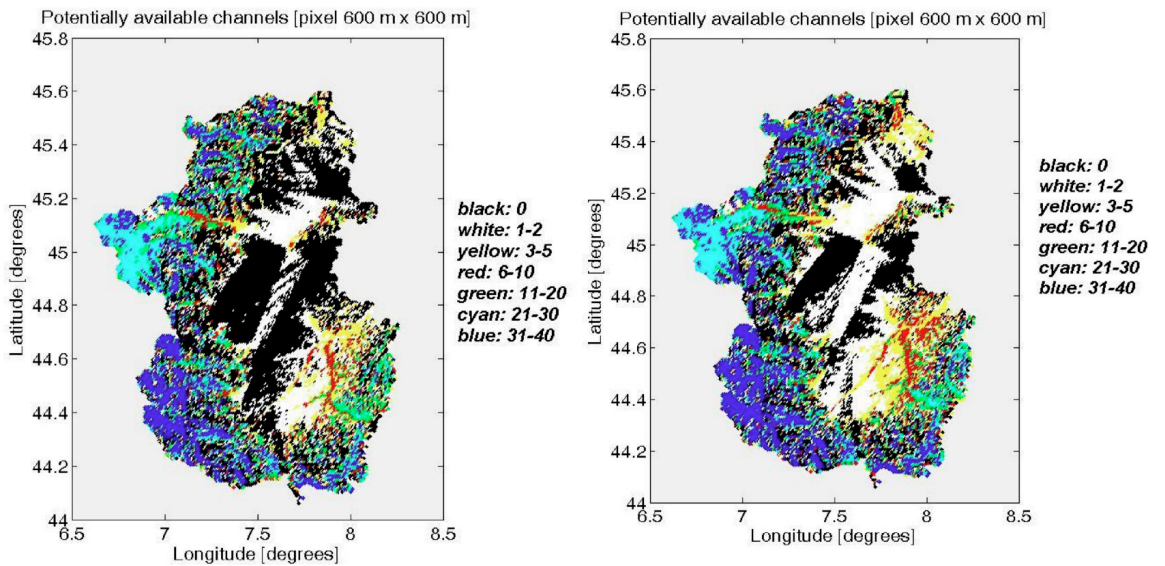


Figure 2.6: $h=1.5$ m, $DT=-120$ dBm (left) and $DT=-114$ dBm (right).

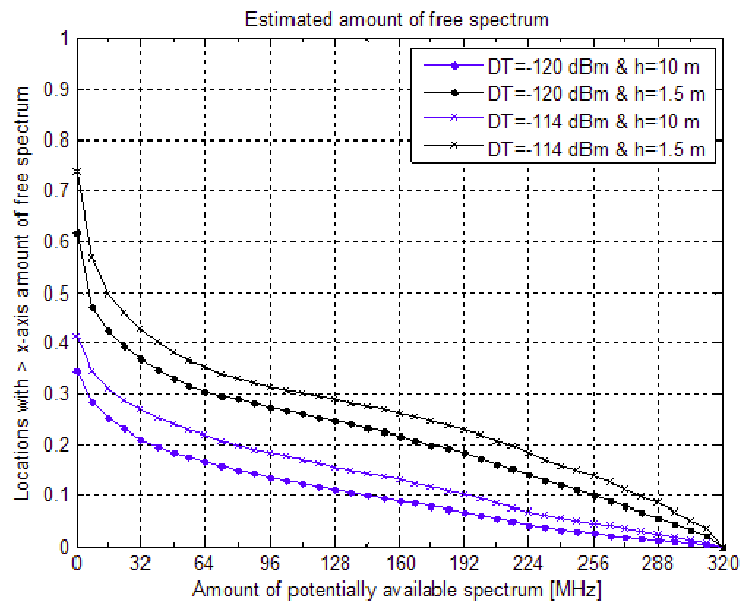


Figure 2.7: CCDF of the amount of white space per pixel.

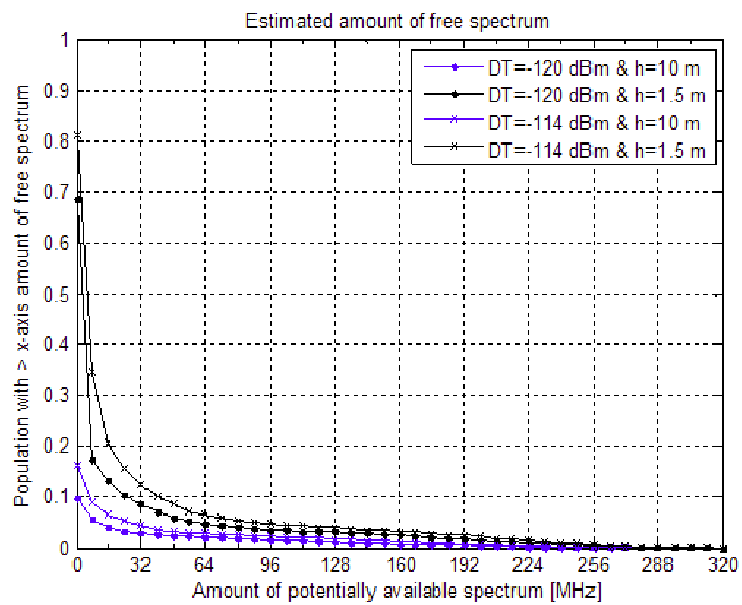


Figure 2.8: CCDF of the amount of white space per population.

Figure 2.7 and figure 2.8 show the Complementary Cumulative Distribution Function (CCDF) of the estimated amount of spectrum available as white space. These figures confirm that the areas where there are more available channels are rural, as the CCDF referring to the population percentage (figure 2.8) has a steeper descent than the one referring to the location percentage (figure 2.7). For example, while almost 20% of locations have more than 64 MHz available with $DT = -120$ dBm and $h = 10$ m, only 2% of population actually resides in these areas. Although these results refer to delimited area of Italy, a similar behaviour is observed in other studies on EU and non-EU countries [47, 48, 49, 50], where it has been shown that the percentage value of available white spaces is higher when expressed by area rather than by population. Similarly the number of available channels is generally higher in less populated or rural areas (see figure 7 in [49]).

2.4.2 Location Probability-based Approach

DTT coverage simulations have been performed in a real scenario in different Italian regions. Predictions have been carried out using a proprietary prediction tool, where the propagation model takes also into account the diffraction phenomena according to ITU-R Recommendation P.526 [51]: occupied and vacant DTT channels are identified according to different levels of protection of the incumbent service (i.e., different percentage of Location Probability LP).

Figure 2.9 shows an example of calculation of the employment of a DTT channel in Northern Italy, using the coverage reference level of RPC1 provided by GEO-06 (table 2.1) of $56 \text{ dB } \mu\text{V/m}$, which corresponds to a LP of 95%. According to the adopted criteria for DTT protection, it is possible to identify those pixels where specific channels could be available for WSDs. In figure 2.9 potentially available WS location for the considered DTT channel correspond to pixels outside the DTT coverage areas highlighted with different colours for each operator. Higher protection can be granted to the incumbent service referring to different LP values. In figure 2.10 the usage of three different DTT channels in some Italian regions is considered and the percentage of population living in the white space locations is calculated on a regional basis. It can be noticed that there are regions where the chosen channels are almost completely un-occupied (e.g. mountain regions such as Valle d'Aosta) and Trentino Alto Adige), while in more densely populated areas (e.g. Lazio) the considered channels are potentially available to serve a lower percentage of population.

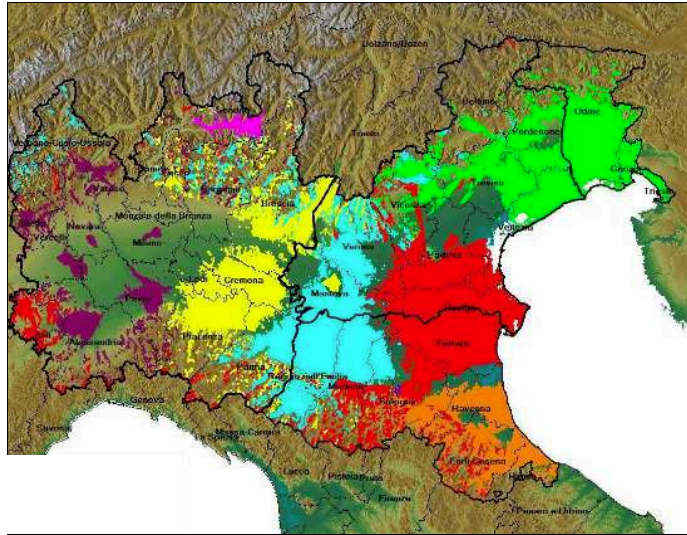


Figure 2.9: DTT coverage area for LP = 95% for the same channel used by different operators.

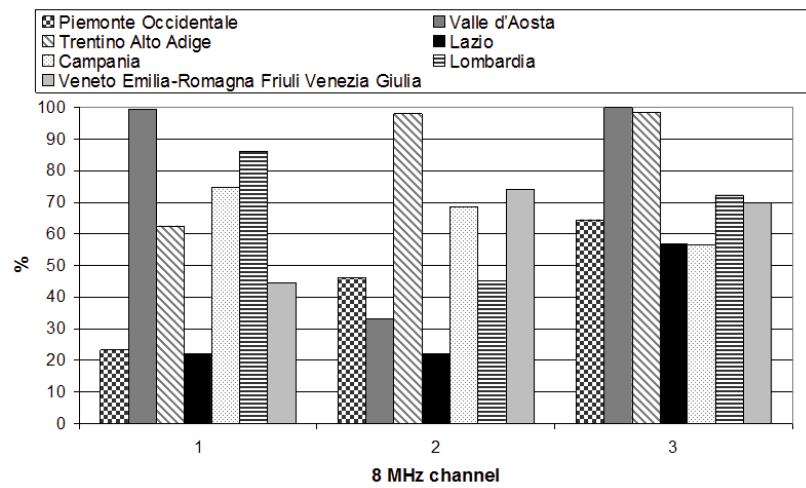


Figure 2.10: Percentage of population living in potential white space areas for three different channels in several Italian Region.

2.4.3 Combined Geo-location and Sensing Approach

The combined sensing and geo-location approach has been applied in a real scenario in Iatly, in the province of Bologna.

2.4.3.1 Geo-location Database

In the considered area, field strength levels for DVB-T channels from 21 to 60 are calculated over square pixels (400 m x 400 m). The path loss between each DVB-T transmitter and virtual receivers located in the centre of the pixels is computed considering a free space term to which the diffraction path loss component is added. For diffraction loss due to natural obstacles along the propagation path, the Recommendation ITU-R P.526 [51] model has been referred and the Deygout method has been adopted with maximum of 3 obstacle, selected with the stretched string method. For calculations, the actual height of the antennas above the level has been considered and the terrain model has been taken from public *Shuttle Radar Topography Mission* SRTM database [52].

For each pixel and for each channel from 21 to 60, the simulation tool evaluates the maximum field strength level E_{rx} (dB μ V/m) considering all possible DVB-T transmitters located in the investigated area and in the neighbourhood:

$$E_{rx}(dB\mu V/m) = Max(E_{tx}(dB\mu V/m) - A_{tot}(dB)), \quad (2.4)$$

where E_{rx} (dB μ V/m) is a function of each considered DVB-T transmitter effective radiated power ERP_{tx} (dBW) and A_{tot} is the path loss.

The simulation results are then compared with the proper threshold based on the RPCs specified in [46] for the protection of the DVB-T service (see table 2.1). In figure 2.11 simulated field strength levels (dB μ V/m) are shown for a DVB-T channel. It can be noticed that most of the pixel of the province of Bologna are occupied, as only some hilly and mountainous areas quite far from Bologna are not reached by the DVB-T. Similar results have been computed with the employed simulation tool for all DVB-T channels in the 470-790 MHz band (channels 21-60).

Based on this analysis the geo-location database can be populated: for each pixel and for each channel, the proper value of D_G parameter (1 or 0) is stored. In figure (2.12) the geo-location database results obtained for channels 21-60 are reported for

Table 2.2: WS POTENTIALLY AVAILABLE FROM GEO-LOCATION DATABASE

Threshold (dB μ V/m)	Percentage of available white space (%)
≤ 34	20.08
≤ 48	38.89
≤ 56	46.15
≤ 60	50.43

the six locations (Villa Griffone, Ristorante Joli, Giardino Sasso Marconi, Val di Setta, Piccolo Paradiso, Mongardino), where also measurements are available. The selected locations are those shown in figure .

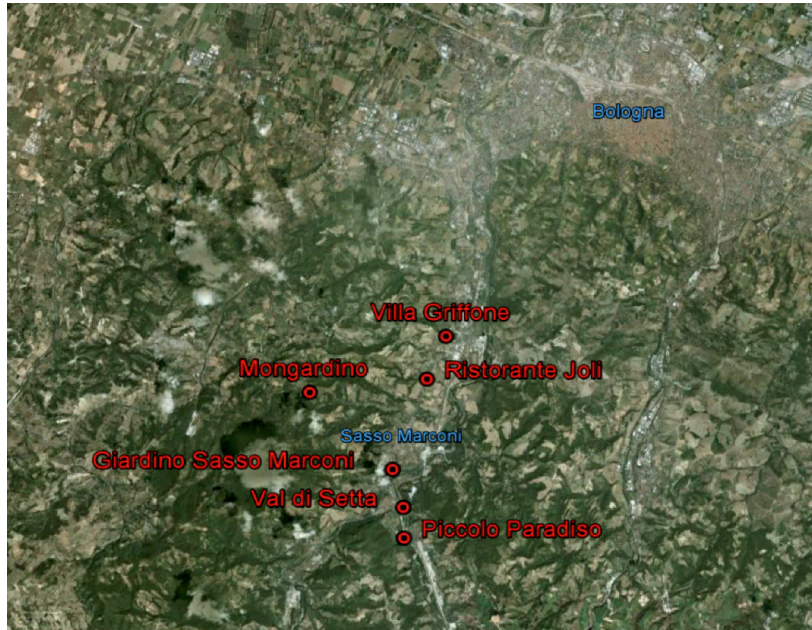


Figure 2.13: Measurement locations: Villa Griffone, Ristorante Joli, Giardino Sasso Marconi, Val di Setta, Piccolo Paradiso, Mongardino.

Four different thresholds of 34 (dB μ V/m), 48 (dB μ V/m), 56 (dB μ V/m), 60 (dB μ V/m) have been addressed in order to identify if the channel is occupied (red) or not (green). Channel occupancy is shown in figure (2.12) for the different locations and selected thresholds. From table 2.2, it can be observed that the percentage of white space potentially available varies with the selected threshold, even though most of the DVB-T channels results to be occupied in the considered locations.

2.4.3.2 Measurements for Spectrum Sensing

Further information on channel occupancy can be achieved by means of sensing techniques. To this aim several measurements have been realised in a number of locations of the considered area (province of Bologna).

In this work, a Narda SRM 3000 portable spectrum analyser has been adopted for spectrum sensing. The instrument has been equipped either with a tri-axial isotropic antenna, which can operate in the frequency range 75 MHz -3 GHz, or with a log-periodic dipole array antenna, which can operate in the frequency range 200 MHz -2.75 GHz. The two different antennas were chosen in order to have different sensitivity thresholds for the measurement set up: sensitivity threshold is as high as -80 dBm with the isotropic antenna and falls to -105 dBm with the log-periodic antenna.

In line with ECC Report 159 [17], the detection threshold have been expressed in dBm. It is also always possible to refer to field strength, once the antenna factor is known: the antenna factor is equal to 50 [1/dBm] for the omnidirectional antenna and approximately 17.7 [1/dBm] for the log-periodic antenna in the frequency range of interest.

It has to be noted that, according to the ECC Report 159, the detection threshold should be set to -120.71 dBm, in case sensing-alone is applied in the considered scenario. However, the measurement equipment available for this study does not permit to lower the sensitivity threshold below -105 dBm; therefore sensing-alone is not a viable approach with this set up.

Measurements have been performed using the "channel power" mode, in order to evaluate the total amount of power received in the DVB-T channel bandwidth of 8 MHz. A resolution bandwidth of 30 kHz has been adopted and for each selected frequency range the Integration Bandwidth function has been used.

Measurements have been performed in the six different locations listed in table 2.3 and shown in figure 2.13.

In figure 2.14 measurement results obtained for channels 21-60 are reported in the six different observed locations, for the two different probes: omnidirectional and log-periodic antenna. According to measurements, unoccupied channels correspond to field strength level below the set up sensitivity floor (-80 dBm for omnidirectional antenna and -105 dBm for log-periodic antenna). As expected, the number of vacant

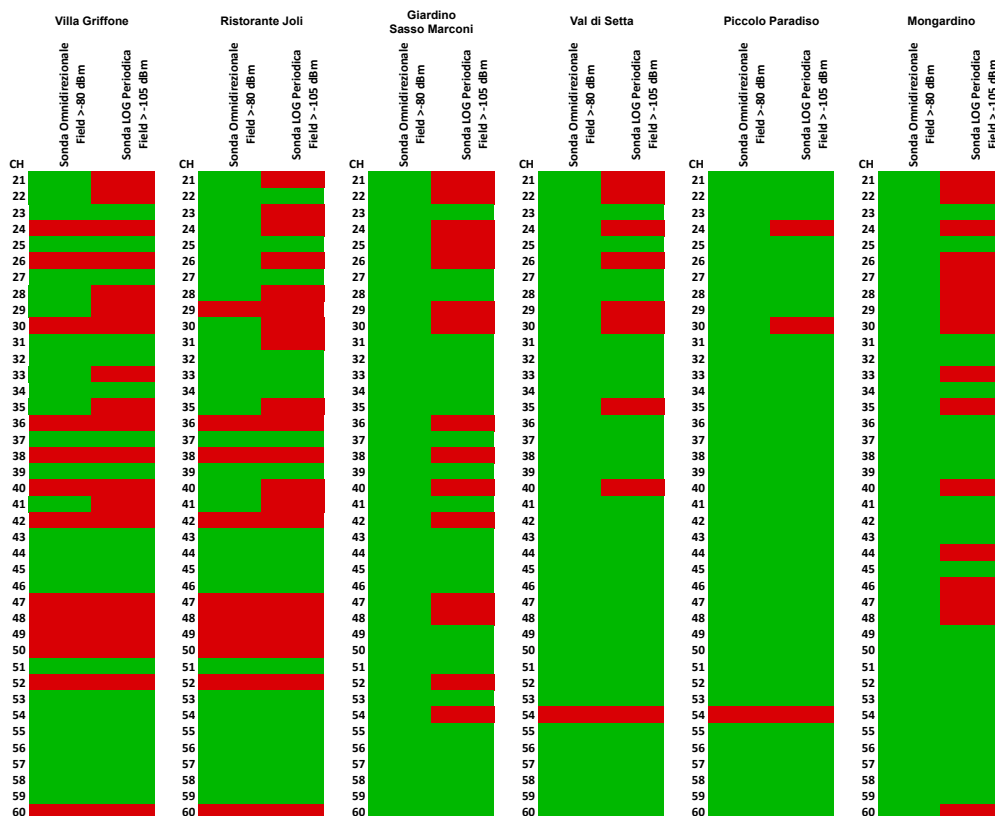


Figure 2.14: Measured data: comparison in each location (Villa Griffone, Ristorante Joli, Giardino Sasso Marconi, Val di Setta, Piccolo Paradiso, Mongardino) for different the two different instrument floor level (-80 dBm and -105 dBm).

Table 2.3: MEASUREMENT LOCATIONS

Measurement point	X-UTM (ED50)	Y-UTM (ED50)	Height (m)
Villa Griffone	680409	4922261	1.5
Ristorante Joli	679948	4920824	1.5
Sasso Marconi	679010	4917863	1.5
Val di Setta	679329	4917863	1.5
Piccolo Paradiso	679384	4915586	1.5
Mongardino	676364	4920300	1.5

channel is negligible, while in other cases the number of unoccupied channels varies with the sensitivity floor value.

Figures 2.15 and 2.16 show the percentage of contiguous available channels that have been identified with geo-location based approach (figure 2.15) and through measurements (figure 2.16).

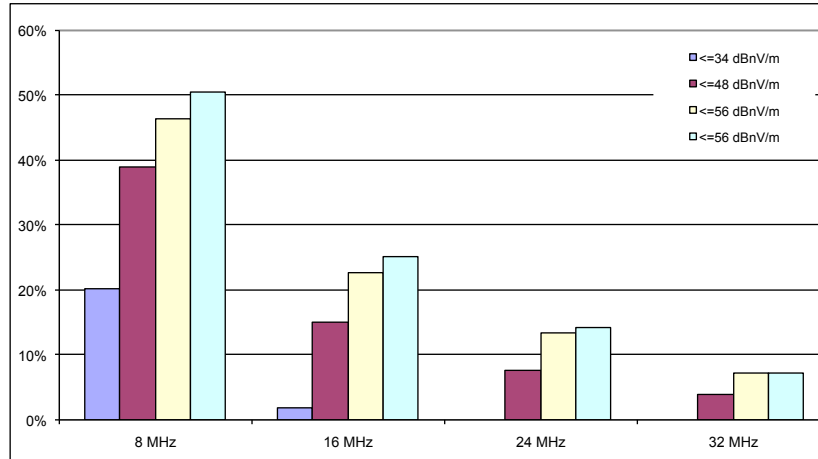


Figure 2.15: Geo-location database: percentage of contiguous channels for different field strength thresholds ($34\text{ dB}\mu\text{V/m}$, $48\text{ dB}\mu\text{V/m}$, $56\text{ dB}\mu\text{V/m}$, $60\text{ dB}\mu\text{V/m}$).

2.4.3.3 Combined Approach

In order to assess the effect of combined approach, both results from the simulations (i.e. geo-location approach) and measurements (i.e. spectrum sensing approach) have been considered.

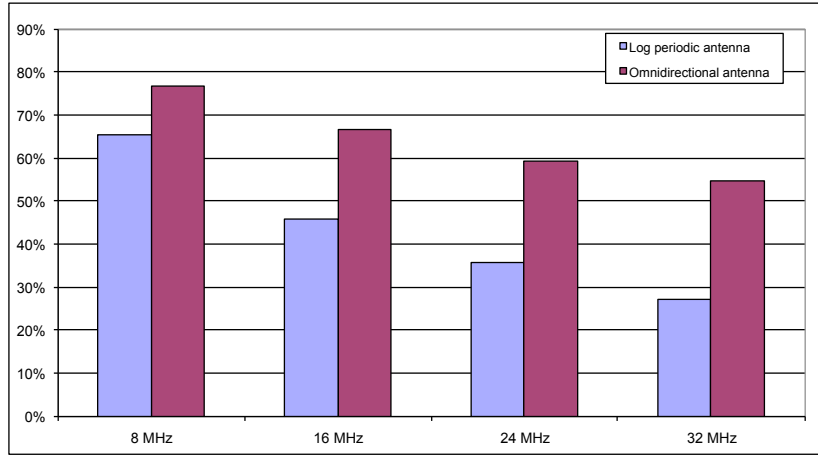


Figure 2.16: Measured data: percentage of contiguous channels for different the two different instrument floor level (-80 dBm and -105 dBm).

Table 2.4: DOUBLE GREEN PERCENTAGE

Different field strength levels for DVB-T reference planning consigurations (dB μ V/m)	Different instrument threshold (dBm)	
	-80	-105
	≤ 34	20.08
≤ 48	38.89	34.19
≤ 56	46.15	38.89
≤ 60	50.43	41.88

In table 2.4, the percentage of channels where both geo-location database and sensing identify unoccupied channels (*double green*) is reported. With a detection threshold of -80 dBm any additional protection for the incumbent service is gained with respect to the geo-location alone approach (compare with table 2.2) whereas adopting a detection threshold of -105 dBm the total amount of white space potentially available decreases. As expected, the smaller percentage of *double green* channels is related to higher protection of the DVB-T service and to more stringent values for the sensing threshold

Chapter 3

White Space Device Emission Limits

The prevailing consensus among stakeholders and regulators is that the only reliable way (at least in the short to medium term) to ensure that WSDs can use the spectrum efficiently, while incumbent DTT services are appropriately protected, is to allow WSDs to operate with assistance from TV white space databases (WSDBs).

The framework developed in the United Kingdom (UK), and being adopted more widely in Europe, is based on the premise that the impact of harmful interference on a DTT receiver is a strong function of the quality of the DTT coverage in the geographical area where the DTT receiver is located. The implication being that the regulatory emission limits for a database-assisted WSD can be significantly increased in areas where the DTT signal-to-noise-plus-interference ratio is high in the absence of WSDs; i.e., where the DTT coverage quality is good. This not only significantly improves the utility of the WSDs, but also removes the need for sensing and detection of very low-power DTT signals (as required by autonomous WSDs). A WSD would only need to report its location to the database and in return receive information with regards to the maximum emission levels with which it can radiate.

This European approach is considerably different from TV white space regulation in the US. FCC has specified the contours of the protected incumbent service areas directly, including safety margins which depend on WSD deployment and type. Outside of the protected contours, WSDs are immediately allowed to use the respective maximum allowed transmit power, which then also does not increase further away from the edge of the contour. Different fixed transmit power limits are defined depending on WSD antenna height and device type.

This chapter addresses the location specific maximum power approach. In particular, in section 3.1, all the information that a database needs to have in order to calculate the maximum permitted WSD EIRP are summarized. Then, the DTT location probability as a measure for quantifying the quality of DTT coverage is presented and the commonly used approach by which broadcasters calculate the DTT location probability, outlining its shortcomings, is described (section 3.1.1). A new approach which considerably improves on the accuracy of the estimated DTT location probability is presented and the performance of the new approach are illustrated by means of numerical examples.

In section 3.1.2 a novel and computationally efficient methodology for the calculation of the maximum permitted WSD EIRP is described. This algorithm is suitable for implementation in TV white space databases. The numerical results show that it provides accurate results in a wide range of DTT coverage conditions.

The operations that are undertaken by a white space database in order to specify location specific WSD emission limits are summarized in section 3.1.3. Furthermore the reference interference-victim geometries for protection of DTT channels are presented.

3.1 TV White Space Database for WSD Emission Levels

In order to afford appropriate levels of protection to the DTT service, it is necessary for the database to specify the maximum permitted WSD emission levels across all DTT channels and in all geographic locations where the DTT service is being used. To accomplish this, the database needs access to the following information:

1. The quality of national DTT coverage to within a suitable spatial resolution.
2. A suitable criterion (or metric) for quantifying and specifying a permitted level of interference to the DTT service.
3. Specified interferer-victim reference co-existence geometries for which the WSD regulatory emission limits would result in the aforementioned permitted level of interference.
4. Appropriate values of WSD-to-DTT protection ratios defined as a function of interferer-victim frequency separation and as a function of the received wanted DTT power at the victim DTT receiver.

5. A methodology for deriving appropriate and consistent WSD regulatory emission limits for simultaneous protection of multiple DTT channels.

Each of the above items have been examined in [45], and addressed the regulatory and standardization issues involved in the implementation of such TV white space databases. There it was introduced the idea of using the degradation in DTT location probability as a metric for assessing the impact of WSD interferers to the DTT service. A mathematical framework for calculating the maximum permitted WSD EIRP subject to a target degradation in location probability was presented, and an analytical (albeit approximate) solution for such a calculation was derived. The proposed solution was approximate, in the sense that it was based on an assumption which only applies in circumstances where DTT self-interference is small compared to the wanted DTT signal; i.e., in noise-limited DTT coverage. In the following, a new methodology which avoids the above assumption is proposed.

3.1.1 DTT Location Probability

The DTT location probability is defined as the probability with which a DTT receiver would operate correctly at a specific location; i.e., the probability with which the median wanted signal level is appropriately greater than a minimum required value. Location probability is widely used in the planning of DTT networks in order to quantify the quality of coverage, and in the UK is calculated for every 100 m x 100 m pixel across the country.

The presence of any interferer naturally results in a reduction of the DTT location probability. Such a reduction is therefore a highly suitable metric for specifying regulatory emission limits for WSDs operating in DTT frequencies.

There are in principle, two types of terrestrial digital broadcasting networks to be considered:

- Multi-Frequency Networks (MFN) which allow the same or different programmes to be carried by individual transmitters using different frequencies; and
- Single Frequency Networks (SFN) in which distributed emission is implemented whereby the required coverage is provided through the use of multiple transmitters operating on the same frequency and carrying the same programmes.

The type of network implemented will depend on the availability of frequencies, the type of coverage required, and the number of multiplexes to be provided and may depend on further national constraints or strategies.

The aim of SFNs is efficient utilization of the radio spectrum, allowing a higher number of radio and TV programs in comparison to traditional MFN transmission. General description of network topologies for SFNs and MFNs is given in [53] and in [54]. In section 3.3 a comparison between a MFN and a SFN deployment in terms of spectrum opportunities for WSDs is provided considering real DTT transmitters in different Italian scenarios.

In Europe, some countries, like UK, are working on MFN while other countries like Italy are employing SFNs across a national network. In the following section the definition of location probability for both MFN and SFN is provided.

3.1.1.1 Definition of location probability

Consider a pixel where the DTT location probability is in the absence of interference from systems other than DTT. Then, for a MFN it can be written (in linear domain):

$$q_1 = Pr \left\{ P_S \geq P_{S,min} + \sum_{k=1}^K r_{U,k} P_{U,k} \right\} \quad (3.1)$$

In a SFN several transmitters simultaneously send the same signal over the same frequency channel, so that it is necessary to sum the wanted signals. Then the location probability can be written as:

$$q_1 = Pr \left\{ \sum_{j=1}^J P_{S,j} \geq P_{S,min} + \sum_{k=1}^K r_{U,k} P_{U,k} \right\} \quad (3.2)$$

where $Pr\{A\}$ is the probability of event A, P_S is the received power of the wanted DTT signal, $P_{S,j}$ is the received power of the j^{th} wanted DTT signal that composes the SFN, $P_{S,min}$ is the DTT receiver's (noise-limited) reference sensitivity level¹, $P_{U,k}$ is the received power of the k^{th} unwanted DTT signal, and $r_{U,k}$ is the DTT-to-DTT protection ratio (co- and adjacent-channel) for the k^{th} DTT interferer. Equation 3.1 and 3.2 are direct results of the definition of protection ratio; i.e., the minimum ratio of wanted signal power to interferer signal power (as measured at the input to the receiver) required for the correct operation of the receiver.

¹The reference sensitivity level of a receiver is the minimum wanted signal power for which the receiver can operate correctly in a noise-limited environment.

In the planning of DTT networks, $P_{S(dBm)}$ and each of the individual terms $P_{S,j(dBm)}$ and $P_{U,k(dBm)}$ are modelled as real Gaussian random variables. Note that in 3.1 and 3.2, the powers are summed in the linear domain. For this reason, the most accurate way of calculating the probability q_1 is to use Monte Carlo simulations, whereby a large number of trials are performed with values for each variable in 3.1 and 3.2 generated according to their log-normal distributions. The probability q_1 can then be calculated by counting the proportion of trials in which the inequalities in 3.1 and in 3.2 are satisfied. A key benefit of Monte Carlo analysis is that it avoids the need for any assumptions with regards to the statistical distribution of the various power sums. In practice, however, undertaking large numbers of Monte Carlo trials for each pixel over large geographic areas is computationally demanding. It is for this reason that analytical and numerical (albeit approximate) solutions for the calculation of location probability are preferred. In what follows, two approaches are presented for the calculation of q_1 . The first approach is commonly used by broadcasters in the planning of DTT networks. The second approach is a new technique proposed in [10].

3.1.1.2 Common approach for calculation of location probability

In order to predict the location probability, it is necessary to estimate the mean values and standard deviations of the power of the wanted and of the unwanted signals. The common approach for the calculation of DTT location probability can be described as three steps:

1. The term $P_{S(dBm)}$ and each of the individual terms $P_{S,j(dBm)}$ are modelled as Gaussian random variable, with median m_S and $m_{S,j}$ and standard deviation σ_S . The value of σ_S is typically assumed to be 5.5 dB in every pixel.

When considering the coverage of a single-frequency network the signals contributing to the wanted input have to be determined and summed. Different algorithms are deployed [55] for carrying out summations of log-normally distributed random variables. Some of the methods commonly applied in network planning are described in [54]. In this context the commonly used methods are k-LNM method and Schwartz-Yeh algorithm. The Schwartz-Yeh algorithm is a computationally efficient technique for the evaluation of the median and standard deviation of the sum of log-normal random variables. Details can be found in Annex B.1. In this work, k-LNM method for the summation of

$P_{S,j(dBm)}$ terms has been applied. It is an approximation method for the statistical computation of the sum distribution of several log-normally distributed variables. The method is based on the assumption that the resulting sum distribution is also log-normal. In Annex B.2 detailed descriptions including formulas can be found. From equation 3.2 q_1 results:

$$q_1 = Pr \left\{ P_S \geq P_{S,min} + \sum_{k=1}^K r_{U,k} P_{U,k} \right\} \quad (3.3)$$

2. Also in the case of the power sum of the unwanted DTT signals, the assumption that the sum of a large number of log-normal random variables is log-normal is considered, from equations 3.1 and 3.3 the expression of the location probability can be written as:

$$\begin{aligned} q_1 &= Pr \{ P_S \geq P_{S,min} + P_V \} \\ &= Pr \{ P_S \geq U \} \end{aligned} \quad (3.4)$$

The power sum $P_{V(dBm)}$ is also modelled as a Gaussian random variable with median, m_V , and standard deviation σ_V , whose values are derived again via numerical techniques such as the Schwartz-Yeh algorithm or k-LNM method [56, 57, 54].

3. The term $U_{(dBm)}$ is approximated as a Gaussian random variable with median, m_U , and standard deviation σ_U . These values are derived via a final application of numerical techniques such as the Schwartz-Yeh algorithm, whereby the deterministic variable $P_{S,min}$ is simply treated as a Gaussian random variable with a 0 dB standard deviation. The relationship between the variables q_1 , $P_{S(dBm)}$ and $U_{(dBm)}$ in a specific pixel is illustrated in figure 3.1 below. From Equation 3.4, and based on the results of the above three steps, the location probability can be expressed in closed form as:

$$q_1 = 1 - \frac{1}{2} \operatorname{erfc} \left\{ \frac{1}{\sqrt{2}} \frac{m_S - m_U}{\sqrt{\sigma_S^2 + \sigma_U^2}} \right\} \quad (3.5)$$

It should, however, be noted that step 3 above involves an approximation based on the premise that the sum of a log-normal random variable and a

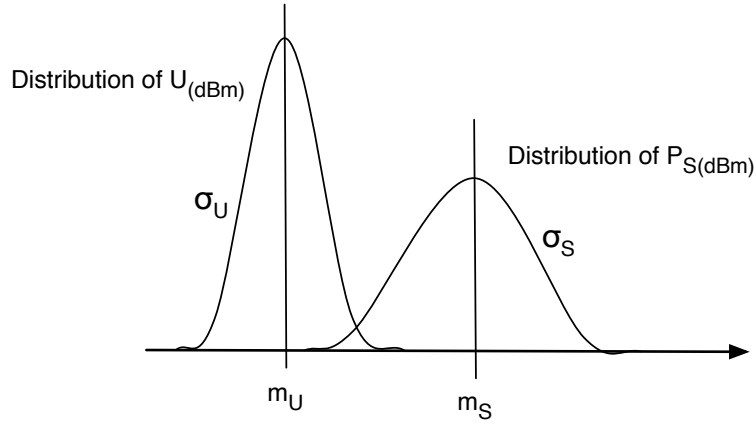


Figure 3.1: Distributions of wanted DTT power and the right-hand-side of the inequality in equation 3.4, as commonly modelled in DTT planning.

deterministic variable is also a log-normal random variable. This assumption is not strictly correct. In Annex C a demonstration of this is provided. In the next it is described a new approach whereby the approximation in step 3 can be avoided.

3.1.1.3 A new approach for derivation of q_1

In [10], equation 3.4 is reformulated in such a way so as to avoid the summation of a deterministic variable and a stochastic random variable. Specifically, q_1 can be written as:

$$\begin{aligned}
 q_1 &= Pr \left\{ 1 \geq \frac{P_{S,min}}{P_S} + \frac{P_V}{P_S} \right\} \\
 &= Pr \{ 1 \geq A + B \} \\
 &= Pr \{ 1 \geq X \}
 \end{aligned} \tag{3.6}$$

Where A_{dBm} and B_{dBm} are Gaussian random variables (on account of the fact that A and B are ratios involving log-normal random variables and a deterministic variable).

Note that the terms A_{dBm} and B_{dBm} are correlated. This is an added complication in comparison with the commonly used approach of section 3.1.1.2, where the log-normal variables were uncorrelated. The relevant correlation coefficient can be readily calculated as follows:

$$\begin{aligned}\rho_{A,B} &= \frac{\text{cov}(A_{dB}, B_{dB})}{\sqrt{\text{var}(A_{dB})\text{var}(B_{dB})}} \\ &= \frac{\sigma_S}{\sqrt{\sigma_S^2 + \sigma_V^2}}\end{aligned}\quad (3.7)$$

In detailed calculation of 3.7 can be found in Annex D

The term $X_{(dB)}$ can then be modelled as a Gaussian random variable, with its median and standard deviation m_X and σ_X derived via the Schwartz-Yeh algorithm for the sum of the two log-normal random variables A and B with correlation, $\rho_{A,B}$. Equation 3.6 can be rewritten as:

$$q_1 = Pr \{0 \geq X_{(dB)}\} \quad (3.8)$$

so the location probability can be readily expressed in closed form as:

$$q_1 = \frac{1}{2} \text{erfc} \left\{ \frac{1}{\sqrt{2}} \frac{m_X}{\sigma_X} \right\} \quad (3.9)$$

3.1.1.4 Numerical Results

In section 3.1.1.3 an approach for the calculation of the DTT location probability, q_1 , was presented. It is the common approach used in the planning of DTT network. This approach approximates the sum of a deterministic variable and a log-normal random variable as another log-normal random variable. Then a new approach was proposed whereby the above approximation is avoided. In the following, the performance of the proposed new approach for the calculation of DTT location probability, q_1 is examined. Results derived from Monte Carlo simulations (50,000 trials) as a benchmark for comparison is used. In this analysis, a range of DTT coverage conditions is examined, considering different levels of DTT self-interference in relation to the wanted DTT signal.

Figures 3.2 -3.5 illustrate the results of three approaches for the calculation of DTT location probability, q_1 under a range of DTT self-interference levels and characterised by the median m_V . The three approaches include:

1. Monte Carlo simulations;
2. the approximate numerical approach commonly used in DTT planning (equation 3.5);

3. the proposed new numerical approach (equation 3.9)

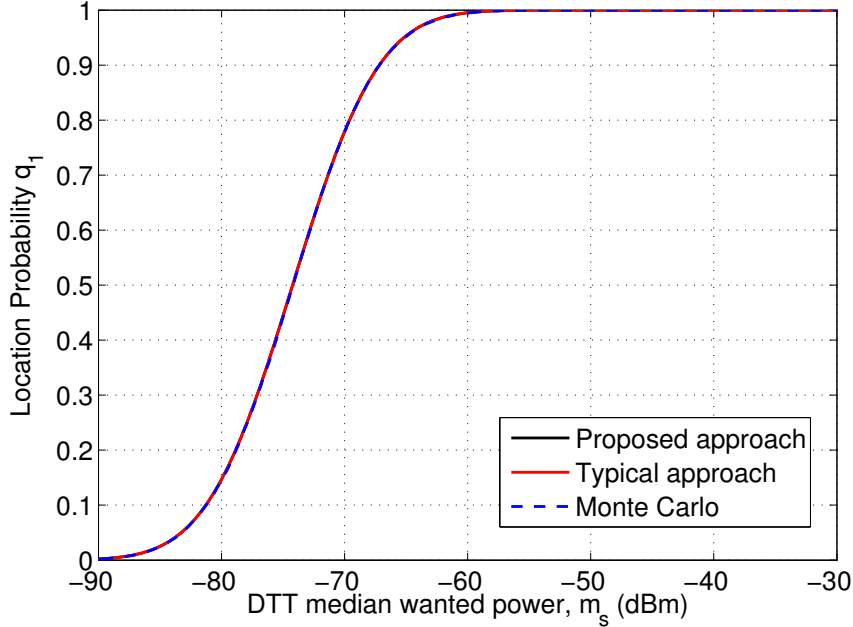


Figure 3.2: DTT location probability. Noise-limited environment.

Figure 3.2 is for the case where there is not DTT self-interference; i.e., where reception is purely noise-limited. As might be expected, in this instance the three approaches generate similar results, since $m_V = -\infty$.

However, figures 3.3, 3.4 and 3.5 indicate that as the DTT self-interference level increases from zero, the commonly used approach calculates location probabilities that can be as much as 10% to 15% lower those estimated via Monte Carlo simulations. The figures also show that the location probabilities calculated via the new approach are virtually indistinguishable from those estimated via Monte Carlo simulations.

The results suggest that, in order to more accurately characterize DTT networks, it might be prudent to account for the fact that the sum of the DTT receiver minimum sensitivity level, $P_{S,min}$, and the weighted sum of DTT interferer powers, P_V , is not strictly a log-normal random variable, as shown in Annex C.

3.1.2 Calculation of the Maximum Permitted WSD EIRP

In the previous section it is showed how the DTT location probability in a pixel can be calculated as a function of the medians and standard deviations of the received

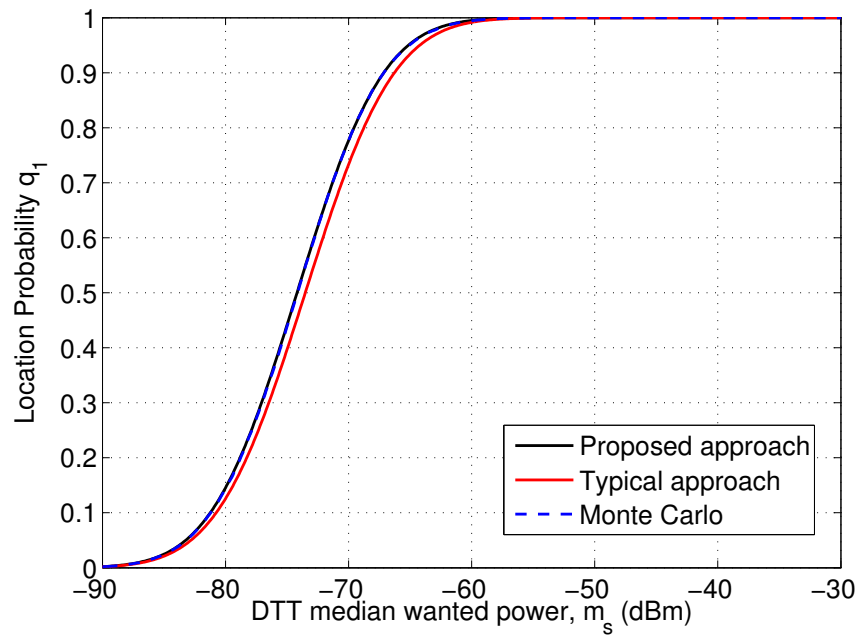


Figure 3.3: DTT location probability. $m_V = -96$ dBm, $\sigma_V = 3.2$ dB.

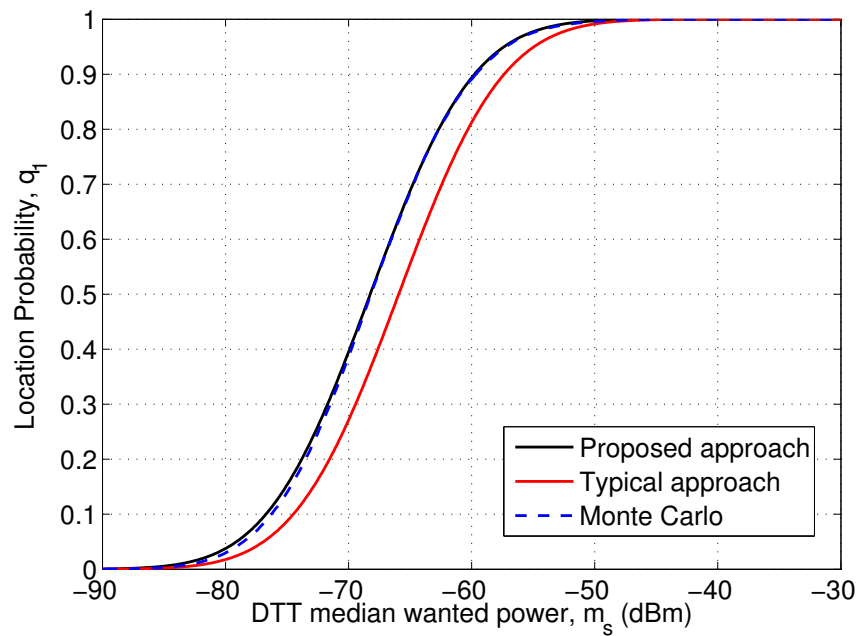


Figure 3.4: DTT location probability. $m_V = -70$ dBm, $\sigma_V = 4.9$ dB.

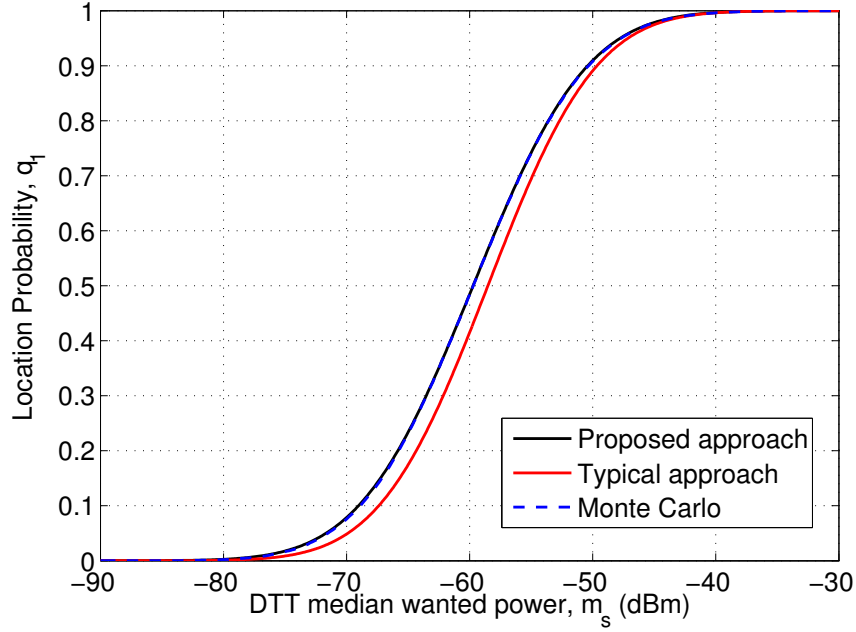


Figure 3.5: DTT location probability. $m_V = -60$ dBm, $\sigma_V = 5$ dB.

wanted DTT signal power and the received DTT interferer powers. In this section two approaches for the calculation of the maximum permitted WSD in-block EIRP in a given pixel, subject to a specified reduction (degradation), Δq , in the DTT location probability, q_1 , are investigated.

3.1.2.1 Problem formulation

Consider a WSD which operates at a carrier frequency $f_{WSD} = f_{DTT} + \Delta f$, where f_{DTT} is the DTT carrier frequency. For the special case of co-channel operation with DTT, $\Delta f = 0$. Let also assume that the WSD radiates with an in-block²EIRP of P_{IB} over a channel bandwidth of 8 MHz. As stated in [45], the maximum permitted WSD out-of-block EIRP level is given (in logarithmic domain) as:

$$P_{OOB(dBm)}(\Delta f) = P_{IB(dBm)} - ACLR_{WSD}(\Delta f)_{(dB)} \quad (3.10)$$

Where $ACLR_{WSD}$ is the adjacent-channel leakage ratio ACLR of the WSD [17].

As explained in [45], the presence of the WSD interferer will inevitably reduce the DTT location probability from q_1 to $q_2 = q_1 - \Delta q$.

²Emissions corresponding to those segments of a radiated signal's frequency spectrum which carry information intended for a receiver. The width of the in-block segment of the frequency spectrum is the nominal bandwidth of the signal.

Assuming a coupling gain, G , between the WSD and the DTT receiver, the (co- and adjacent-channel) WSD interferer power at the DTT receiver is given by the product GP_{IB} . Following the framework described in equation 3.4, q_2 can be written (again in the linear domain):

$$q_2 = Pr \left\{ P_S \geq P_{S,min} + \sum_{k=1}^K r_{U,k} P_{U,k} + r(\Delta f, m_S) GP_{IB} \right\} \quad (3.11)$$

The coupling gain includes path loss, receiver antenna gain, as well as receiver antenna angular and polarization discriminations. The coupling gain, $G_{(dB)}$ is typically modelled as a Gaussian random variable with a median value, m_G , and a standard deviation σ_G (see section 3.1.3).

The protection ratio $r(\Delta f, m_S)$ is defined as the ratio of the received wanted DTT signal power to the received WSD interferer power at the point of failure of the DTT receiver. The protection ratio is a function of the spectral leakage of the WSD signal into the adjacent DTT channel, as well as the adjacent-channel selectivity (ACS) of the DTT receiver. The ACS characterizes the overall behaviour of the receiver in response to the adjacent channel interferer, and captures effects ranging from frequency discrimination (i.e., various stages of filtering) to receiver susceptibility to the interferer's signal structure (e.g., inability of gain control to respond to large interferer power fluctuations). The protection ratio broadly decreases with increasing frequency separation, Δf , between the WSD and DTT signals. Following the framework adopted in recent co-existence studies involving 4G mobile networks and DTT [58, 59], in this analysis the protection ratio is modelled as a function of the received median wanted DTT signal power as well. This dependence implicitly characterizes the non-linear behaviour (including hard overload) of the DTT receiver.

In equation 3.11 the presence of a single WSD interferer is considered. In practice if multiple device operates, interference aggregation can occur. To account the proliferation of WSDs and an increase in the potential for aggregate interference from multiple WSDs to DTT services, an interference safety margin has to be set [45, 17].

In what follows, two approaches for the calculation of the maximum permitted WSD EIRP, P_{IB} subject to a given degradation, Δq , in DTT location probability in the geographic vicinity of the WSD are outlined.

Table 3.1: MONTE CARLO SIMULATIONS FOR THE CALCULATIONS OF THE MAXIMUM PERMITTED WSD EIRP

Initialize: Set the target location probability to q_T

1. Select an initial value, P , for P_{IB} .
2. In each Monte Carlo trial generate a realisation of the log-normal random variables in 3.11.
3. Use L Monte Carlo trials to calculate the DTT location probability q , by counting the number of trials for which the inequality in 3.11 is satisfied.
4. If q is suitably close to q_T , then STOP, otherwise appropriately increment/decrement P and go to (2).

Terminate: The maximum permitted WSD EIRP, P_{IB} , is the value of P when the loop is existed at step (4).

3.1.2.2 Monte Carlo simulations

As explained for the case of q_1 in 3.1 and 3.2, the location probability q_2 can be calculated as a function of P_{IB} via Monte Carlo simulations. Specifically, the maximum permitted WSD EIRP can be derived as outlined in 3.1.

3.1.2.3 New approach

While the Monte Carlo approach avoids the need for any assumptions with regards to the statistical distribution of various power sums, it can be computationally prohibitive when performed for each pixel over large geographical areas. It is for this reason that analytical and numerical (albeit approximate) solutions are preferred. An analytical expression for the calculation of the maximum permitted WSD in-block EIRP was derived in [45, 60]. [45] was based on an approximation³ that is accurate only in noise-limited environments; i.e., where $P_S \gg U$. In [10] a new approach for the evaluation of the maximum permitted WSD EIRP is proposed. This approach applies in both noise-limited and interference-limited environments; i.e., whether the received DTT self-interference is small or large in comparison with

³Specifically, the assumption was that the term $P_S - U$ is log-normally distributed. This is not strictly correct, since $P_S - U$ can take on negative values.

the DTT wanted signal.

By expanding 3.11, q_2 is:

$$\begin{aligned}
q_2 &= Pr \left\{ P_S \geq P_{S,min} + \sum_{k=1}^K r_{U,k} P_{U,k} + r(\Delta f, m_S) G P_{IB} \right\} & (3.12) \\
&= Pr \{ P_S \geq P_{S,min} + P_V + r(\Delta f, m_S) G P_{IB} \} \\
&= Pr \left\{ 1 \geq \frac{P_{S,min}}{P_S} + \frac{P_V + r(\Delta f, m_S) G P_{IB}}{P_S} \right\} \\
&= Pr \left\{ 1 \geq A + \frac{P_V + C}{P_S} \right\} \\
&= Pr \left\{ 1 \geq A + \frac{D}{P_S} \right\} \\
&= Pr \{ 1 \geq A + E \} \\
&= Pr \{ 1 \geq Y \} \\
&= Pr \{ 0 \geq Y_{(dBm)} \}
\end{aligned}$$

The term $C_{(dBm)}$ is a Gaussian random variable with median and standard deviation:

$$\begin{aligned}
m_C &= r(\Delta, m_S)_{(dB)} + m_G + P_{IB(dBm)} & (3.13) \\
\sigma_C &= \sigma_G
\end{aligned}$$

Since P_V and C are uncorrelated log-normal random variables, $D_{(dBm)}$ can be modelled as a Gaussian random variable, whose median, m_D , and standard deviation, σ_D , can be calculated via the Schwartz-Yeh algorithm. Furthermore, since D and P_S are both log-normal random variables, it follows that $E_{(dBm)}$ is also Gaussian, with median and standard deviation:

$$\begin{aligned}
m_E &= m_D - m_S & (3.14) \\
\sigma_E &= \sqrt{\sigma_D^2 + \sigma_S^2}
\end{aligned}$$

Finally, since A and E are log-normal random variables, $Y_{(dBm)}$ can be modelled as a Gaussian random variable, whose median, m_Y , and standard deviation, σ_Y , can be calculated via the Schwartz-Yeh algorithm. Note that $A_{(dBm)}$ and $B_{(dBm)}$ are correlated, with correlation coefficient:

Table 3.2: NEW METHODOLOGY FOR THE CALCULATION OF THE MAXIMUM PERMITTED WSD EIRP

<p><u>Initialize</u>: Set the target location probability to q_T</p> <ol style="list-style-type: none"> 1. Select an initial value, P, for P_{IB}. 2. Use Schwartz-Yeh to derive $m_{Y_{dBm}}$ and $\sigma_{Y_{dB}}$. 3. Use the <i>erfc</i> expression in 3.16 to calculate the DTT location probability q. 4. If q is suitably close to q_T, then <u>STOP</u>, otherwise appropriately increment/decrement P and go to (2). <p><u>Terminate</u>: The maximum permitted WSD EIRP, P_{IB}, is the value of P when the loop is existed at step (4).</p>

$$\begin{aligned}\rho_{A,E} &= \frac{\text{cov}(A_{dB}, E_{dB})}{\sqrt{\text{var}(A_{(dB)})\text{var}(E_{(dB)})}} \\ &= \frac{\sigma_S}{\sqrt{\sigma_S^2 + \sigma_D^2}}\end{aligned}\quad (3.15)$$

and this must be used within the Schwartz-Yeh algorithm. Having calculated m_Y and σ_Y , it follows from 3.12 that:

$$q_2 = \frac{1}{2} \text{erfc} \left\{ \frac{1}{\sqrt{2}} \frac{m_Y}{\sigma_Y} \right\} \quad (3.16)$$

However, note that the random variable Y is itself a function of P_{IB} (the unknown). For this reason, an iterative algorithm to calculate P_{IB} is adopted. This is outlined in table 3.2.

3.1.3 Database Calculations

To place the materials of sections 3.1.1 and 3.1.2 into context, in this section the type of calculations which a white space database must perform in order to specify location-specific WSD regulatory emission limits for the simultaneous protection of all relevant DTT channels are summarized. Specifically, for a WSD operating in

a specific channel and in a given geographic pixel, the database must examine all relevant co-channel and adjacent-channel interference scenarios with respect to the victim DTT channels. Each WSD-to-DTT frequency separation, Δf , then results in specific maximum permitted WSD in-block EIRP level required for a permitted level of interference to the DTT service. The lowest EIRP level represents WSD regulatory emission limit for that specific channel and given pixel.

The following calculations apply in each pixel:

1. The white space database must be aware of the frequencies, median m_S and standard deviation σ_S of the received DTT signal power (in dBm), the median m_V and standard deviation σ_V of the DTT interferer powers (in dBm), as well as the resulting DTT location probability q_1 in each geographic pixel. The above variables can all be extracted from the national DTT network planning model (e.g. in UK the UK Planning Model is used [61]). In the absence of such a model, the above variables can be calculated explicitly based on the technical characteristics and locations of the DTT transmitters, and appropriate propagation models (e.g. ITU-R P.526 [51]) which use the information on terrain and clutter data. In 3.1.1 three approaches for calculating q_1 are described.
2. The white space database must then establish the median and standard deviation of the coupling gain, $G_{(dB)}$, between the WSD interferer and victim DTT receiver. This requires the use of appropriate propagation models and interferer-victim geometries. For victim DTT channels that are used by the DTT service in the same (or immediately adjacent) pixel as the WSD, the coupling gain must be based on a *reference* coexistence geometry (see section next section) that is deemed suitable in the context of protecting the DTT platform. Such a reference geometry is necessary because the precise spatial separation between the WSD and a victim DTT receiver within a given pixel (or in immediately adjacent pixels) cannot be known by the database. For victim DTT channels that are not used by the DTT service in the same (or immediately adjacent) pixel as the WSD, the coupling gain can be based on the actual spatial separation between the pixel where the WSD operates and the pixel where the DTT channel is used by the DTT service. Such scenario is termed *non-reference* geometry (see section next section).
3. The white space database must also assume a maximum permitted degrada-

tion, $\Delta q = q_1 - q_2$, in the DTT location probability of pixels where the DTT services are used. The permitted degradation can be different in different pixels. For example, it may be set according to the number of households in each pixel.

4. The white space database must assume appropriate WSD-to-DTT protection ratios, $r(\Delta f, m_S)$. These can be derived via laboratory measurements of WSD and DTT equipment.
5. Finally, with the above variables evaluated, the database can readily compute the maximum permitted WSD in-block EIRPs as described in section 3.1.2.

Figure 3.6 shows the logical architecture of calculations that the database has to perform in order to calculate the maximum permitted WSD EIRP for each pixel considering the methodology described in table 3.2.

3.1.3.1 Interferer-victim geometries

In order to evaluate the impact of interference from WSDs to DTT receivers, the co-existence geometries need to be defined. Different national regulatory authorities may use different reference and non-reference geometries in the context of co-existence between WSD and DTT services. For example, in one country only the protection of fixed roof-top DTT reception might be considered, whereas in another country DTT reception with set-top aerial might be protected. Reference and non-reference geometries have been introduced in [17, 45].

In this work a reference and a non-reference interferer-victim geometries are examined. These geometries will be considered for numerical examples in section 3.2.

Reference geometries have been introduced to take into account that WSDBs can only account for the locations of victim TV aerials within a spatial resolution of a pixel. This means that it is not possible to know with any degree of certainty, whether or not a victim TV aerial exists in the close proximity of a WSD interferer. Specifically, reference geometries are helpful in cases where the interferer and victim are deemed to be located within the same pixel (or in immediately adjacent pixels). Reference geometries tend to over-estimate the extent of interference.

Non-reference geometries are used to characterise interference where the interferer and victim are multiple pixels apart, and the limited spatial resolution of the information on TV aerial locations is less important.

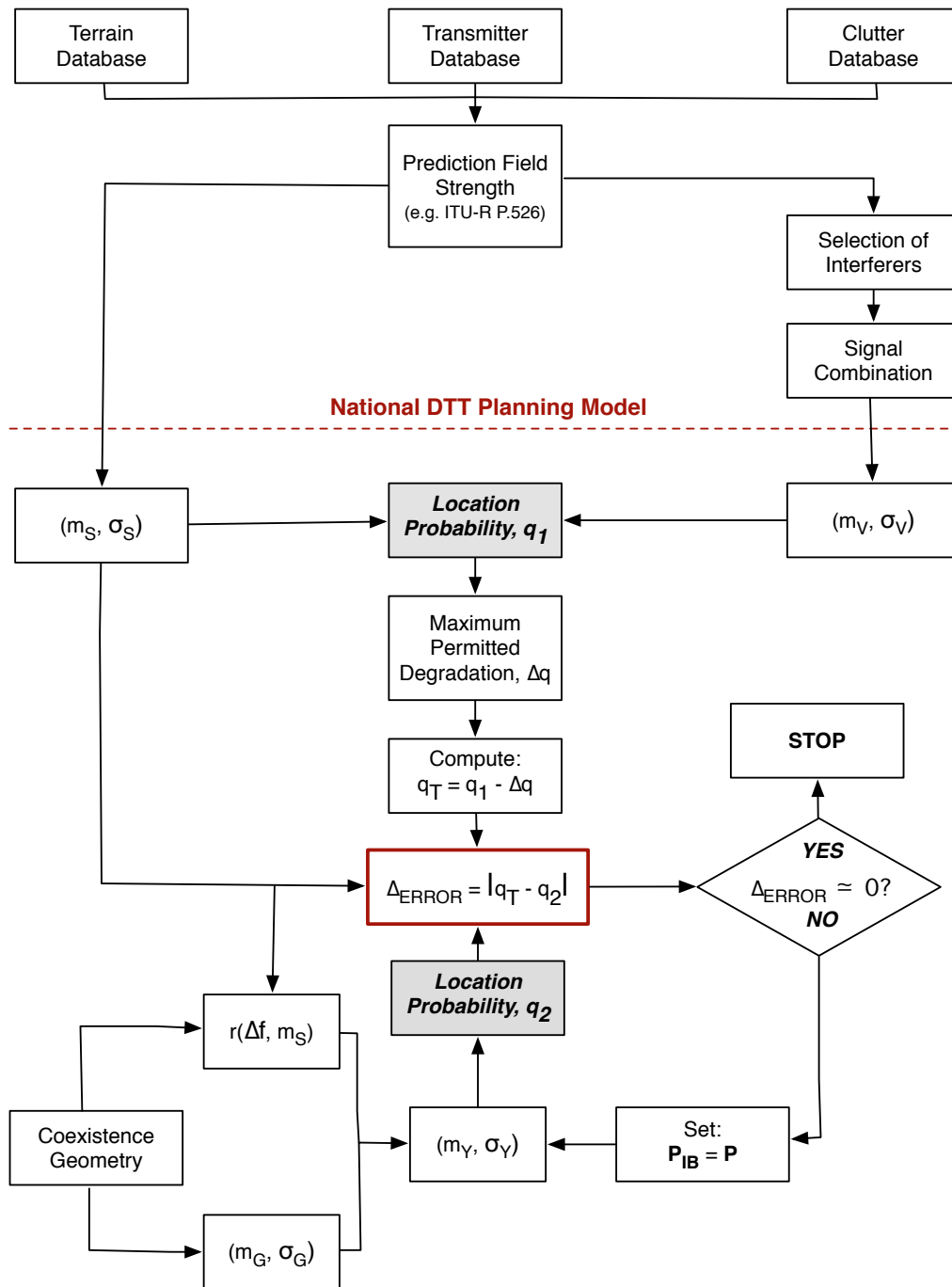


Figure 3.6: Logical architecture of database calculations.

Figure 3.7 illustrates the difference between reference and non-reference geometry.

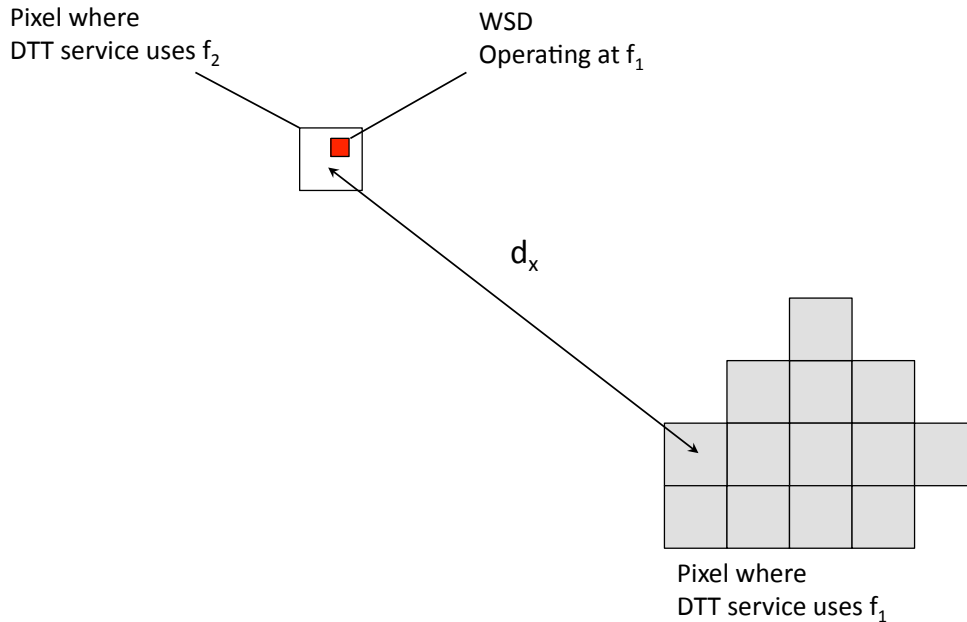


Figure 3.7: Reference and non-reference geometries. Interference from the WSD (radiating at f_1) to DTT reception at f_2 will be quantified via reference geometry (WSD and TV aerial in the same pixel). Interference from WSD (radiating at f_1) to DTT reception at f_1 will be quantified via non-reference geometries.

Interference from the WSD (radiating at f_1) to DTT reception at f_2 will be quantified via reference geometry (WSD and TV aerial in the same pixel). Interference from WSD (radiating at f_1) to DTT reception at f_1 will be quantified via non-reference geometry.

It is assumed that the WSD interferer is not allowed to operate at the same frequency of DTT service. This assumption has been made because WSDs are operating inside of a DTT coverage area, where the extremely high interference potential of co-channel usage, would lead to very low permitted power levels, P_{IB} , not useful for a real transmission. Different national regulatory authorities may use different reference and non-reference geometries in the context of co-existence between WSDs and DTT services both within the same pixel, or in immediately adjacent pixels and in some pixels apart. In the following, statistics of coupling gains between white space devices and TV receivers for both reference and non-reference geometries are presented.

3.1.3.2 Statistics of coupling gains between white space devices and TV receivers within a pixel

Reference geometries are considered in circumstances where the WSD interferer and TV aerial are deemed to be within the same (or immediately adjacent) pixels.

Figure 3.8, depicts the reference geometry that has been considered in this framework. This geometry is proposed in [10]. It is representative of scenarios where a fixed outdoor WSD and the victim DTT receiver are located on opposite sides of the road (a nominal 20 m separation), with the WSD located along the azimuth bore-sight of the DTT receiver's antenna. The assumed horizontal polarisation of the DTT receiver antenna would provide a 16 dB polarization with respect to vertically polarized fixed-WSD transmitter antenna and a DTT antenna angular discrimination of 0 dB. Both WSD and TV antennas are at a height of 10 m. It is assumed a net TV aerial gain of 9.15 dBi ⁴ and a free-space path-loss. The free-space path gain is given by:

$$G_{FS}(d) = \frac{\lambda^2}{(4\pi d)^2} = \frac{c^2}{(4\pi df)^2} \quad (3.17)$$

or in dB :

$$\begin{aligned} G_{FS}(d) &= 147.56 - 20 \log(f) - 20 \log(d) \\ &= 121.54 - 20 \log(f) \end{aligned}$$

Where f is the frequency in Hz, λ is the wavelength in metres, c is the speed of the light in m/s, and d the interferer-victim separation in metres. Note that "log" indicates common (base 10) logarithm.

The reference geometry defines a possible coupling geometry between the WSD and a DTT receiver and ideally takes into account the closest separation possible upon the type of WSD to guarantee that interference to the DTT receiver will not occur. Then, the coupling gain (in dB) from the WSD to the TV receiver can be calculated as:

$$G_{(dB)} = G_{P(dB)} + G_{A,TV(dB)} + g_{A,TV}(\alpha)_{(dB)} + g_{polar}(\alpha)_{(dB)} \quad (3.18)$$

Where

⁴This is equivalent to an aerial gain of 12 dBd and 5 dB cable loss.

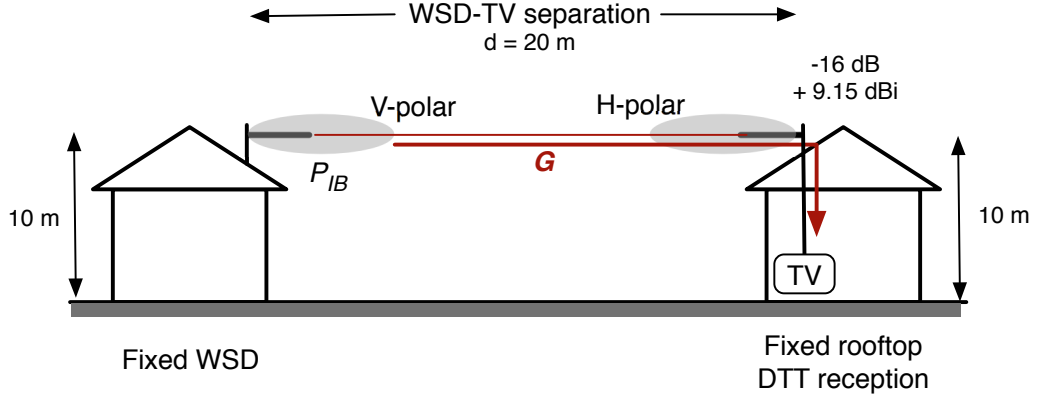


Figure 3.8: Reference geometry for fixed WSDs.

G_P is the propagation gain,

$G_{A,TV}$ is the TV aerial gain,

$g_{A,TV}(\alpha)$ is the TV aerial angular discrimination,

$g_{polar}(\alpha)$ is the TV aerial polarisation discrimination, and

α is the angle from the TV aerial bore-sight.

It has to be noted that for any given separation, the propagation gain is a log-normal random variable, i.e.,

$$G_{P(dB)} \sim N\left(m_{P(dB)}, \sigma_{P(dB)}^2\right) \quad (3.19)$$

Where

$m_{P(dB)}$ is the median path gain. In this scenario it corresponds to the free-space path gain given by 3.17

$\sigma_{P(dB)}$ is the log-normal standard deviation. In this work it is set at 3.5 dB.

3.1.3.3 Statistics of coupling gains between white space devices and TV receivers that are some pixels apart

Non-reference geometries are considered in circumstances where the WSD interferer operates outside of a DTT coverage area. Due to the great separation distance between WSD interferer and DTT receiver, a free-space path gain model might be

not suitable to characterize the terrestrial environment reliably. In this case a *dual slope* model has been considered. A dual slope model is based on a two-ray model and takes into account the effect of ground reflection and the antenna heights above it.

Basically the model takes free-space loss of 20dB/decade up to a range of the breakpoint distance (defined by equation 3.21) and 40dB/decade there after. This model is very well suited for analyses involving line-of-sight scenarios.

A simplified closed-form algorithm for UHF frequency range, characterized by two slopes and a single breakpoint, has been considered. The approximate path gain in dB is given by:

$$G_{LoS}(d) = -G_{BP} - \begin{cases} 20 \log \left(\frac{d}{R_{BP}} \right), & \text{for } d \leq R_{BP} \\ 40 \log \left(\frac{d}{R_{BP}} \right), & \text{for } d > R_{BP} \end{cases} \quad (3.20)$$

Where R_{BP} is the breakpoint distance and is given by

$$R_{BP} \approx \frac{4h_{Tx}h_{Rx}}{\lambda} \quad (3.21)$$

where λ is the wavelength in metres. h_{Tx} and h_{Rx} are respectively the transmitter and receiver antenna heights and correspond to interferer WSD device and the victim DTT receiver antenna heights. Assuming both WSD and DTT receiver antennas at a height of 10 m, for UHF frequencies, the breakpoint distance results at about 90 metres.

G_{BP} is a value for the basic transmission loss at the break point, defined as:

$$G_{BP} = \left| 20 \log \left(\frac{\lambda^2}{16\pi h_{Tx}h_{Rx}} \right) \right| \quad (3.22)$$

Figure 3.9 represents free-space path gain and two-ray path gain.

Figure 3.10 below shows the geometry of two-ray propagation. It is representative of scenarios where a fixed outdoor WSD and the victim DTT receiver are located some pixel apart (at a distance of d metres), with the WSD located along the azimuth bore-sight of the DTT receiver's antenna. Also in this case, it is assumed an horizontal polarisation of the DTT receiver antenna that provides a 16 dB polarization with respect to vertically polarized fixed-WSD transmitter antenna and a DTT antenna angular discrimination of 0 dB. Both WSD and TV antennas are at a height of 10 m. It is assumed a net TV aerial gain of 9.15 dBi .

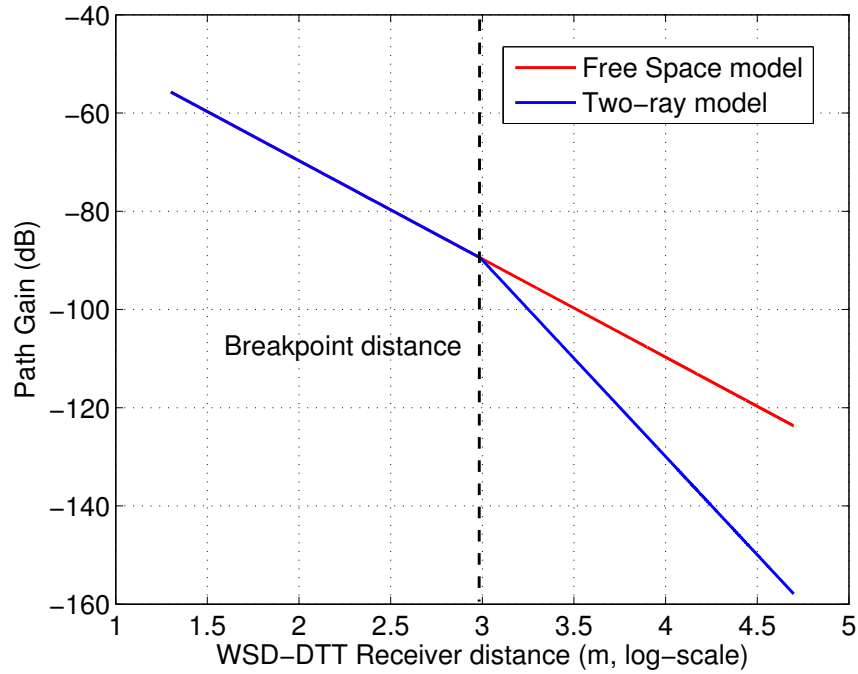


Figure 3.9: Free-space path gain for reference geometry and two-ray path gain for non-reference geometry.

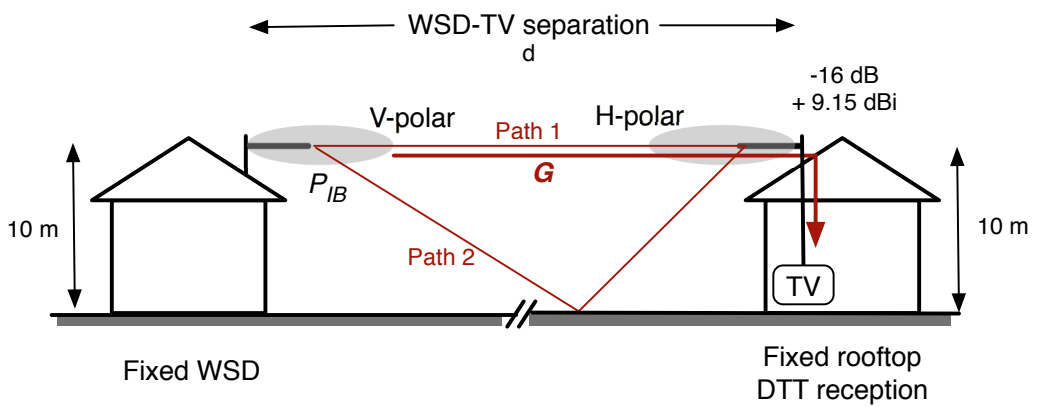


Figure 3.10: Non-reference geometry for fixed WSDs.

The coupling gain G in equation 3.18, is calculated using the actual distance from the WSD to the pixel under consideration, applying the two-ray propagation model. In non-reference geometry the median path gain in 3.19 corresponds to G_{LoS} .

3.1.4 Numerical Results of Maximum Permitted Emission Levels

In section 3.1.2.3 a novel methodology for the calculation of the maximum permitted WSD in-block EIRP, P_{IB} was presented. Firstly the various parameter values used in following calculations are summarized. Then the performance of the novel methodology for the derivation of maximum permitted WSD EIRP P_{IB} , are demonstrated, again using the results derived from Monte Carlo simulations (50,000 trials) as benchmark.

Table 3.3 summarizes the values of the various parameters used in the numerical examples of this section. The reference geometry illustrated in figure 3.8 has been considered.

Figures 3.11-3.14 illustrate the results of two approaches for the calculation of the maximum permitted WSD EIRP, P_{IB} , under a range of DTT self-interference levels, as characterised by the median m_V , and subject to 1% degradation in DTT location probability. The two approaches include:

1. Monte Carlo simulations;
2. the proposed new numerical approach (equation 3.12 and table 3.2).

Figure 3.11 is for the case where there is no DTT self-interference; i.e., where reception is purely noise-limited. As can be seen, the proposed approach calculates maximum permitted WSD EIRP values that are in broad agreement with those estimated via Monte Carlo simulations. Nevertheless, for certain values of median received wanted DTT signal power, m_S , the approaches can diverge by 2 to 3 dB. This is not particularly significant given the overall range of EIRP values, and is due to the fact that Monte Carlo simulations make no assumptions regarding the log-normality of the sum of log-normal random variables.

As might be expected, the maximum permitted WSD EIRP reduces with a reduction in received median received wanted DTT signal power, m_S , and location probability, q_1 . However, this trend is reversed at low values of m_S and q_1 , where the received WSD interference levels move to the upper long tail of log-normal distribution of the wanted DTT signal power, P_S .

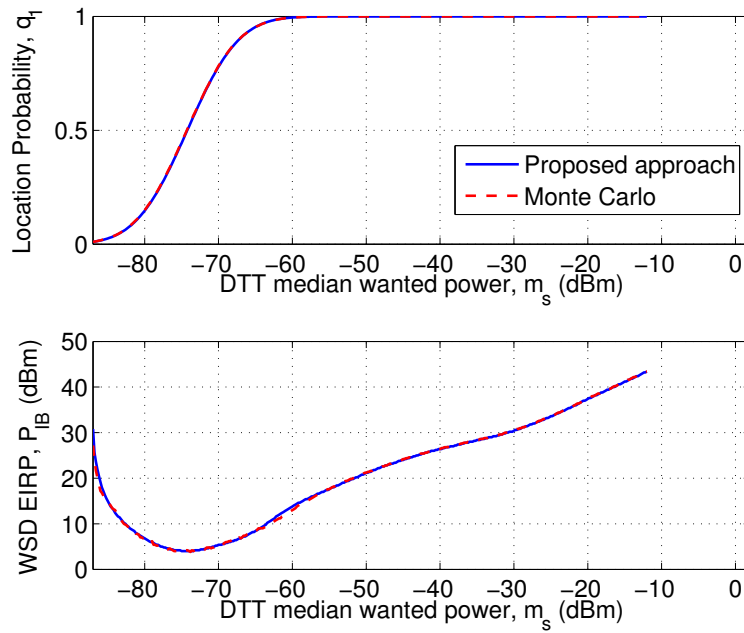


Figure 3.11: Maximum permitted WSD EIRP. Noise-limited DTT coverage. $m_V = -\infty$.

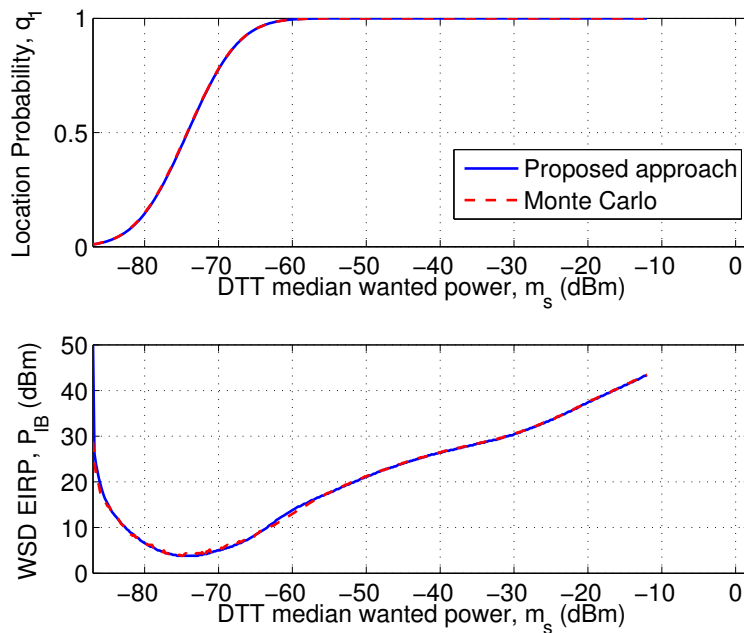


Figure 3.12: Maximum permitted WSD EIRP. Interference-limited DTT coverage, $m_V = -96$ dBm, $\sigma_V = 3.2$ dB.

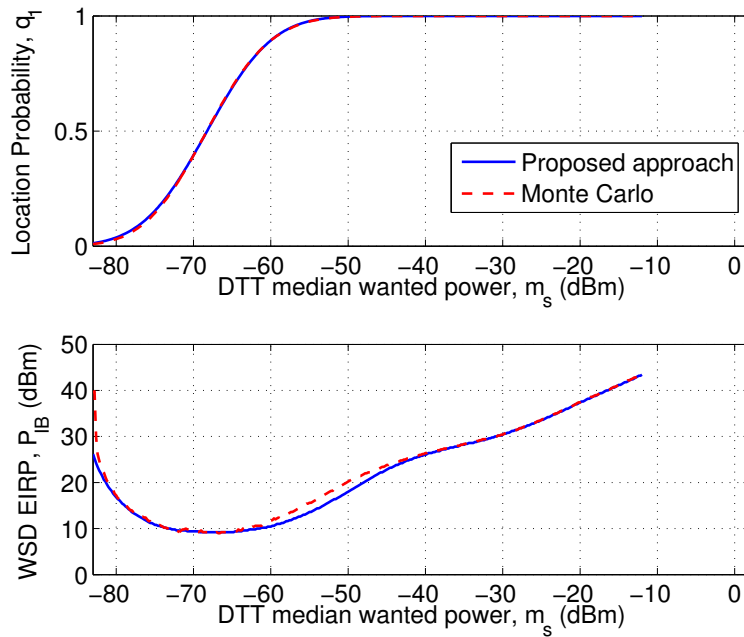


Figure 3.13: Maximum permitted WSD EIRP. Interference-limited DTT coverage, $m_V = -70$ dBm, $\sigma_V = 4.9$ dB.

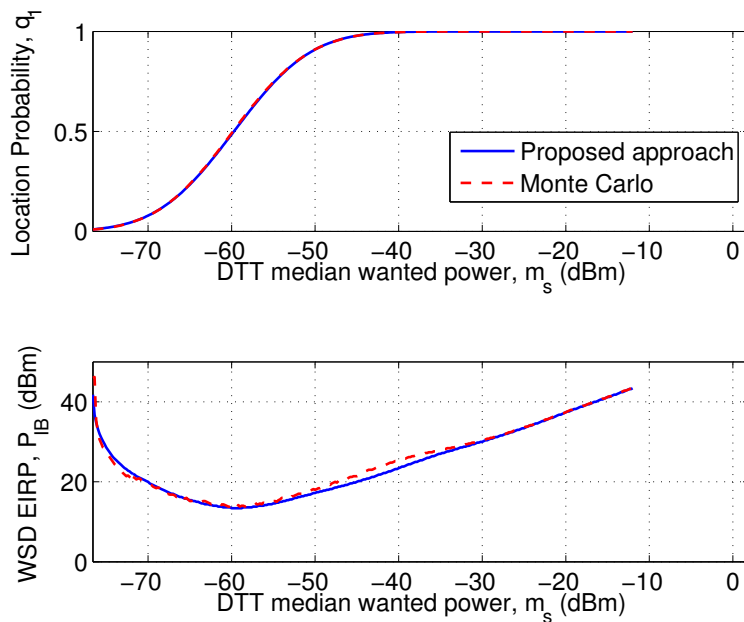


Figure 3.14: Maximum permitted WSD EIRP. Interference-limited DTT coverage, $m_V = -60$ dBm, $\sigma_V = 5$ dB.

To better understand the trend of P_{IB} curve, let consider the cumulative distribution of P_S and define the CDF in absence and in presence of the WSD interference as:

$$CDF_1 = 1 - q_1; \tag{3.23}$$

$$CDF_2 = 1 - q_2.$$

Figures 3.15-3.17 illustrate three different zones that can be identified. Assuming the system is operating in low DTT coverage (see figure 3.15), i.e. in the lower part of the cumulative distribution of P_S , where the derivative is low, a degradation of 1% leads to a maximum permitted WSD EIRP, P_x . Going towards greater values of P_S , where the derivative of the cumulative distribution of P_S increases, the maximum permitted WSD EIRP decreases respect to P_x , until the point where the derivative reaches the maximum value (see figure 3.16). In correspondence of this point the maximum permitted WSD EIRP reaches the minimum value. Moving towards the upper part of the cumulative distribution curve, the derivative starts to decrease and the maximum permitted WSD EIRP increases (see figure 3.17).

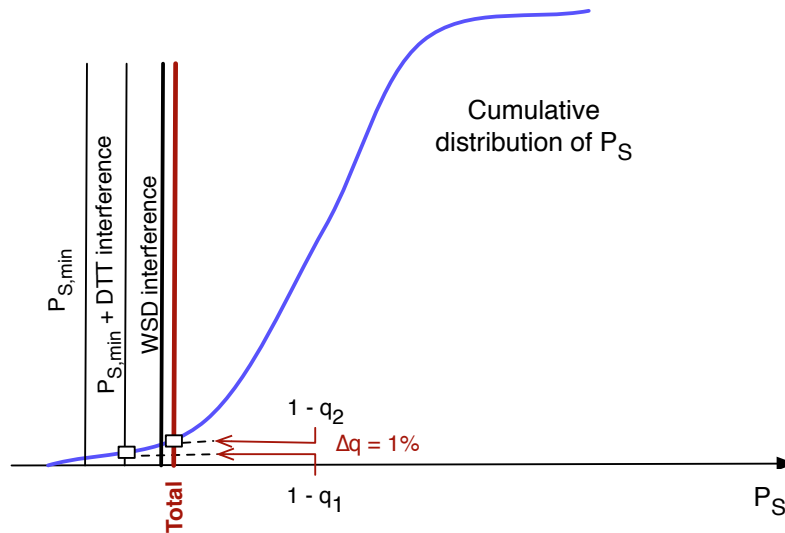


Figure 3.15: P_{IB} trend explanation. Low DTT coverage condition

It has to be noted that large increases in WSD interfering power may lead to saturation effects in the DTT receiver. To avoid this type of situation, a WSD EIRP limit must be set.

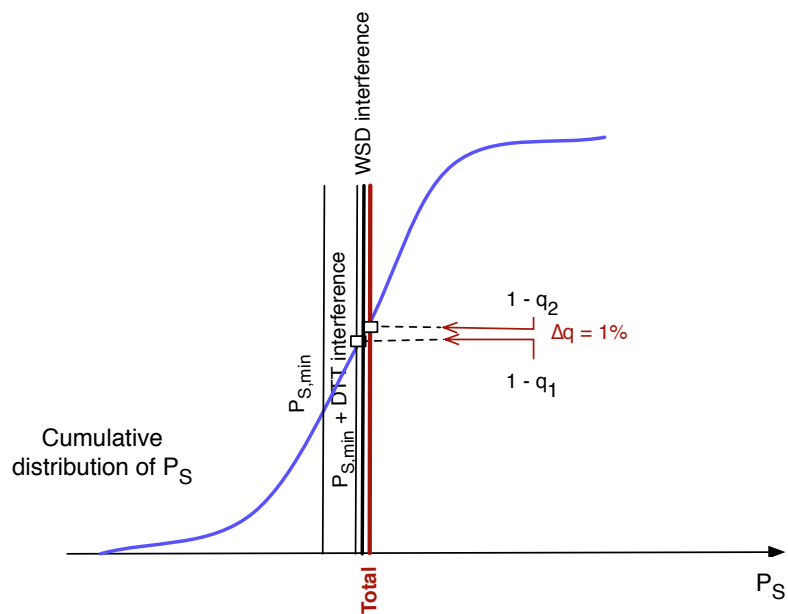


Figure 3.16: P_{IB} trend explanation. Mean DTT coverage condition.

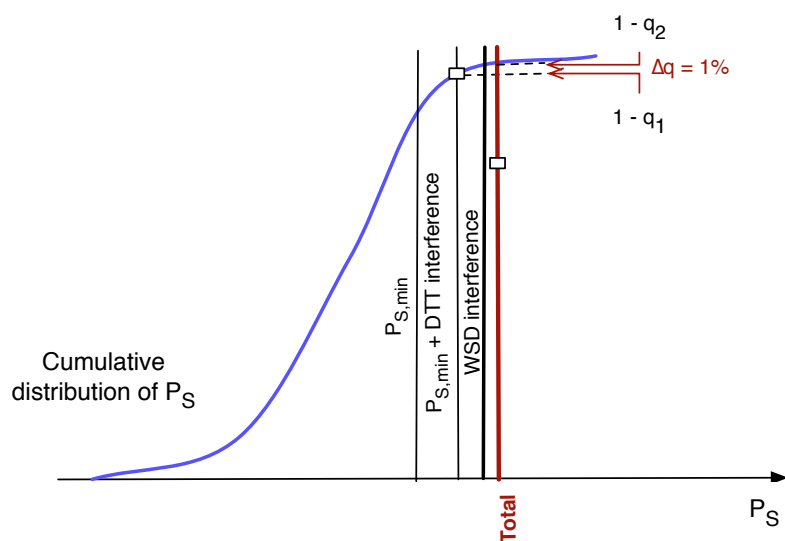


Figure 3.17: P_{IB} trend explanation. High DTT coverage condition.

Figures 3.12-3.14 show similar results for increasing levels of DTT self-interference, m_V . These confirm that the proposed new approach calculates the maximum permitted WSD EIRP with reasonable accuracy, at a fraction of the computational complexity of Monte Carlo simulations.

It has to be noted that for the considered scenarios, the DTT coverage area, i.e. pixels where the location probability is $\geq 70\%$, should admit only the operation of a WSD using frequencies adjacent to that of the DTT service in the area in question.

Table 3.3: PARAMETER VALUES USED IN THE NUMERICAL EXAMPLES OF THIS SECTION

$m_S, \sigma_S, m_V, \sigma_V$
The median and standard deviations of $P_{S,min}$ and $P_{V(dBm)}$. The values used correspond to those observed in the coverage area of a specific DTT transmitter in the UK ($\sigma_S = 5.5$ dB in all pixels). The location probability q_1 is calculated as described in section 3.1.1.3.
$\Delta q, \quad q_2 = q_1 - \Delta q$
Δq is the maximum permitted degradation in DTT location probability within a given pixel. The maximum permitted WSD in-block EIRP is the value which results in degradation Δq . For illustration, it is assumed to be $\Delta q = 0.01$.
f_{DTT}
The frequency of the DTT carrier. This is assumed to be 730 MHz (DTT channel 53).
Δf
The frequency offset between the WSD and DTT carriers. This is assumed to be 16 MHz.
$P_{S_{min}}$
The minimum required DTT wanted signal power at the input to DTT receiver (reference sensitivity level). This is assumed to be -74.2 dBm.
WSD-to-DTT adjacent channel protection ratios, $r(\Delta f, m_S)$
<p>Values derived from recent measurements of protection ratios performed in the UK have been used [62].</p> <p>Specifically, for $\Delta f = 16$ MHz it is assumed that</p> $r(\Delta f, m_S) = \{-32, -32, -28, -24, -19, -13, -10, -8\} \text{ dB for}$ $m_S = \{-80, -70, -60, -50, -40, -30, -20, -12\} \text{ dBm respectively}$ <p>The dependence of $r(\Delta f, m_S)$ on m_S implicitly models the non-linear behaviour for DTT receiver.</p> <p>For intermediate values of m_S, protection ratios are determined via linear interpolation. Furthermore, it is assumed that the protection ratios $r(\Delta f, m_S)$ increase by 1 dB for every 1 dB increase in m_S above - 12 dBm. This models a hard overload of the DTT receiver.</p>
Coupling gain, $G_{(dB)}$
From equation 3.17 and considering the WSD is operating at frequency $f_{WSD} = f_{DTT} + \Delta f$, the median path gain results to be - 55.9 dB. The considered reference geometry (see figure 3.8) defines the values of antenna angular discrimination and DTT antenna polar discrimination. Then, taking account of equation 3.18, the resulting median coupling gain m_G is then equal to - 62.75 dB. The coupling gain standard deviation σ_G is assumed to be 3.5 dB, for illustrative purposes.

3.2 Numerical Examples and Further Considerations on White Space Device Emission Limits

In this section the basic methodology to calculate the WSD maximum emission power described in section 3.1.2.3 is extended to other scenarios and further considerations are made. In particular, considerations supported by calculation examples are provided on:

- an analysis on different fixed values of location probability degradation, Δq (see section 3.2.1);
- an approach that considers the location probability degradation varying across the coverage area of the broadcasting service (see section 3.2.2);
- a co-channel analysis considering both a fixed value of location probability degradation, $\Delta q = 1\%$ (see section 3.2.3), and Δq varying across the coverage area (see section 3.2.4);
- an analysis on variation of DTT self-interference considering $\Delta q = 1\%$ (see section 3.2.5).

3.2.1 Analysis on different fixed values of location probability degradation, Δq

In order to understand the impact of variations in degradation of location probability on the maximum permitted WSD EIRP, different values of fixed location probability degradation are examined.

Reference scenario described in section 3.1.3.2 has been considered. The WSD-to-DTT adjacent channel protection ratios, $r(\Delta f, m_S)$, values are assumed to be the same summarized in table 3.3. A median path gain of - 55.9 dB and a median coupling gain, m_G , equal to -62.75 dB are used.

Figures 3.18 - 3.20 illustrate the results in terms of maximum permitted WSD EIRP under a range of DTT self-interference levels, as characterised by the median m_V . Each curve represents a different degradation in location probability. A loss in location probability of 0.1%, 0.5%, 1%, 2%, 3%, 4% is applied.

Figures indicate that if the admitted degradation is fairly high, i.e. 3%, a small increase in WSD EIRP leads to a degradation of 4%, while greater values of WSD

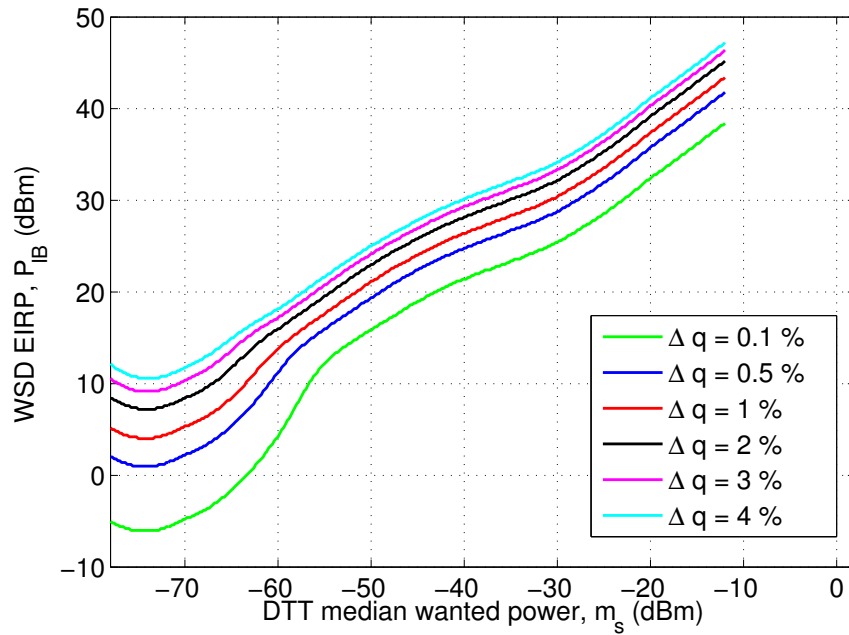


Figure 3.18: Maximum permitted WSD EIRP for different values of Δq . Noise-limited DTT coverage. $m_V = -\infty$.

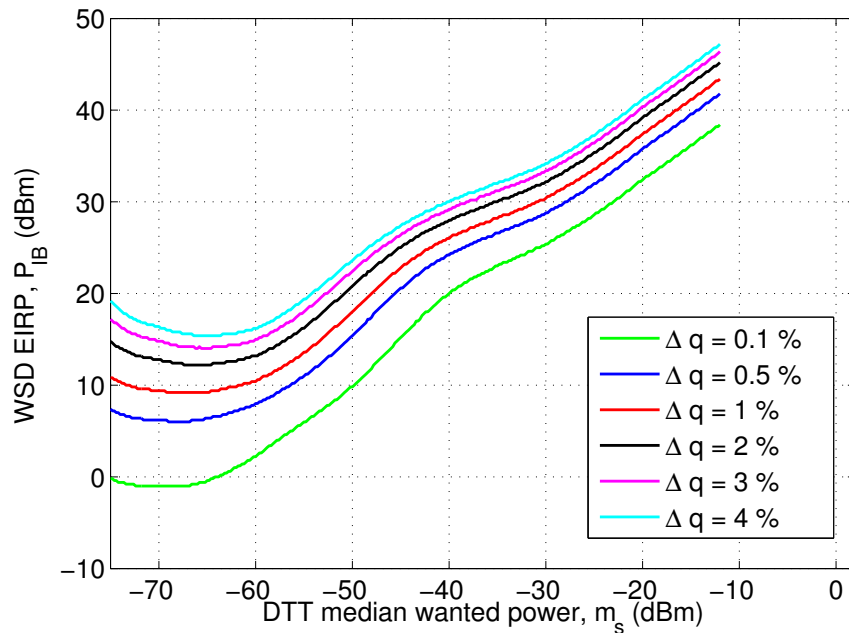


Figure 3.19: Maximum permitted WSD EIRP for different values of Δq . $m_V = -70$ dBm, $\sigma_V = 4.9$ dB.

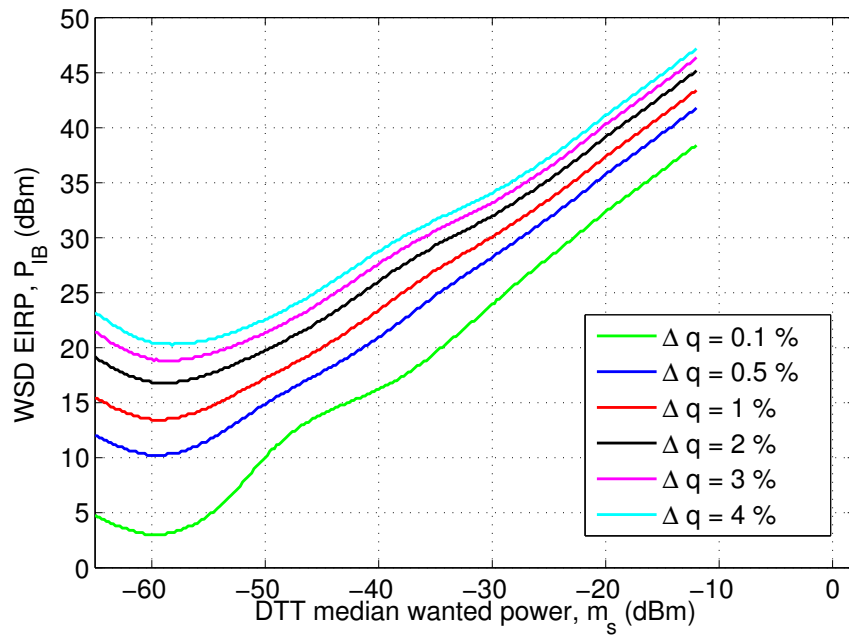


Figure 3.20: Maximum permitted WSD EIRP for different values of Δq . $m_V = -60$ dBm, $\sigma_V = 5$ dB.

EIRP are needed to pass from 1% of location probability degradation, to 2%. This is more evident for low values of median received wanted DTT signal power, m_S .

3.2.2 Analysis on Δq varying across the coverage area

Limiting the location probability degradation to a fixed value, i.e. 1%, everywhere in the coverage area of the DTT transmitter may have a twofold effect:

1. lead to an unacceptable degradation in DTT service in very well covered areas (e.g. close to DTT transmitter);
2. restrict the WSD transmission possibilities in areas where the location probability is low, i.e. approaching the DTT coverage edge.

As stated in section 3.1.1.1, the location probability defines the fraction of the unit area, known as a pixel, where the DTT service can be received. To point out the different impact of the same degradation in location probability on pixels with different quality of coverage, two pixels having a location probability of 99% and 70% respectively will be considered.

A fixed degradation for example of 1% leads to different consequences in the two pixels.

In the pixel where the location probability is 99%, the outage probability, which is the complement of the location probability, is 1%. Then a degradation of the location probability of 1% leads the outage probability to be 2%. This means that the percentage increase of the outage probability is 100%, i.e. the outage probability doubles.

The impact on the other pixel is less important in terms of outage probability. In fact in the case of location probability of 70% the outage probability is 30% and a location probability degradation of 1% causes a percentage increase of only 3.33%.

It is also worth noting that the planning cost of a DTT network is very related to the mean location probability that has to be guaranteed over the territory. Particularly in territories like Italy that have wide mountain and hilly areas, planning cost does not increase linearly with the location probability. In fact, in such territories, in order to reach a mean location probability that approaches the 100%, the number of DTT transmitters installations could be noticeably greater than to reach lesser mean location probability values over the territory.

It has also to be noted that the degradation in location probability will result in a reduction in coverage and a loss in the number of viewers who can receive the broadcasting service - the larger degradation, the larger loss. The DTT broadcasting systems are usually planned to guarantee an high location probability in most

populated pixels. A location probability degradation of 1% in those pixels would cause a loss of the DTT service of a great number of households. This confirms that a fixed value of degradation could be not completely satisfactory.

In the following, the possibility of adopting variable acceptable degradation of coverage probability is investigated. To this end, it has been considered that the degradation in location probability varies as a function of the location probability across the territory. Two different trends of the degradation have been analysed according to functions Δq_A and Δq_B . Δq_A and Δq_B are defined as:

$$\begin{aligned}\Delta q_A &= -0.058 \cdot q_1 + 0.059; \\ \Delta q_B &= \frac{0.029}{q_1} - 0.028.\end{aligned}\tag{3.24}$$

Functions Δq_A and Δq_B are obtained by fixing two targets in maximum degradation:

- a degradation of 3% for a location probability of 50%;
- a degradation of 0.1% for a location probability of 100%.

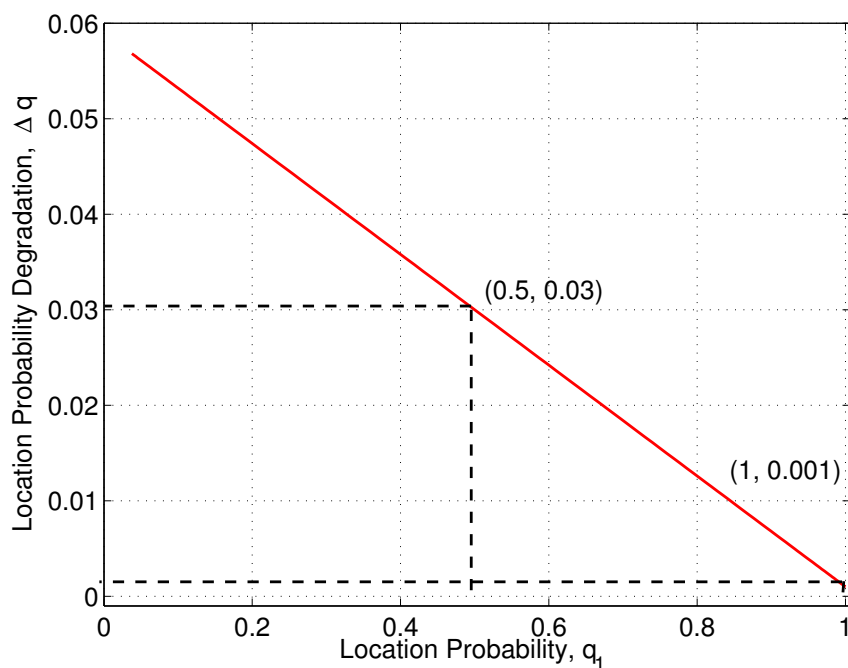
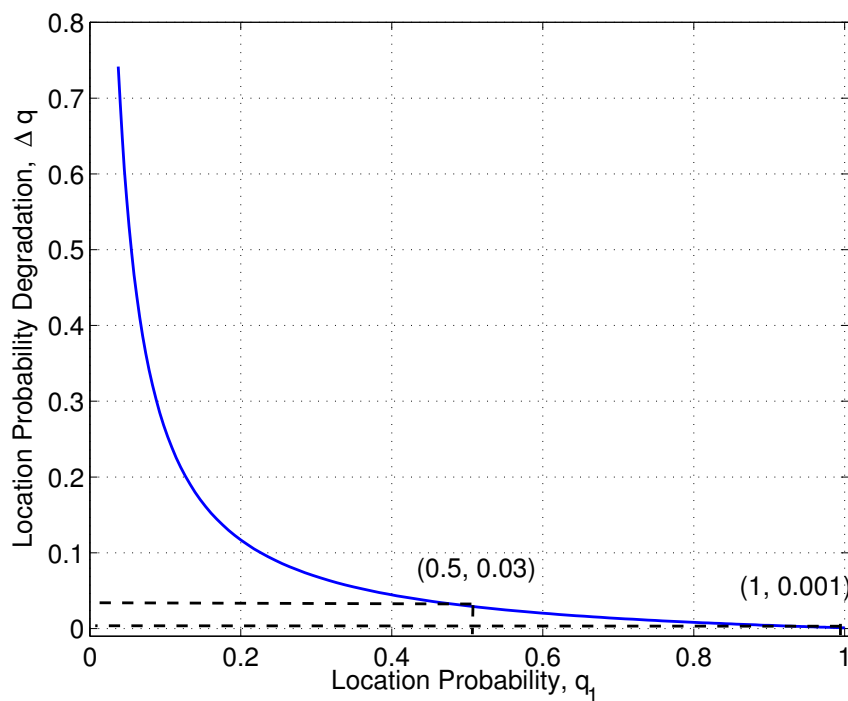
Figures 3.21 and 3.22 show the variation of degradation in location probability related to the location probability.

Figures 3.23 - 3.25 illustrate the results in terms of maximum permitted WSD EIRP considering a fixed value of degradation in location probability equal to 1% and the approach when the probability degradation varies across the coverage area as the functions Δq_A and Δq_B , under a range of DTT self-interference levels, m_V .

The scenario and values of the various parameters used to obtain the results are the same considered in section 3.1.4. The curves red and blue are obtained considering the functions Δq_A and Δq_B respectively. As can be seen from the figures, the minimum of these curves is shifted respect to the case $\Delta q = 1\%$, black curve.

Let consider that the functions Δq_A and Δq_B provide a degradation of $\Delta q = 1\%$ for $q_1 = 84\%$ and $q_1 = 74\%$ respectively.

Referring to figure 3.25 and considering the upper part of figure 3.11, the intersection between blue and red curve is obtained for $q_1 = 50\%$. The corresponding value of WSD EIRP is greater than the value obtained considering $\Delta q = 1\%$ because Δq_A and Δq_B for low values of location probability are set to admit a degradation of 3%.

Figure 3.21: Location probability degradation function, Δq_A .Figure 3.22: Location probability degradation function, Δq_B .

The intersection of red and blue curves with the black one, corresponds $q_1 = 84\%$ and $q_1 = 74\%$ respectively, i.e. $\Delta q = 1\%$. From values of DTT median wanted power, m_s greater than -68 dBm, the location probability assumes values greater than 84% . For these values Δq_A and Δq_B admit a location probability degradation lower than 1% and for this reason the WSD EIRP assumes lower values than those provided from black curve.

As expected, a variable Δq , compared to a fixed value, provides stricter protection in case of higher values of m_s , i.e. when the DTT service has high location probability; particularly in the range $[-50$ dBm, -30 dBm] of DTT wanted power, corresponding to most frequent and significant situations of DTT service, the reduction in WSD EIRP is remarkable, in the order of $5-8$ dB and almost identical for Δq_A and Δq_B . This confirms the crucial role of the choice of allowed degradation criteria.

On the other hand, when the DTT quality is already below threshold, towards the left side of the graph, variable allowed Δq results in noticeably higher WSD EIRP with respect to a fixed value, again consistently with practical considerations.

Same considerations can be done for the other figures.

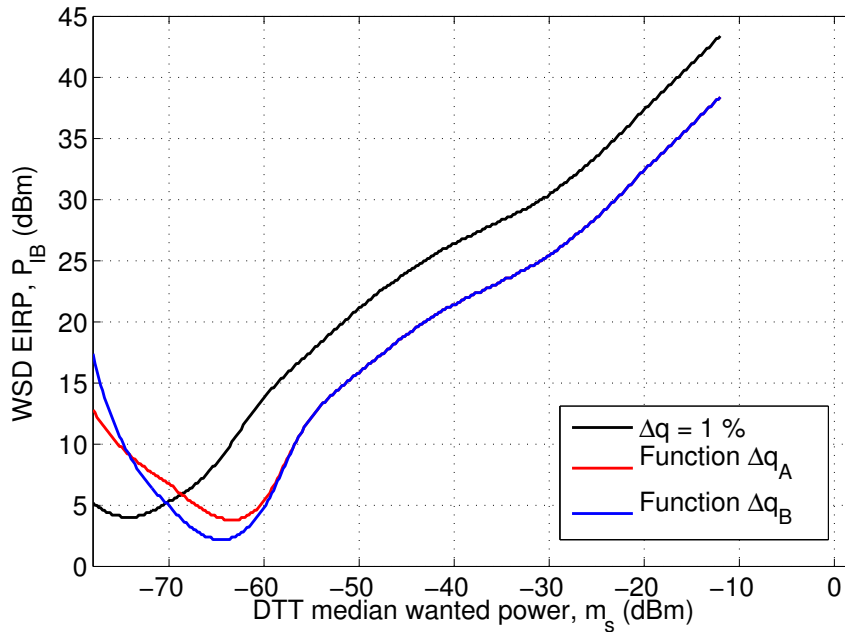


Figure 3.23: Maximum permitted WSD EIRP for three different Δq functions. Noise-limited DTT coverage. $m_V = -\infty$.

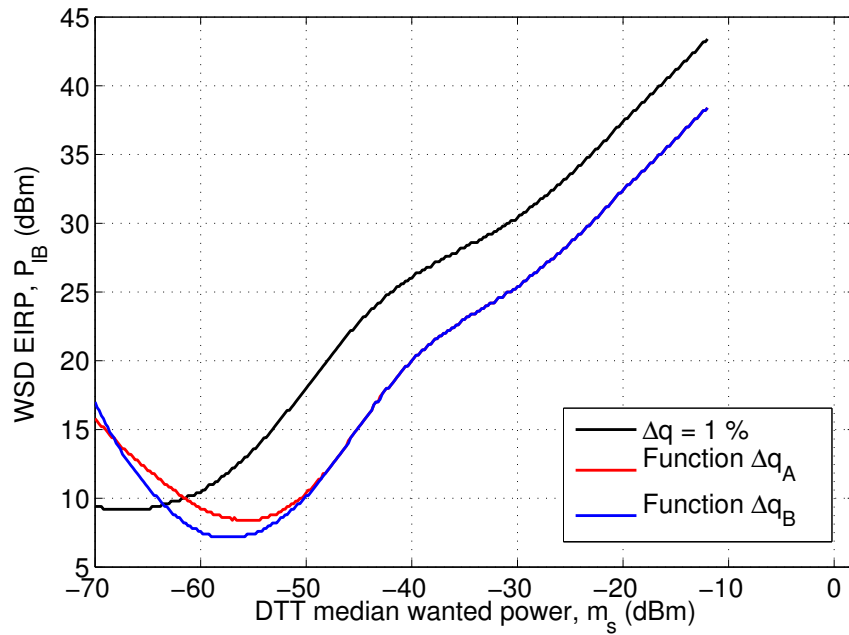


Figure 3.24: Maximum permitted WSD EIRP for three different Δq functions. $m_V = -70$ dBm, $\sigma_V = 4.9$ dB.

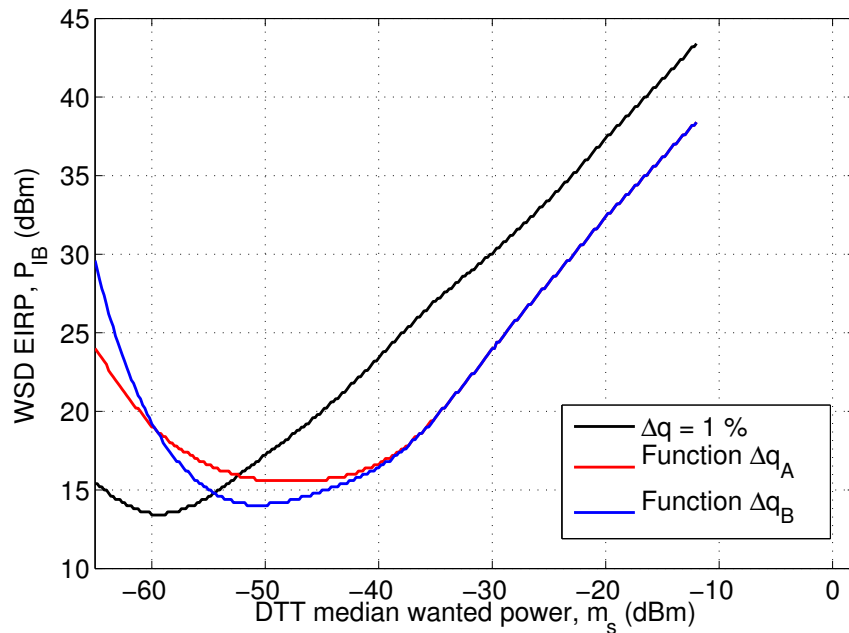


Figure 3.25: Maximum permitted WSD EIRP for three different Δq functions. $m_V = -60$ dBm, $\sigma_V = 5$ dB.

3.2.3 WSDs operating outside of a DTT coverage area: co-channel analysis considering $\Delta q = 1\%$

In the next two paragraphs, some considerations on WSD transmission using co-channel of the DTT service are made. Let consider a WSD operating inside of a DTT coverage area. The extremely high interference potential of co-channel usage, provides one of the main constraints on WSD EIRP limits. This effect is highlighted in figure 3.26, where maximum permitted WSD EIRP is shown considering reference scenario, co-channel transmission and protection ratio value of 21 dB.

It can be seen that this scenario provides very low values of maximum permitted WSD EIRP, not consistent with a real transmission.

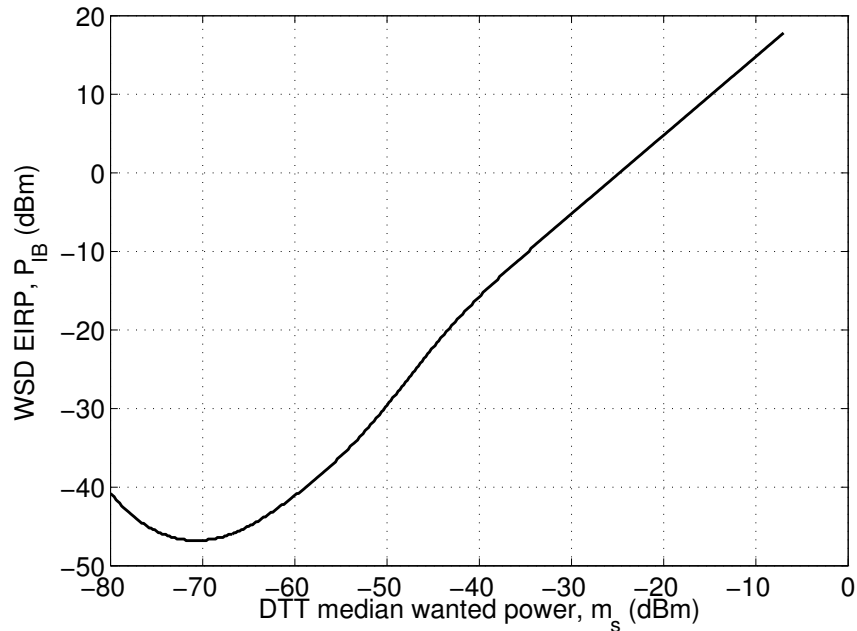


Figure 3.26: Maximum permitted WSD EIRP. Co-channel usage, reference geometry, $\Delta q = 1\%$. $m_V = -70$ dBm, $\sigma_V = 4.9$ dB.

Consideration of "short distance" WSD interference, i.e. 20 m of reference geometry, limits the possible operation of WSDs. Figures 3.27 - 3.29 illustrate the minimum separation between a WSD operating on the same channel of the victim DTT receiver for different fixed values of maximum permitted WSD EIRP and for a range of self-interference, m_V . The results are obtained considering free-space propagation model to calculate the coupling gain, WSD -to- DTT co-channel protection ratio of 21 dB and location probability degradation, Δq , equal to 1%.

The results show that the WSD co-channel transmission is allowed only with

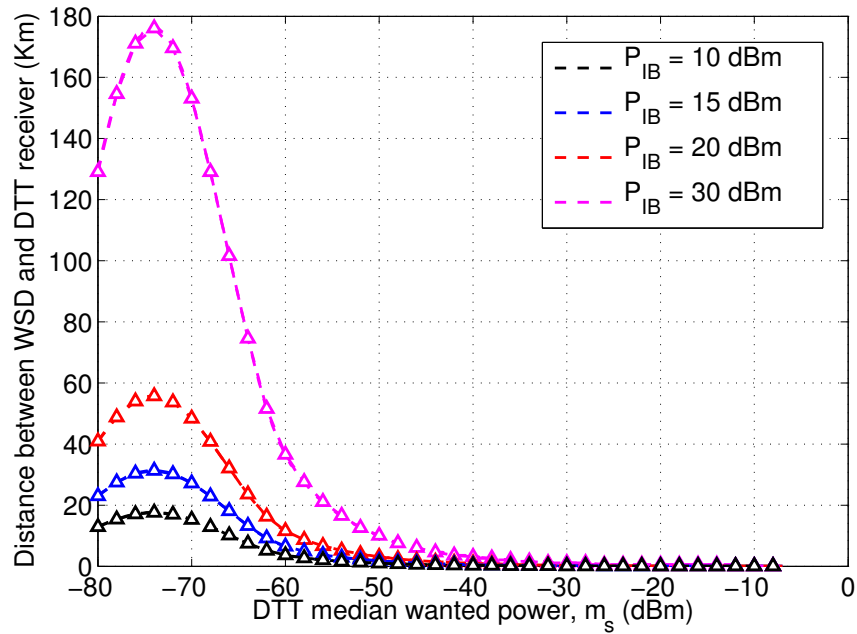


Figure 3.27: WSD interferer - DTT receiver distance for different WSD EIRP values. Co-channel usage, actual distance between WSD and DTT receiver, free-space propagation, $\Delta q = 1\%$. Noise-limited DTT coverage. $m_V = -\infty$.

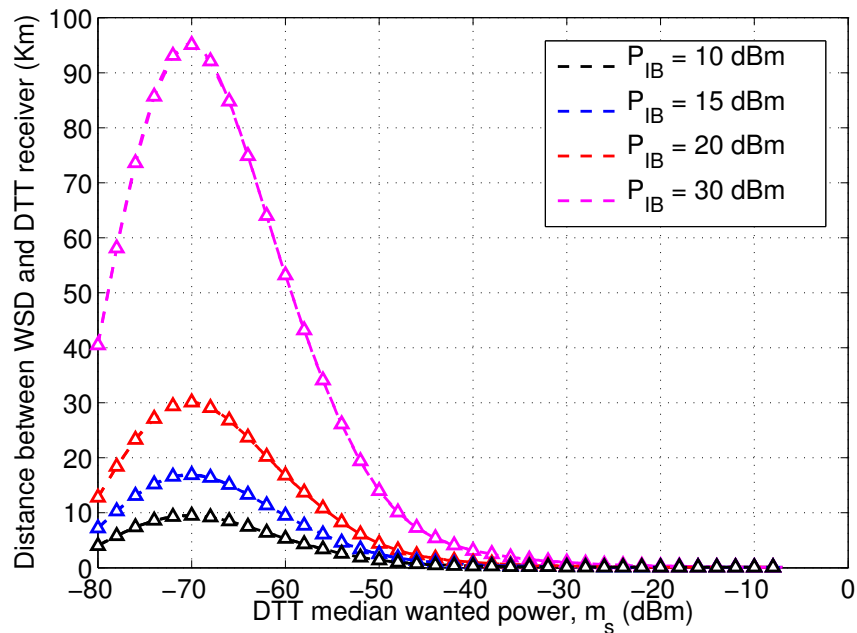


Figure 3.28: WSD interferer - DTT receiver distance for different WSD EIRP values. Co-channel usage, actual distance between WSD and DTT receiver, free-space propagation, $\Delta q = 1\%$. $m_V = -70$ dBm, $\sigma_V = 4.9$ dB.

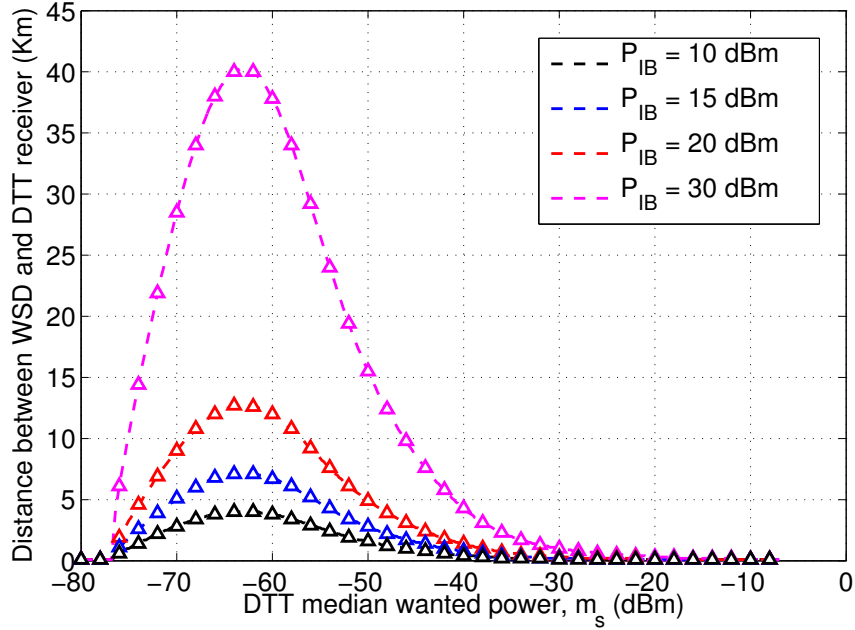


Figure 3.29: WSD interferer - DTT receiver distance for different WSD EIRP values. Co-channel usage, actual distance between WSD and DTT receiver, free-space propagation, $\Delta q = 1\%$. $m_V = -60$ dBm, $\sigma_V = 5$ dB.

an high separation between the WSD interferer and the DTT receiver, i.e. 5 Km to transmit 10 dBm for $m_V = -60$ dBm. The distance increases, increasing the maximum permitted WSD EIRP as well as decreasing the DTT self-interference, m_V .

For long distance, the free-space model is not representative of the real environment. For this reason, the same scenario is analysed, assuming a dual-slope model to calculate the coupling gain, i.e. non-reference geometry.

Figures 3.30 - 3.32 show the results that have been obtained. As can be seen, the minimum separation decreases with respect to the case of assuming the free-space path loss between WSD interferer and DTT receiver.

The slope change in the curves refers to the break-point distance. The zone where the values of the DTT median wanted power, m_S , are very high, i.e. where m_S is 50-60 dB greater than the DTT receiver's reference sensitivity, the separation between WSD and DTT receiver is very small (30-40 metres); nevertheless, these DTT power values do not represent common service situations.

Approaching the zones of most common DTT service, in the range [-50 dBm,-30 dBm], Δq_A and Δq_B functions admit a location probability degradation lower

than 1%, thus the separation between WSD and DTT receiver is significantly higher than in case of fixed degradation. For instance, the minimum separation distance for $m_S = -50$ dBm increases from 1.5 km in case of fixed Δq to 2.5 km in case of variable Δq , for WSD EIRP equal to 15 dBm, and from 3.5 Km to 5.8 km for WSD EIRP equal to 30 dBm. This confirms the sensitiveness of system to the setting of the allowed degradation.

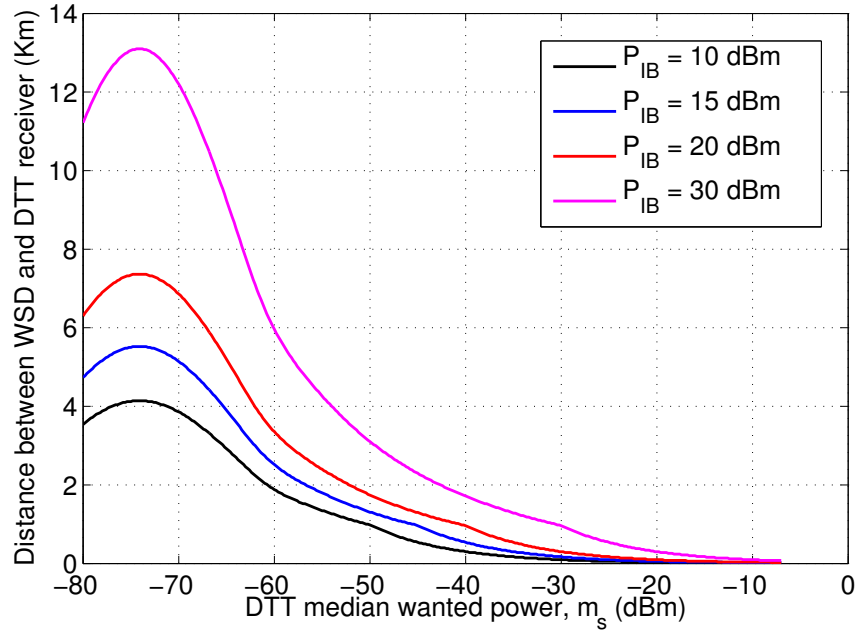


Figure 3.30: WSD interferer - DTT receiver distance for different WSD EIRP values. Co-channel usage, non-reference geometry, dual-slope propagation, $\Delta q = 1\%$. Noise-limited DTT coverage. $m_V = -\infty$.

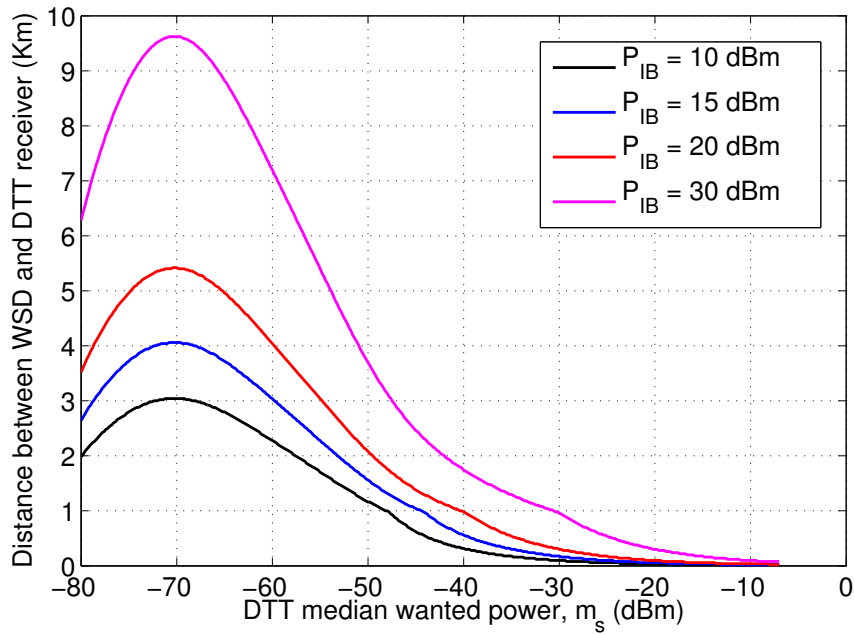


Figure 3.31: WSD interferer - DTT receiver distance for different WSD EIRP values. Co-channel usage, non-reference geometry, dual-slope propagation, $\Delta q = 1\%$. $m_V = -70$ dBm, $\sigma_V = 4.9$ dB.

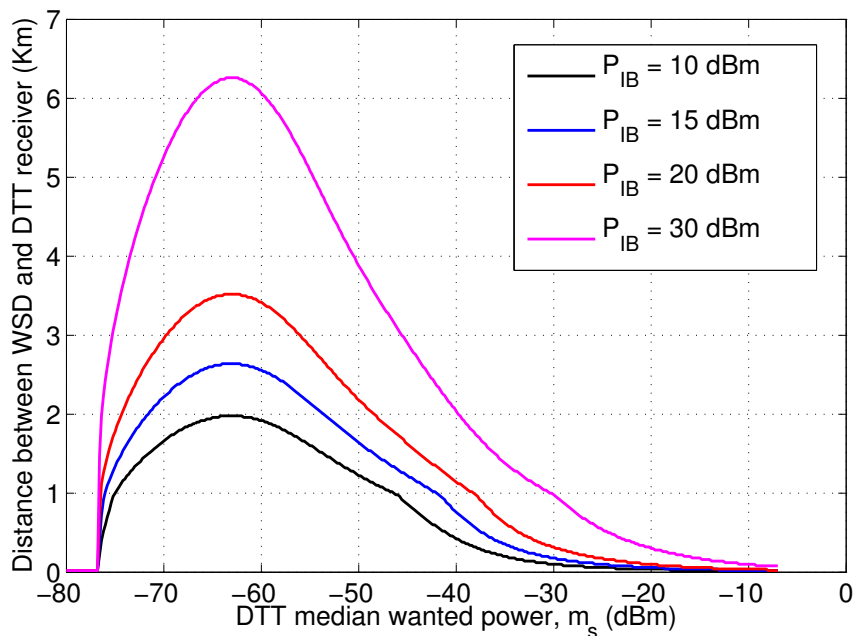


Figure 3.32: WSD interferer - DTT receiver distance for different WSD EIRP values. Co-channel usage, non-reference geometry, dual-slope propagation, $\Delta q = 1\%$. $m_V = -60$ dBm, $\sigma_V = 5$ dB.

3.2.4 WSDs operating outside of a DTT coverage area: co-channel analysis considering Δq varying across the coverage area

In this section it is analysed the scenario where the WSD operates outside of a DTT coverage area using the same channel of the DTT receiver under consideration. The non-reference geometry is assumed, i.e. actual distance between WSD and the protected DTT pixel and dual slope propagation model are used to determine the coupling gain. Furthermore the location probability degradation is assumed to vary across the coverage area of the broadcasting service according to function Δq_A and Δq_B defined in section 3.2.2.

Figure 3.33 - 3.36 show the minimum separation between the WSD and the DTT receiver for a range of maximum WSD EIRP and considering the DTT self-interference, m_V equal to -70 dBm. Co-channel WSD - to - DTT protection ratio equal to 21 dB is assumed. Each curve represents a different location probability degradation function. The curves red and blue are obtained considering the functions Δq_A and Δq_B respectively while the black one refers to the case of a fixed value equal to 1%.

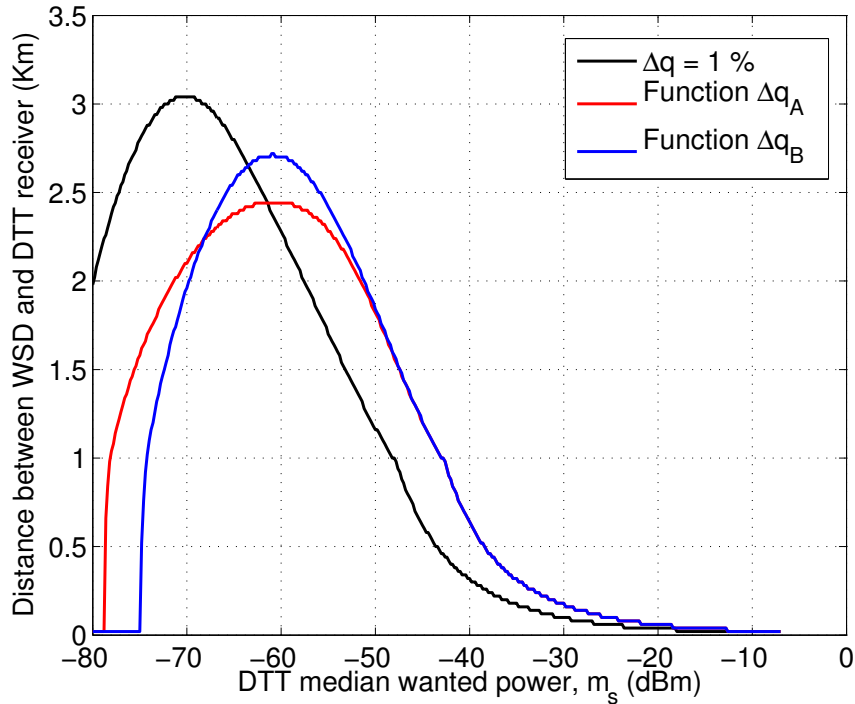


Figure 3.33: WSD interferer - DTT receiver distance for three different Δq functions. Co-channel usage, non-reference geometry, dual-slope propagation, WSD EIRP = 10 dBm, $m_V = -70$ dBm, $\sigma_V = 4.9$ dB.

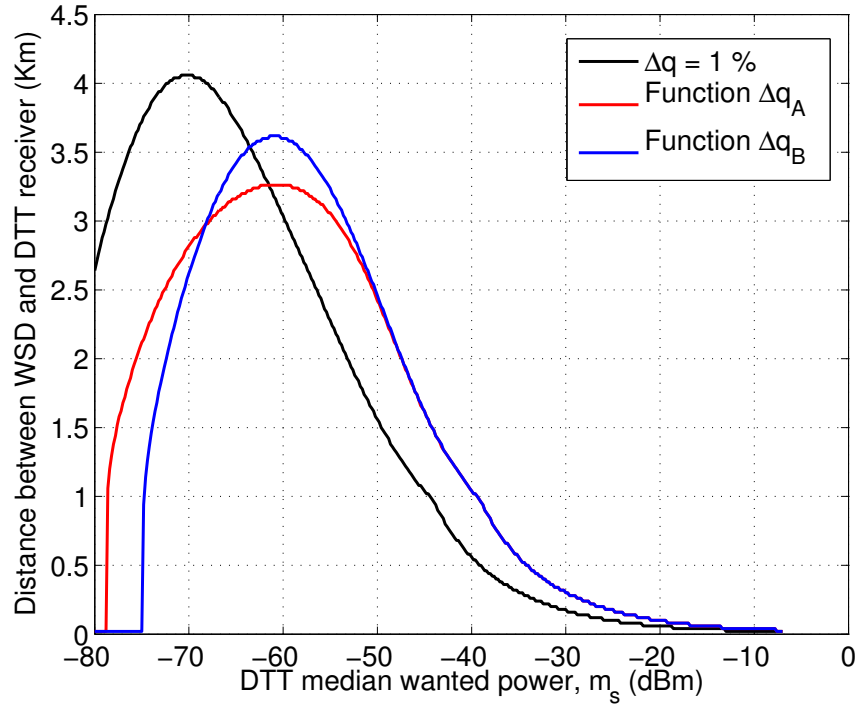


Figure 3.34: WSD interferer - DTT receiver distance for three different Δq functions. Co-channel usage, non-reference geometry, dual-slope propagation, WSD EIRP = 15 dBm, $m_V = -70$ dBm, $\sigma_V = 4.9$ dB.

The intersection between blue and red curve corresponds to $q_1 = 50\%$. For this value of location probability, Δq_A and Δq_B admit 3% of degradation in location probability. As might be expected, the separation between WSD and DTT receiver is lower than for the case of $\Delta q = 1\%$.

For low values of location probability, i.e. corresponding to m_S values lesser than -67 dBm, better results in terms of separation between the WSD and the DTT receiver are obtained considering Δq_A curve. For greater values of location probability, Δq_A and Δq_B functions admit a degradation of location probability lower than 1% and for this reason the distance between WSD and DTT receiver increases while the DTT median wanted power, m_S , increases.

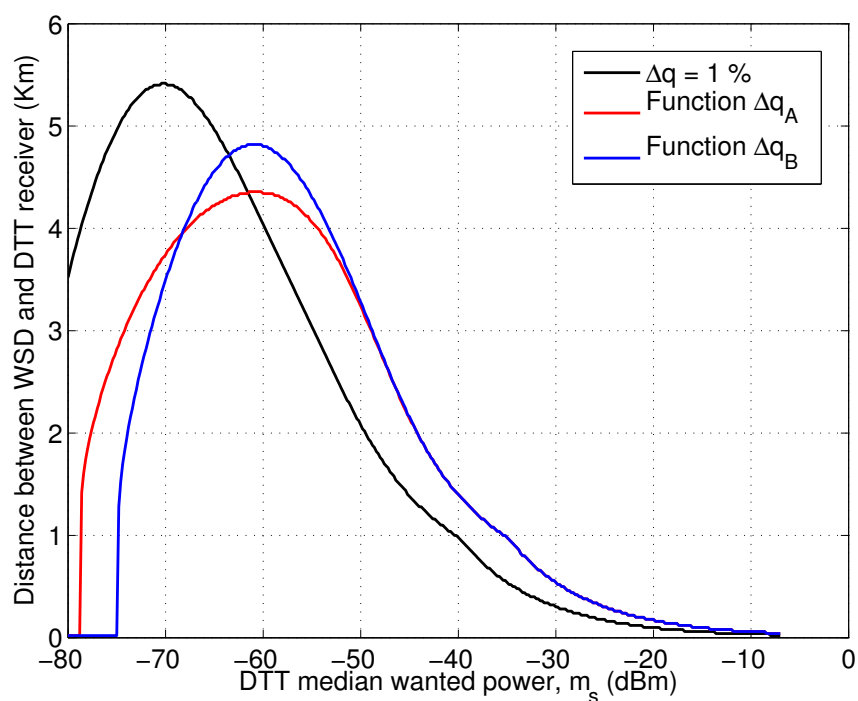


Figure 3.35: WSD interferer - DTT receiver distance for three different Δq functions. Co-channel usage, non-reference geometry, dual-slope propagation, WSD EIRP = 20 dBm, $m_V = -70$ dBm, $\sigma_V = 4.9$ dB.

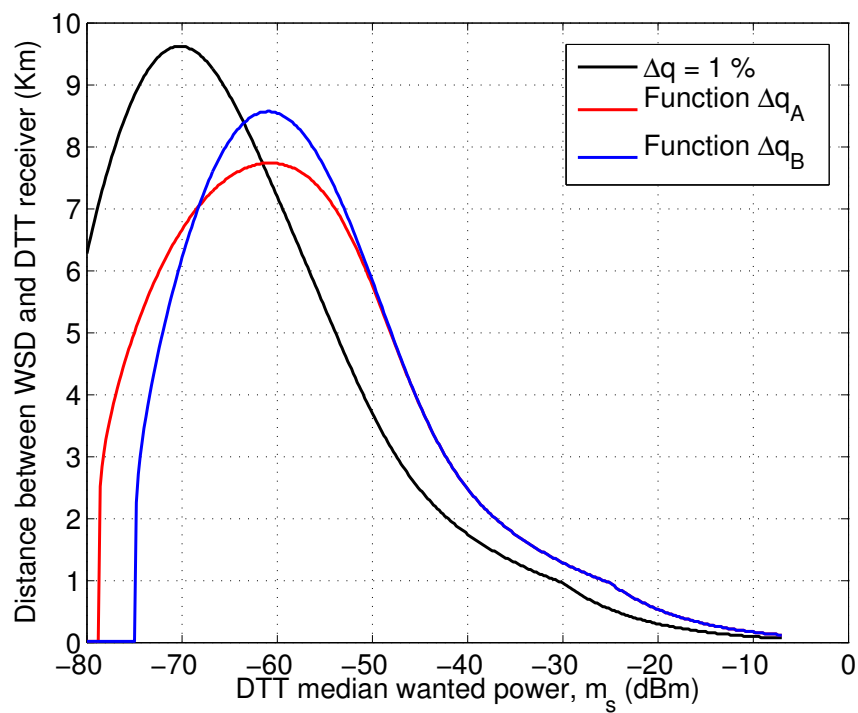


Figure 3.36: WSD interferer - DTT receiver distance for three different Δq functions. Co-channel usage, non-reference geometry, dual-slope propagation, WSD EIRP = 30 dBm, $m_V = -70$ dBm, $\sigma_V = 4.9$ dB.

3.2.5 Analysis on variation of DTT self-interference considering $\Delta q = 1\%$

In previous paragraphs, a range of DTT coverage conditions have been analysed considering fixed levels of DTT self-interference in relation to the wanted DTT signal. In this section the location probability and the maximum permitted WSD EIRP are examined in relation to the DTT self-interference, considering different values of wanted DTT signal.

In all pixels the standard deviation of the wanted signal, σ_S , is set to 5.5 dB while the standard deviation of the DTT self-interference, σ_V , is set to 4 dB. The reference geometry is considered and the values of the various parameters used in the following numerical examples are the same used in section 3.1.4 and summarized in table 3.3.

Figure 3.37 illustrates the location probability, q_1 , in relation to the unwanted DTT median power, m_V , i.e. the median value of DTT self-interference, for a range of DTT median wanted power, m_S . As might be expected, the location probability decreases as the unwanted DTT power increases. For very low values of DTT wanted power, i.e. $m_S = -64$ dBm and $m_S = -74$ dBm, the maximum achievable value of the location probability results to be lesser than 1. Furthermore, figure 3.37 indicates that the location probability increases as well as the DTT median wanted power level increases.

Figure 3.38 shows the maximum permitted WSD EIRP in relation to the unwanted DTT median power, m_V , for different values of the wanted DTT signal level, m_S .

As can be seen, in noise-limited zone, i.e. where the unwanted DTT median power, m_V , is low, the maximum permitted WSD EIRP is limited by the noise floor. In order to guarantee the location probability degradation at 1%, for increasing values of the DTT self-interference, the WSD EIRP decreases. The minimum value of the WSD EIRP is reached for that value of m_V in correspondence of the point where the derivative of the cumulative distribution function P_V reaches the minimum negative value. Moving towards greater values of m_V , the WSD EIRP increases as well as the derivative of the cumulative distribution function.

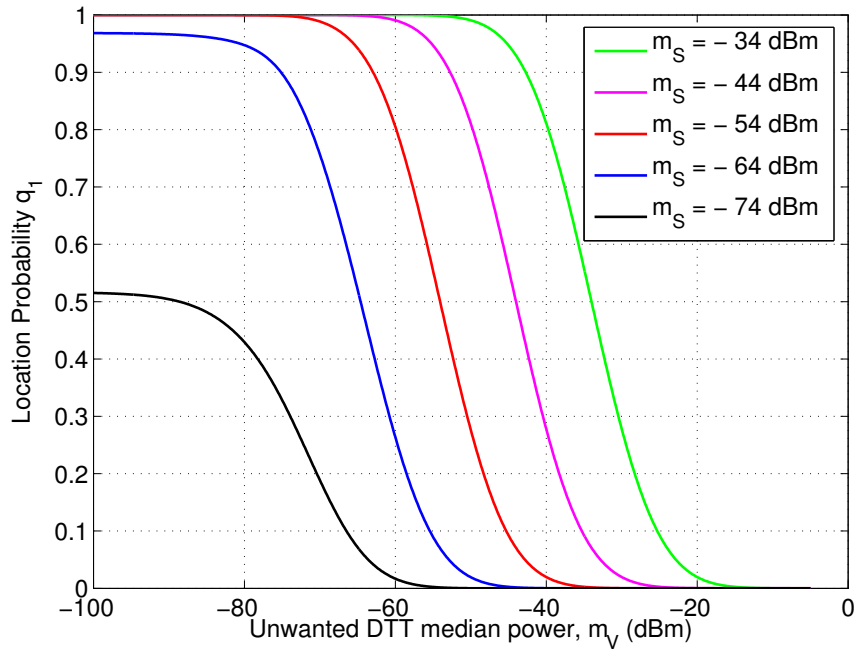


Figure 3.37: DTT location probability for different values of m_S . $\sigma_S = 5.5$ dB, adjacent-channel usage, reference geometry, $\Delta q = 1\%$

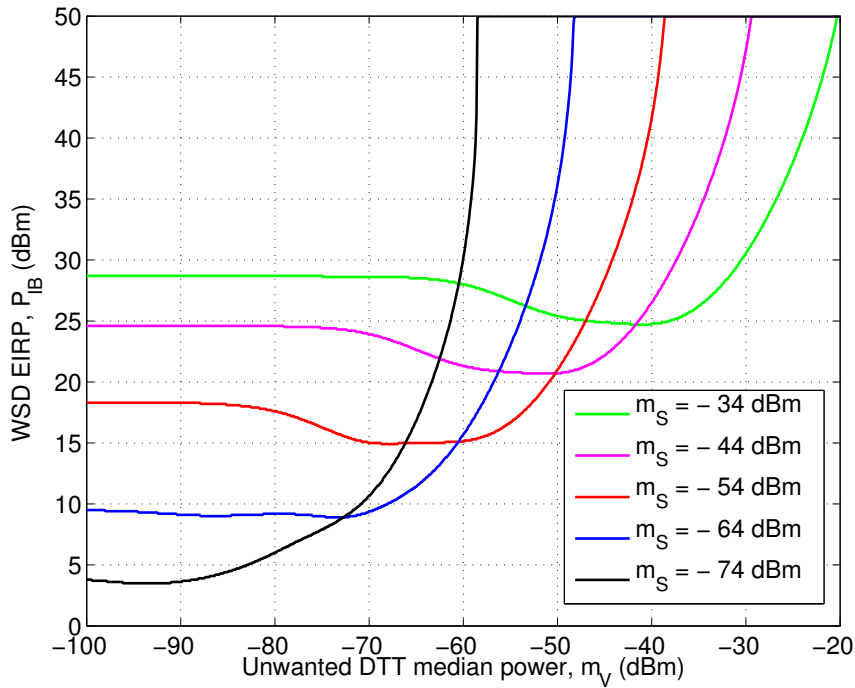


Figure 3.38: Maximum permitted WSD EIRP for different values of m_S . $\sigma_S = 5.5$ dB, adjacent-channel usage, reference geometry, $\Delta q = 1\%$.

3.3 Maximum Permitted WSD EIRP: Comparison Between MFN and SFN Planning Configurations

UHF terrestrial TV networks have historically been planned as a Multi-Frequency Networks (MFNs) to support regional TV programming. Multi-Frequency Networks consist of transmitters each using an individual channel which can be reused only at sufficient distance to avoid destructive interference. Therefore, in order to cover a large area with the same DVB-T multiplex, a certain number of radio-frequency channels is needed [53]. Frequency efficiency of this kind of planning is very poor. A particular UHF channel carrying a TV multiplex for one region cannot be in fact re-used until the signal strength has fallen to a level approaching the thermal noise floor.

Compared with a conventional MFN, a Single-Frequency Network (SFN) allows significant improvements in spectrum utilization. In a SFN, all transmitters are synchronously modulated with the same signal and radiate on the same channel so that large areas can be served with a common multiplex using only one channel. The wanted signal consists of several signal components from different transmitters the variations of which are only weakly correlated and fades in the field strength of one transmitter may be filled by another transmitter. Due to the multi-path capability of the multi-carrier transmission system (COFDM) [63] signal from several transmitters arriving at a receiving antenna may contribute constructively to the total wanted signal.

Then, when operating in a SFN, the signals transmitted from individual transmitters should be:

- synchronous in time (or with a precisely controlled delay);
- nominally coherent in frequency (within a few Hz);
- must have identical multiplex content.

Synchronism of all transmitters composing the SFN is essential. The network should be designed to avoid self-interference and to make use of wanted echoes produced by other transmitters. The power of all signals received within the time width of the guard interval is treated as useful, and contributes to the total useful power. If a signal delay is greater than the guard interval, intersymbol interference occurs and the relevant signal contributes to the total interference. This scheme

allows for much greater spectrum efficiency, at the cost of planning efforts to avoid significant echoes arriving beyond the guard interval period.

In a SFN, self-interference due to a signal extra delay over the guard interval and adjacent-channel incoming interference have to be taken in account. The predictions of wanted coverage and the interference potential for each transmitters should be carried out at 50% of the time for the wanted service and 1% of the time for the interferer.

The features of both MFN and SFN planning techniques are included in k-SFN planning. Such kind of networks are made of $k > 1$ "sub-networks" SFN, each using a different channel from the adjacent ones; the overall coverage is given by the sum of the coverage of all k sub-networks. This is done, for instance, for the planning of local networks, or when the morphology of the land makes it difficult to overcome the synchronisation issues of a single SFN.

In the following subsections, different examples are provided in order to study the WSDs transmit opportunities in different network plans. Maximum permitted WSD emission levels are computed considering real transmitters data of the Italian region of Friuli-Venezia Giulia. The same network composed by the same DTT installations is considered for three strategies of network planning. In particular it is assumed that three channels with a frequency offset between them of 16 MHz, i.e. $f_{DTT_1} = 594$ MHz, $f_{DTT_2} = 610$ MHz and $f_{DTT_3} = 626$ MHz, that correspond to DTT channels 36, 38, 40 respectively, are available and the following configurations have been analysed:

- a SFN, using channel 36 (section 3.3.2);
- a MFN, that uses the three available channels, i.e. channel 36, channel 38 and channel 40. Firstly it is assumed that non-overlapped coverage areas are present, i.e. each pixel is considered covered by a single frequency (section 3.3.3). Then, overlapped coverage areas have been considered, so that a pixel may be covered by up to three frequencies (section 3.3.5);
- a k-SFN, composed by three SFNs and with non-overlapped coverage areas (section 3.3.4). Each available channel is used by a SFN, i.e. a SFN operates on channel 36, a SFN operates on channel 38 and a SFN operates on channel 40;

The hypothetical SFN, MFN and 3-SFN frequency plans have been designed specifically for this analysis, adopting standard criteria of planning optimisation

have been applied, i.e. maximisation of population coverage achievable with the available set of transmitters. In the following section the methodology to calculate the maximum permitted WSD EIRP for each channel is described.

3.3.1 Methodology to derive EIRP limits over all DTT channels

In order to calculate the maximum allowed WSD EIRP in each pixel covered by the DTT service, the methodology described in [45] is applied. This methodology allows to calculate the maximum permitted WSD EIRP in each pixel and for each channel. In particular the most stringent emission requirement is taken for each channel considering both co-channel and adjacent channel interference. This methodology is briefly outlined below.

Denote as f_1 , f_2 and f_3 the frequencies used in the DTT network under consideration and focus on a given pixel where WSD operates. Figure 3.39 illustrates an example of the spatial reference pattern. As can be seen, the WSD operates in a given pixel within which the DTT network uses frequency f_2 , while frequencies f_1 and f_3 are used in other distant pixels, the closest of which are d_x and d_y Km from the pixel of interest, respectively.

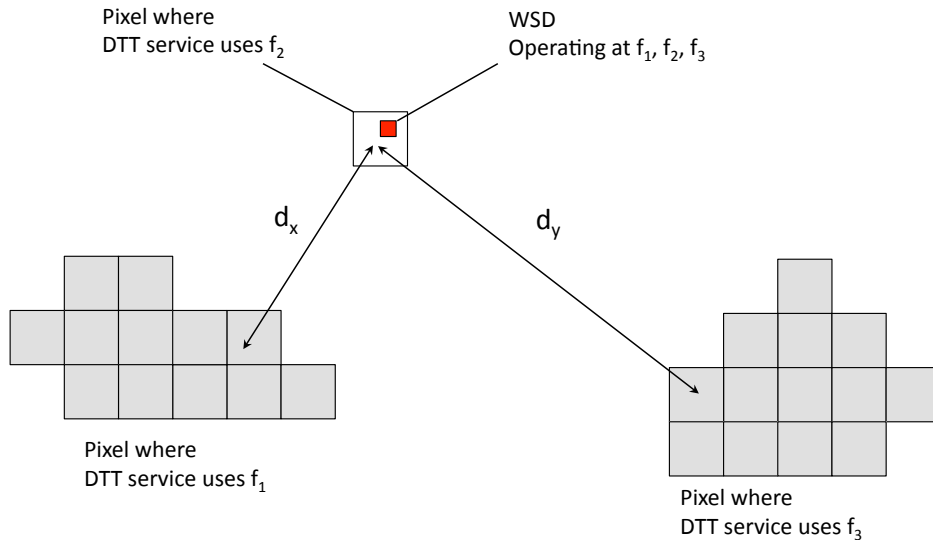


Figure 3.39: Usage of frequencies f_1 , f_2 and f_3 by the WSD and the DTT service. The nearest pixels where f_1 and f_3 are used by DTT service are d_x and d_y away, respectively.

For each pixel, the maximum permitted EIRP for each frequency f_i , $i = 1, 2, 3$, with f_i different from the frequency of the DTT service in the pixel has been derived,

by performing the following calculations:

- the maximum permitted WSD EIRP (P_{IBA}) considering the co-channel interference assuming the non-reference geometry shown in figure 3.10;
- the maximum permitted WSD EIRP (P_{IBB}) considering the adjacent-channel interference assuming the reference geometry shown in figure 3.8;
- the maximum permitted WSD EIRP (P_{IBC}) considering the adjacent-channel interference assuming the non-reference geometry shown in figure 3.10.

Tables 3.4, 3.5 and 3.6 summarise the operations relevant to the pixel shown as example in figure 3.39; the first two tables list the protection ratios to be considered for each evaluation, for both frequencies not used by the DTT system in the pixel, while the third table show how the final emission limit is determined for each frequency, taking the minimum EIRP value among P_{IBA} , P_{IBB} and P_{IBC} .

In order to apply this procedure to all pixels in the region, it is assumed that in pixels where the location probability is $< 70\%$ for all three frequencies, i.e. pixels that are not considered covered by the DTT network, the WSD is allowed to use any of the three frequencies. For each one of them, the maximum permitted WSD EIRP is computed considering co-channel and adjacent channel interference in reference geometry of figure 3.10. Figure 3.40, shows the spatial pattern of a non-covered pixel. Again, powers P_{IBA} , P_{IBB} and P_{IBC} are computed for each WSD operating frequency, i.e. $f_{WSD} = f_1$, $f_{WSD} = f_2$ and $f_{WSD} = f_3$ and three tables such as 3.4 and 3.5 are generated. The emission limits applicable to the WSD over each DTT frequency channel is again the minimum of the calculated permitted EIRP for each interference condition.

Note that in case of non-covered pixels, only non-reference geometry scenarios are considered (see figure 3.40). The emission limits applicable to the WSD over each DTT frequency channel is again the minimum of the calculated permitted EIRP derived for each considered interference condition.

3.3.2 WSDs operating in a SFN

In this section, firstly the location probability of the SFN planned in the Friuli-Venezia Giulia region is evaluated applying the approach described in section 3.1.1.3. Then the maximum WSD EIRP is calculated for each pixel in the area under investigation.

Table 3.4: ILLUSTRATIVE EMISSION LIMITS FOR WSD OPERATING AT FREQUENCY f_1

WSD operates at frequency, $f_{WSD} = f_1$			
DTT frequency, f_{DTT}	Geometry (coupling gain)	Protection Ratio (dB)	WSD EIRP for $f_{WSD} = f_1$
f_1	Non-reference geometry	21 dB	P_{IBA}
f_2	Reference geometry	$r(\Delta f, m_S)$	P_{IBB}
f_3	Non-reference geometry	$r(\Delta f, m_S)$	P_{IBC}

Table 3.5: ILLUSTRATIVE EMISSION LIMITS FOR WSD OPERATING AT FREQUENCY f_3

WSD operates at frequency, $f_{WSD} = f_3$			
DTT frequency, f_{DTT}	Geometry (coupling gain)	Protection Ratio (dB)	WSD EIRP for $f_{WSD} = f_3$
f_1	Non-reference geometry	$r(\Delta f, m_S)$	P_{IBA}
f_2	Reference geometry	$r(\Delta f, m_S)$	P_{IBB}
f_3	Non-reference geometry	21 dB	P_{IBC}

Table 3.6: WSD EMISSION LIMITS

WSD frequency, f_{WSD}	EIRP limits
f_1	$\text{MIN}(P_{IBA}, P_{IBB}, P_{IBC})$
f_2	—
f_3	$\text{MIN}(P_{IBA}, P_{IBB}, P_{IBC})$

The following assumptions have been made:

- the SFN is operating at frequency $f_{DTT} = 594$ MHz (DTT channel 36);
- the DTT interference from other transmitters is evaluated considering only co-channel signals from the network itself (DTT adjacent channel interference

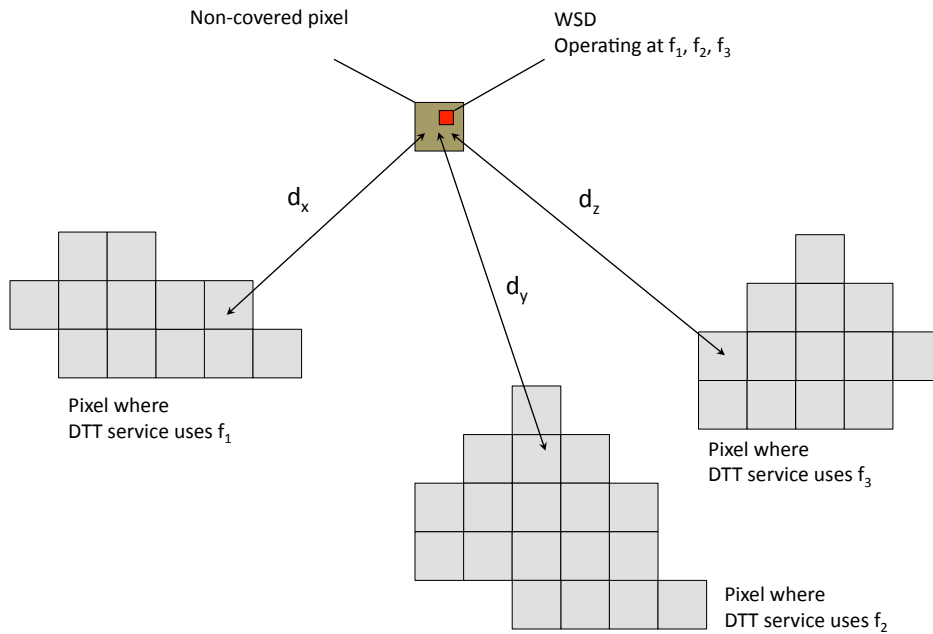


Figure 3.40: Usage of frequencies f_1 , f_2 and f_3 by the WSD and the DTT service. The nearest pixels where f_1 , f_2 and f_3 are used by DTT service are d_x , d_y and d_z away, respectively.

is not considered);

- a pixel is considered as covered if at least one frequency provides a location probability $\geq 70\%$.

The calculation of the location probability for each pixel 400 m x 400 m, is split into five parts:

- the field strength level, considering all DTT transmitters that compose the SFN, is evaluated using a proprietary prediction tool where the propagation model follows the ITU-R Recommendation P.526 [51];
- the discrimination between signals contributing to wanted signal and those contributing to interference signal is carried out considering a guard interval of 224 μs . Then, the calculation of the median and standard deviation values of the wanted sum field strength is performed, considering each signal power as a Gaussian random variable with standard deviation of 5.5 dB;
- calculation of median and standard deviation values of the sum of unwanted DTT signal is carried out, considering each signal modelled as real Gaussian

random variable with standard deviation of 5.5 dB. A co-channel protection ratio of 21 dB is used;

- evaluation of the location probability using the methodology described in section 3.1.1.3. The reference sensitivity level is assumed to be - 74.2 dBm.

Figure 3.41 shows the location probability of the SFN plan in the Italian region of Friuli-Venezia Giulia. Only the values of the covered pixels, i.e. where the location probability ranges between 0.7 and 1 are shown. As can be seen, in the most populated areas, the location probability mainly ranges between 0.95 and 1. In correspondence of mountains and valleys, the location probability values are lower and most of the pixels in those areas results to be not covered.

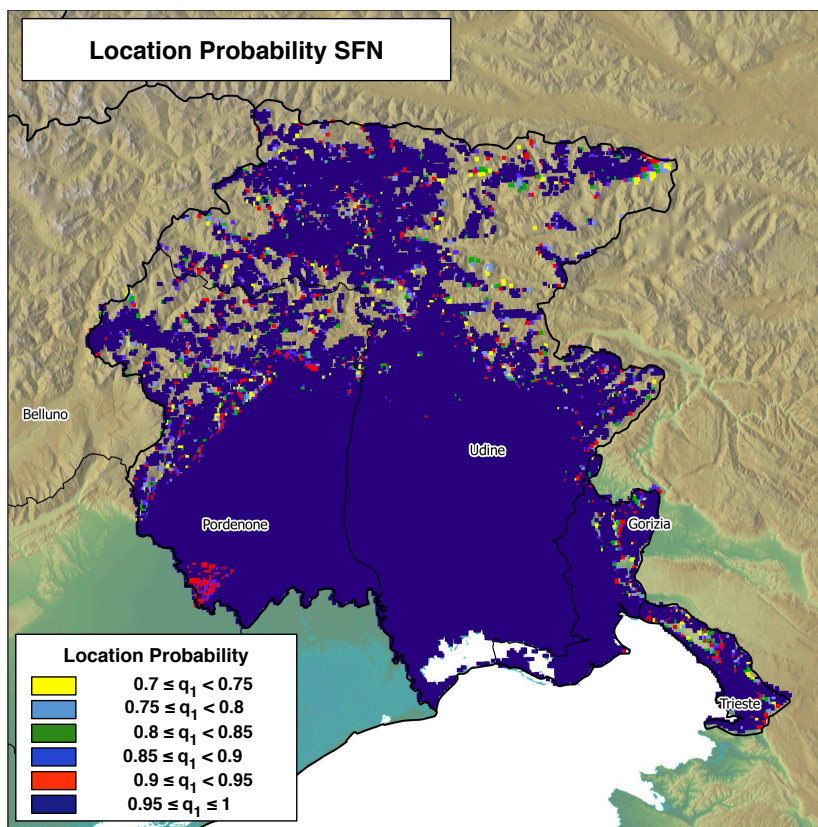


Figure 3.41: Example of a SFN in Friuli-Venezia Giulia: Location Probability of covered pixels ($q_1 \geq 0.7$).

The maximum permitted WSD EIRP is then calculated for each pixel of the considered area. The WSD is assumed to operate in the SFN DTT adjacent-channel

over the whole considered area. In particular, the frequency offset between the WSD and DTT carrier is assumed to be 16 MHz.

The reference geometry described in section 3.1.3.2 is used. The maximum permitted degradation in DTT location probability, Δq , is assumed to be 1% in all pixels and the WSD-to-DTT adjacent channel protection ratio, $r(\Delta f, m_S)$, values are assumed to be the same summarized in table 3.3. It is used a median path gain of -54.39 dB and a median coupling gain, m_G , equal to -61.24 dB.

Figure 3.42 shows the maximum WSD EIRP over the considered area. The value of P_{IB} has been varied between 0 dBm and 40 dBm. The P_{IB} values result to range between 20 dBm and 30 dBm in the densely populated areas while greater values have been obtained in non-covered pixels.

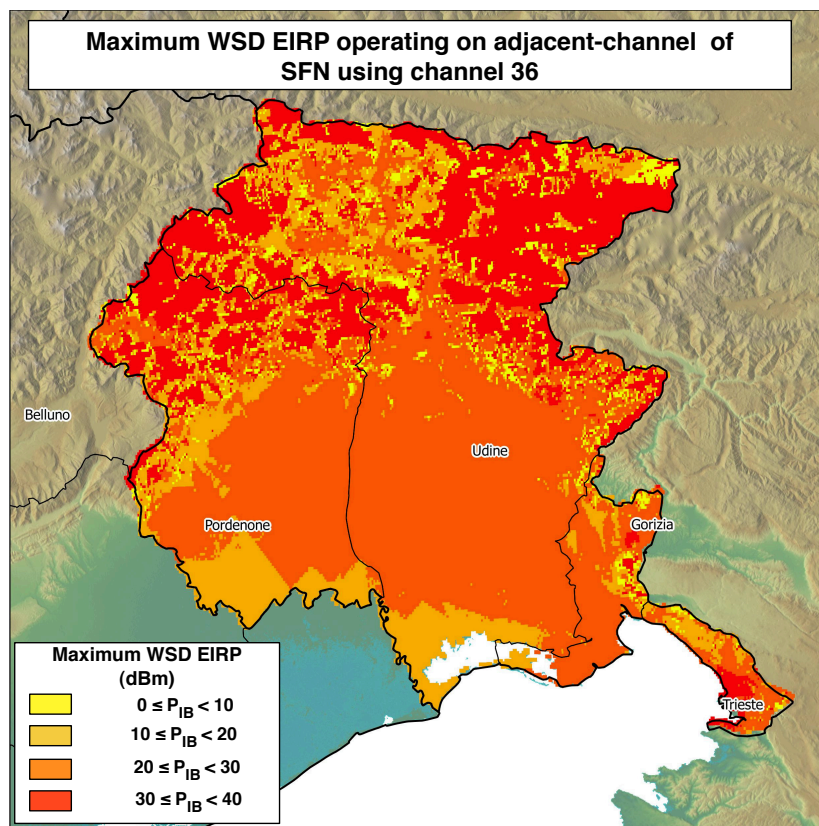


Figure 3.42: SFN in Friuli-Venezia Giulia: maximum WSD EIRP operating on adjacent-channel of SFN using channel 36.

3.3.3 WSDs operating in a MFN with non-overlapped coverage areas

In this section a MFN planning in Friuli-Venezia Giulia region is considered. The results in terms of DTT location probability and maximum permitted WSD EIRP are presented.

In this case, the following assumptions have been made:

- the MFN uses the three available frequencies, i.e. $f_{DTT_1} = 594$ MHz (channel 36), $f_{DTT_2} = 610$ MHz (channel 38) and $f_{DTT_3} = 626$ MHz (channel 40);
- non-overlapping coverage areas are assumed. In each pixel only the channel with the highest DTT location probability is protected;
- Only co-channel interference from the network itself is taken into account;
- a pixel is considered covered if at least one frequency provides a location probability $\geq 70\%$;

The calculation of the location probability for each pixel 400 m x 400 m, is performed as follows:

- the field strength level considering all DTT transmitters in the area is evaluated using the ITU-R Recommendation P.526 propagation model [51];
- calculation of median and standard deviation values of the sum of the unwanted DTT signals is carried out, considering each signal modelled as real Gaussian random variable with standard deviation of 5.5 dB. A co-channel protection ratio of 21 dB is used;
- evaluation of the location probability using the methodology described in 3.1.1.3. The reference sensitivity level is assumed to be - 74.2 dBm.

Figure 3.43 illustrates the DTT transmitters installations of the MFN. Different colors refer to different operating frequencies.

Table 3.7 shows the percentage of population with a given level of location probability for the three frequencies, obtained by the considered planning example. Frequencies f_1 and f_2 provide a location probability ≥ 0.95 to a large percentage of population, i.e. each frequency covers more than half per cent of population. Frequency f_3 serves less percentage of population because some of the installations are located on mountain areas.

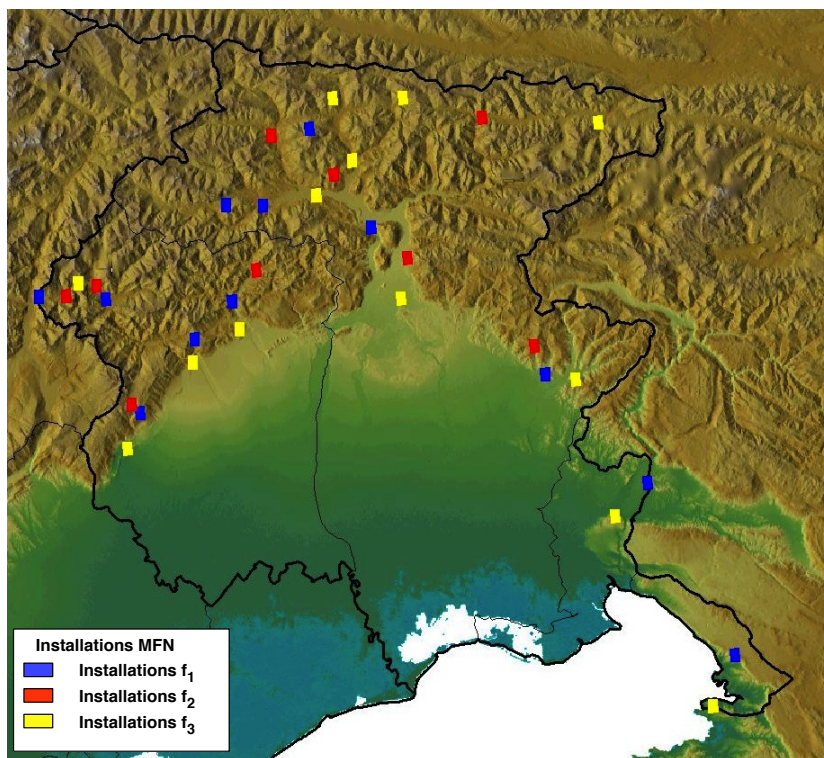


Figure 3.43: DTT installations MFN.

Table 3.7: EXAMPLE OF PERCENTAGE OF POPULATION RELATED TO LOCATION PROBABILITY IN MFN

Location Probability in MFN			
	MFN on f_1	MFN on f_2	MFN on f_3
% of Population $q_1 \geq 0.95$	50.9 %	63.45 %	31.77 %
% of Population $0.9 \leq q_1 < 0.95$	6.15 %	4.23 %	1.73 %
% of Population $0.85 \leq q_1 < 0.9$	5.54 %	2.45 %	1.31 %
% of Population $0.8 \leq q_1 < 0.85$	1.91 %	2.55 %	1.49 %
% of Population $0.75 \leq q_1 < 0.8$	1.06 %	1.79 %	1.11 %
% of Population $0.7 \leq q_1 < 0.75$	0.91 %	1.48 %	1.24 %
% of Population $q_1 < 0.7$	33.5 %	24.05 %	61.34 %

Figure 3.44 shows the location probability between 0.7 and 1, i.e. location probability of covered pixels. Also in this case non-covered pixels are on mountain areas and valleys, while densely populated zones are well covered by at least a channel.

Then, the maximum permitted WSD EIRP in each pixel and for each channel is calculated following the methodology described in previous section.

A maximum permitted degradation in DTT location probability, Δq , of 1% is assumed in all pixels. The considered WSD-to-DTT adjacent-channel protection ratios, $r(\Delta f, m_S)$, values are summarized in table 3.3. The median coupling gain, m_G , values for both reference and non-reference geometry are computed by means of methodology described in sections 3.1.3.2 and 3.1.3.3. The value of P_{IB} has been varied between 0 dBm and 40 dBm.

Figure 3.45 shows the maximum WSD EIRP over the Friuli-Venezia Giulia region in at least a channel. It can be seen that the highest power values are allowed in

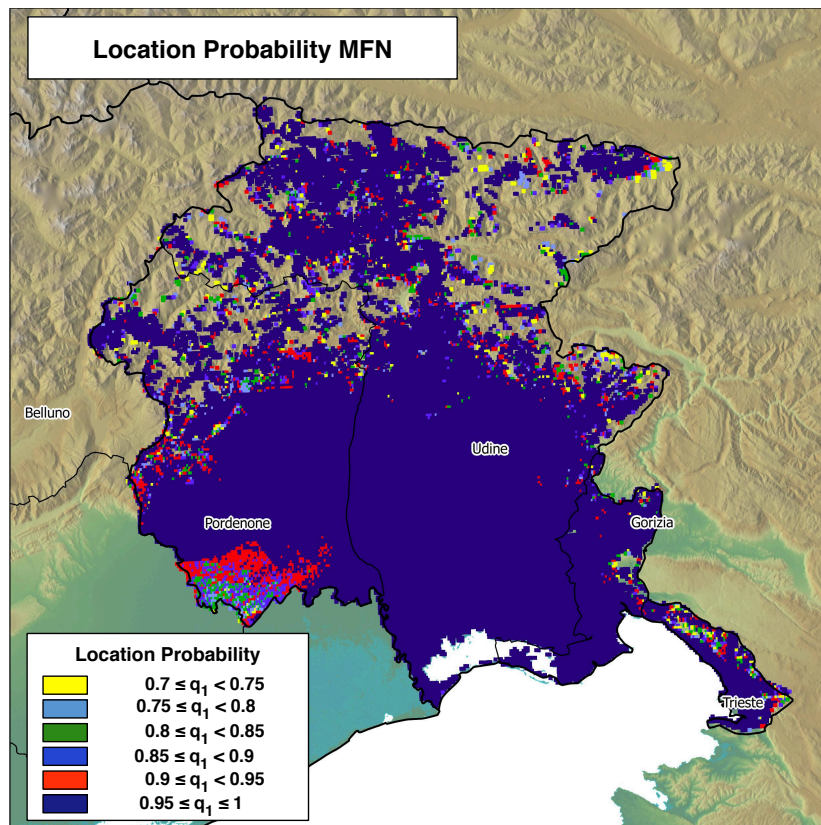


Figure 3.44: Example of a MFN with non-overlapped coverage areas in Friuli-Venezia Giulia: Location Probability of covered pixels ($q_1 \geq 0.7$).

mountain areas. Furthermore it has to be noted that in all pixels of the area, the WSD can use at least a channel.

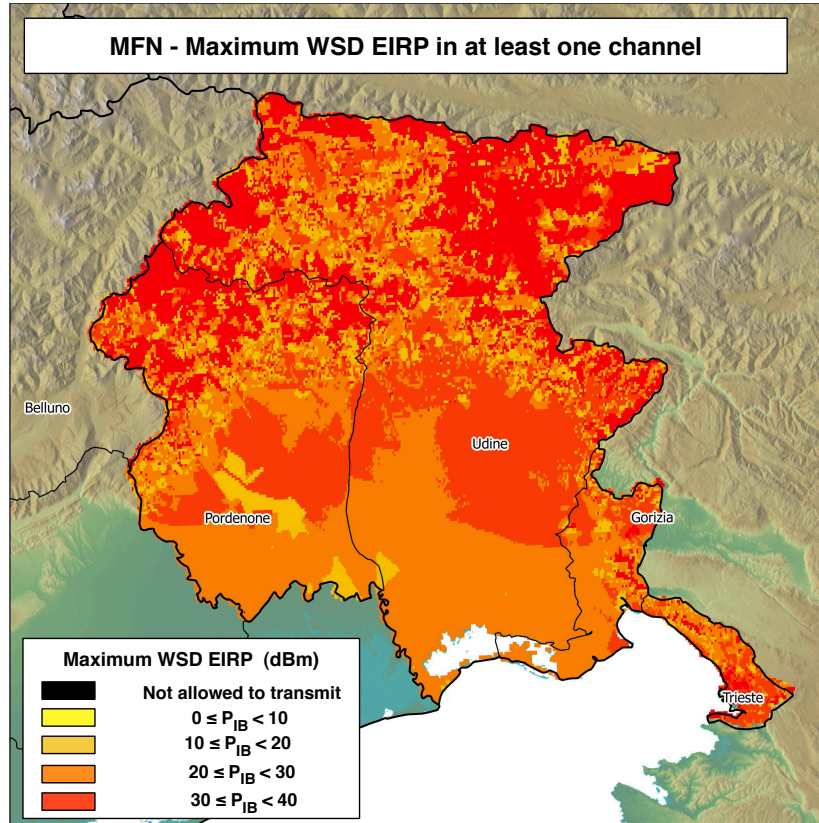


Figure 3.45: MFN with non-overlapped coverage areas in Friuli-Venezia Giulia: maximum WSD EIRP in at least one channel .

3.3.4 WSDs operating in a k-SFN with non-overlapped coverage areas

In this section location probability and maximum permitted WSD EIRP levels over the investigated region are analysed considering an example of k-SFN plan. The network is planned such that all available spectral resources ($k = 3$) are used, i.e. $f_{DTT_1} = 594$ MHz, $f_{DTT_2} = 610$ MHz and $f_{DTT_3} = 626$ MHz frequencies.

The network is composed by three SFNs. For each network and for each pixel, the location probability is calculated by means of the equation 3.2. Then, the calculation of the location probability for each pixel 400 m x 400 m, is performed following the steps presented in section 3.3.2.

Figure 3.46 shows the DTT transmitters installations that compose the k-SFN. Each colour represents a SFN operating on a different channel and figure 3.47 the overall location probability in the range between 0.7 and 1. Also in this case a very good coverage is guaranteed on the populated areas.

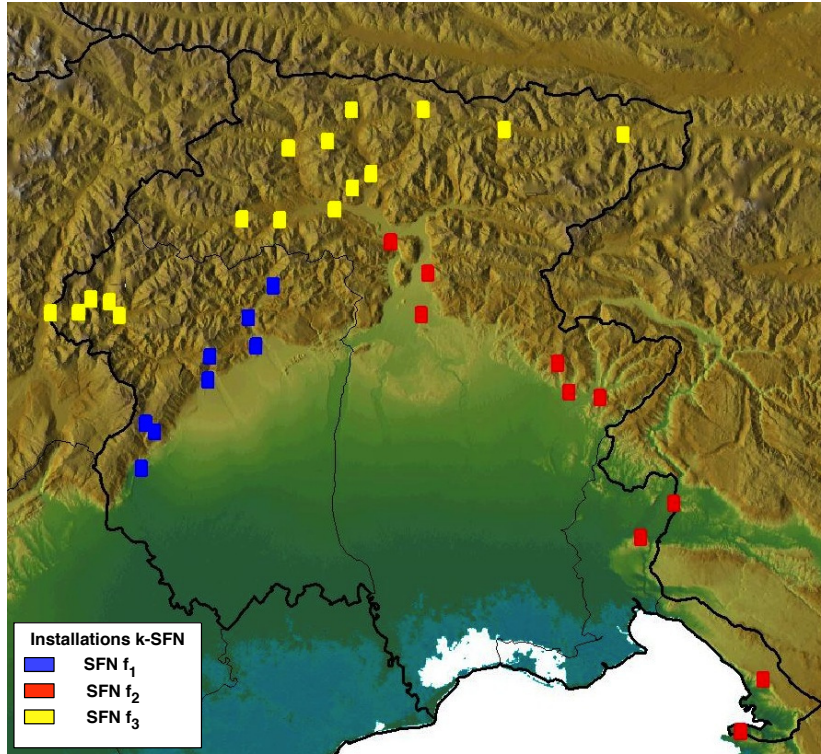


Figure 3.46: DTT installations k-SFN.

In table 3.8 the percentage of population with a given location probability for each SFN frequency is shown. It has to be highlighted that this is a simplified example of plan. As can be expected, the percentage of population covered by frequency f_3 is very low because the installations that use this channel are mainly located on mountain areas. Frequency f_1 and frequency f_2 provides a very good coverage, i.e. $\geq 95\%$, to a very large percentage of population, i. e. 78.82% and 92.04% respectively.

The permitted transmit power is calculated according to the methodology described in section 3.3.1 and assuming the maximum location probability degradation equal to 1% in all pixels. The adjacent-channel protection ratio values, $r(\Delta f, m_S)$, are summarized in table 3.3 and the co-channel protection ratio equal to 21 dB is assumed. The value of P_{IB} has been varied between 0 dBm and 40 dBm.

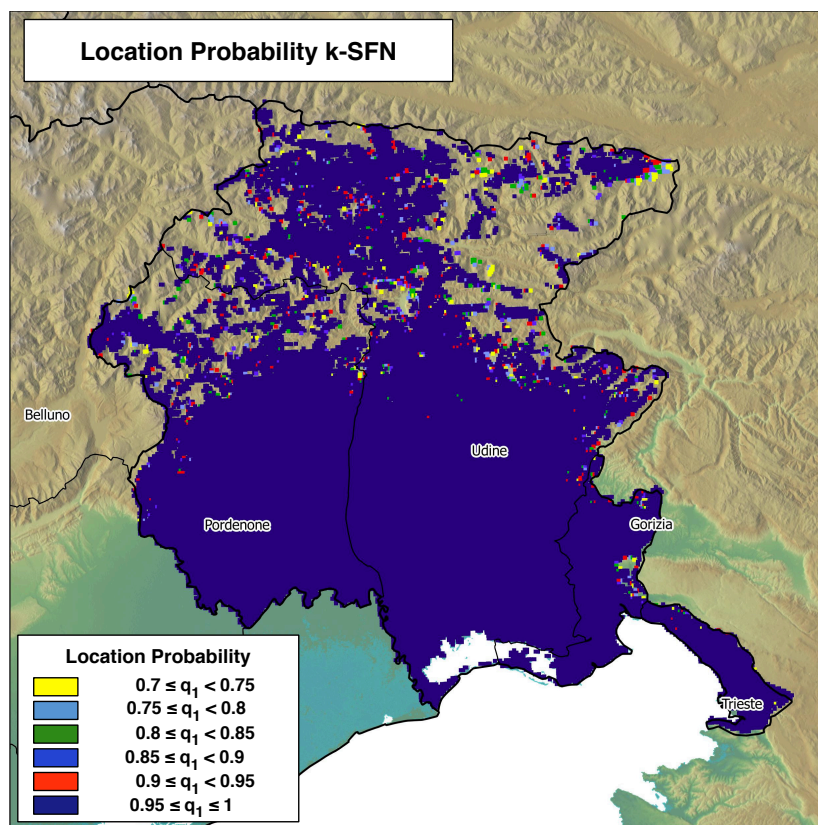


Figure 3.47: Example of a k-SFN with non-overlapped coverage areas in Friuli-Venezia Giulia: Location Probability of covered pixels ($q_1 \geq 0.7$).

Table 3.8: EXAMPLE OF PERCENTAGE OF POPULATION RELATED TO LOCATION PROBABILITY IN k-SFN

Location Probability in k-SFN			
	SFN on f_1	SFN on f_2	SFN on f_3
% of Population $q_1 \geq 0.95$	79.82 %	92.04 %	3.12 %
% of Population $0.9 \leq q_1 < 0.95$	0.61 %	0.48 %	0.04 %
% of Population $0.85 \leq q_1 < 0.9$	0.42 %	0.27 %	0.01 %
% of Population $0.8 \leq q_1 < 0.85$	0.23 %	0.17 %	0.02 %
% of Population $0.75 \leq q_1 < 0.8$	0.33 %	0.22 %	0.03 %
% of Population $0.7 \leq q_1 < 0.75$	0.15 %	0.13 %	0.02 %
% of Population $q_1 < 0.7$	18.44 %	6.69 %	96.76 %

Figure 3.48 illustrates the permitted WSD EIRP in at least one channel. Comparing the WSD emission levels in MFN and k-SFN plans (figure 3.45 and figure 3.48 respectively), it is evident that the permitted power levels in case of k-SFN planning strategy is greater respect to the WSD EIRP values obtained for MFN plan. This is due to the higher robustness to the interference of the SFN planning than the MFN configuration.

3.3.5 WSDs operating in a MFN with overlapped coverage areas

In this section the results in terms of maximum permitted WSD transmit power are shown considering the same MFN plan used in section 3.3.3 assuming, in this case, overlapped covered areas. This means that a pixel can be covered by more than one frequency. Then, in each pixel, a WSD is not allowed to operate at the frequencies which are used by the DTT service in the pixel under consideration. To calculate the permitted WSD transmit power, co-channel and adjacent channel interference

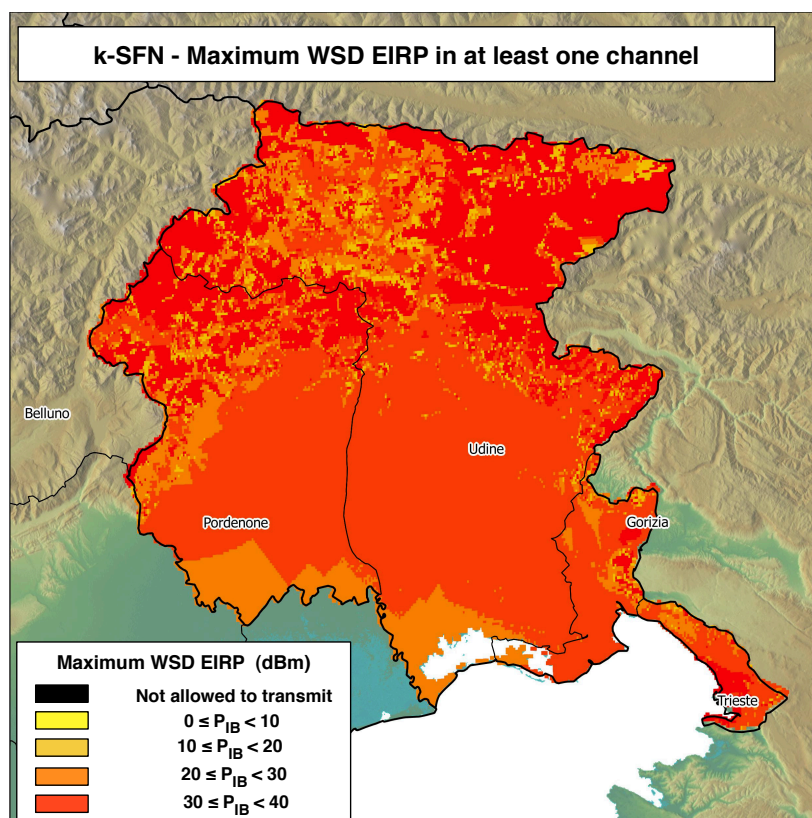


Figure 3.48: k-SFN with non-overlapped coverage areas in Friuli-Venezia Giulia: maximum WSD EIRP in at least one channel .

have to be considered (see section 3.3.3). If the pixel is covered by any frequency, the WSD can use all frequencies, f_1 , f_2 and f_3 . The maximum permitted power on each frequency is given by the minimum value obtained considering both co-channel and adjacent channel interference (see table 3.6).

Figure 3.3.6 show the distribution of the maximum permitted WSD EIRP over the territory. Considering overlapped coverage areas limits the WSD transmission opportunities respect to the case of MFN with non-overlapped coverage areas. As can be seen, in this case, some pixels where the WSD is not allowed to transmit are present. These are pixels where all frequencies provide a location probability greater than 0.7.

Again, high permitted WSD EIRP are allowed in mountain areas.

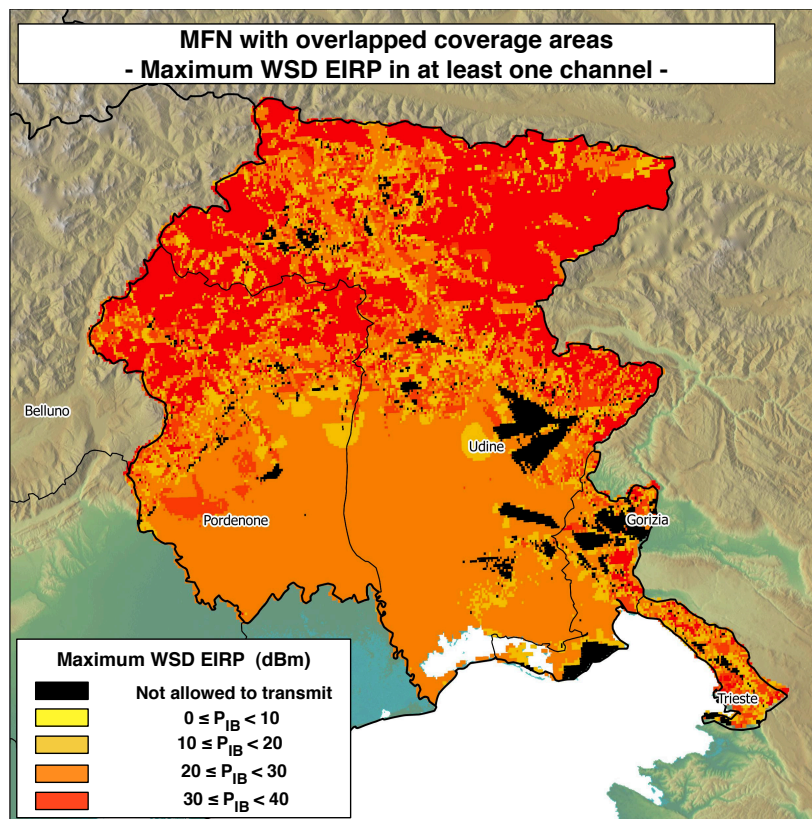


Figure 3.49: MFN with overlapped coverage areas in Friuli-Venezia Giulia: maximum WSD EIRP in at least one channel.

3.3.6 Comparison between MFN, SFN and k-SFN planning strategies

This section provides a comparison between the performance of the planning strategies considered in previous paragraphs. Figure 3.50 shows the complementary cumulative distribution function (CCDF) of the location probability per population for SFN, k-SFN and MFN planning configurations. As shown in previous paragraphs, all planning strategies provide very high location probabilities to a large percentage of population. As can be seen from the figure, k-SFN provides better performance than MFN planning. In fact location probabilities values greater than 0.95 can be provided to 93% of population with MFN, while with k-SFN to 98% of population.

k-SFN provides better performance than other planning strategies also because only self-interference from the network itself is taken into account. Each SFN manages the self-interference so that the interference from far installation is rejected. This does not occur in the single SFN where also self-interference from far installations, i.e. installations whose signal does not fall in the guard interval, is considered.

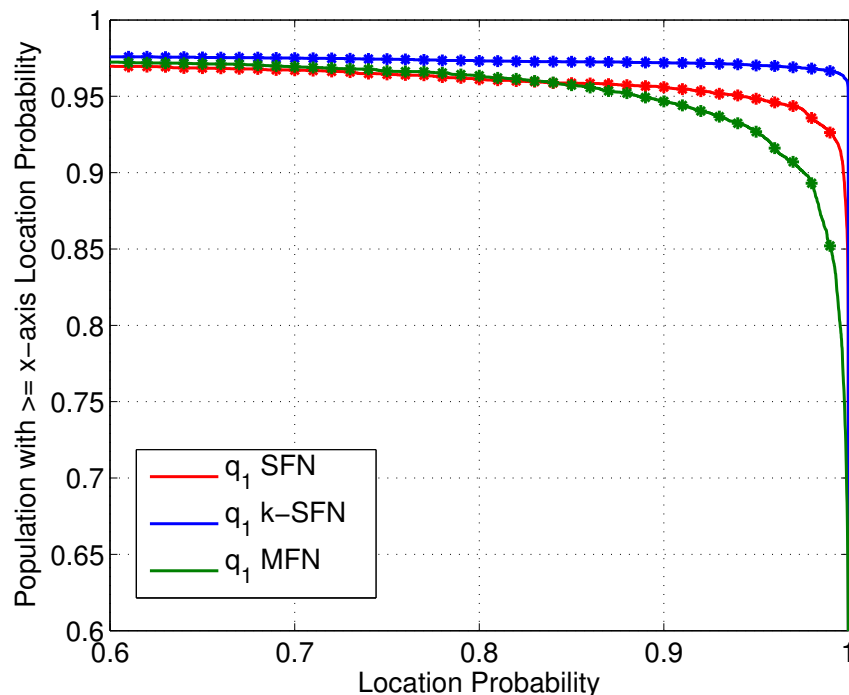


Figure 3.50: Complementary cumulative distribution function of the location probability per population for SFN, k-SFN and MFN planning strategies.

As a comparison measure for the different considered DTT plans, the EIRP limits are evaluated in each pixel. Figure 3.51 shows the cumulative distribution function

(CDF) of the WSD EIRP in at least one channel per population for SFN, k-SFN and MFN planning configurations. The curves represent the percentage of population living in pixels where the allowed WSD EIRP is lower than the corresponding values on the x-axis.

As highlighted in previous paragraph, MFN plan provides greater WSD EIRP if non-overlapped coverage areas are considered. The curve for the k-SFN case lies well below the one for the MFN, meaning that, for a given value of EIRP, a smaller percentage of population live in pixels where the resulting WSD EIRP is lower. We can see, for instance, that in case of k-SFN almost 90% of population live in pixels where a WSD EIRP of at least 20 dBm is allowed, while this value reduces to only 58% of population in case of MFN planning. The separation between two curves, in zones of practical interest, is in the order of 5 dB, which can be roughly taken as the gain of the k-SFN plan in terms of allowed WSD transmissions.

It has to be highlighted that the results of the SFN plan are obtained considering the transmission of the WSD on only one of the adjacent channel of that used by DTT service. Same levels of WSD EIRP can be considered for the use of the other adjacent channel. This translates in a greater efficiency of this planning example.

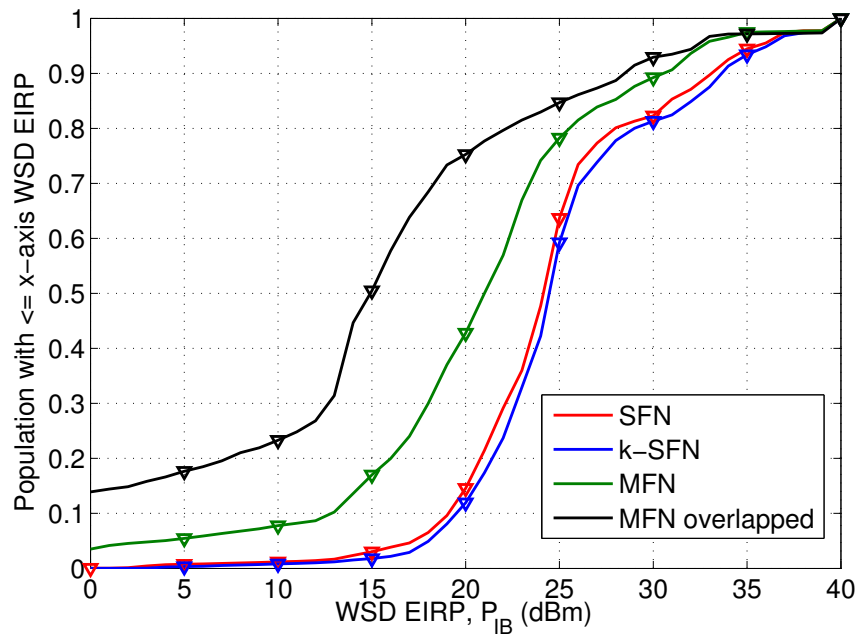


Figure 3.51: Cumulative distribution function of the maximum WSD EIRP in at least one channel per population for SFN, k-SFN and MFN planning strategies.

Chapter 4

Applications of Cognitive Radios

Cognitive radio has been introduced in the last years for better exploiting the limited available spectrum and the efficiency in the spectrum usage. Its main aim is to allow the co-existence of different wireless systems on the same spectral resources by limiting the mutual interference.

Recent developments in spectrum policy and regulatory domains in this context [22] open up interesting opportunities for cognitive radio to enable and support a variety of emerging applications, ranging from smart grid, public safety and broadband cellular, to medical applications [64].

This chapter presents how cognitive radio technology could support applications related to emergency management and could be implemented in hybrid satellite-terrestrial systems.

Emergency management is of the most important areas where technology innovation has direct impact on social well-being and sustainability. In the past few years, Information and Communication Technology (ICT) has proved to be instrumental to improve emergency management with particular focus on resilience, rapidity of response, adaptability to situations. To these ends, joint optimization of communication and computing is a promising cross-layer approach. Section 4.1 is focused on the consideration of both cognitive and autonomic networking approaches when deploying an emergency management system. The cognitive approach was initially considered specifically for wireless communications, while the autonomic approach was initially introduced for managing complex computing systems; however, they share several similarities in dealing with fully reconfigurable systems. The future

trend is to expand their influence toward the global optimization of the ICT infrastructure, as it is shown in this chapter for the specific case of emergency management systems. In section 4.1, firstly a description of the ICT emergency management requirements is provided; then attention will be focused on the communication infrastructure and the distributed computing infrastructure that constitute the two infrastructures combining to form the system. Finally, the cognitive and autonomic approach to emergency management will focus on how the cognitive and autonomic approaches allow to efficiently designing the communication and computing infrastructures in order to exploit them in an emergency scenario.

The second part of the chapter is about the cognitive hybrid satellite-terrestrial system. One of the main challenge in the context of cognitive radio, is to extend the cognitive paradigm also to satellite network by considering hybrid satellite and terrestrial scenarios. Aim of section 4.2 is to evaluate the coexistence of terrestrial and satellite networks by considering a cognitive approach when radio resources sharing is employed. The section deals with the presentation of a statistical interference model that aims at evaluating the mutual interference among the two systems. Firstly, the hybrid cognitive terrestrial satellite scenarios are introduced, by focusing the attention on the two reverse scenarios. Then the attention is focused on the terrestrial cognitive scenario, by introducing a stochastic model for evaluating the interference caused by the terrestrial wireless devices. Finally, numerical results for performance evaluation are described by taking into account the outage probability of having an undesired level of interference at the satellite side.

4.1 CR in Emergency Management Scenario

Emergency management and disaster recovery schemes have great importance in communities throughout the world: large scale emergencies like the earthquake in March 2011 in Japan with the following Tsunami and nuclear plant emergency have dramatically highlighted the need to pay close attention to all those instruments aiming at preventing or, at least, reducing the negative effects of disasters [65]. The main target of emergency management is to design a system having a good grade of resilience and autonomicity [66]. Resilience is intended here as the ability of the system of reacting to disastrous effects in the presence of infrastructural deficiencies. This is particularly important in all situations whereby the disaster seriously damages any critical infrastructure (e.g., electrical energy network, communication

infrastructure). In fact, several studies show that damaging any critical infrastructure can create a cascade effect on other ones, generating a critical scenario that takes a long time to be resolved [67]. Autonomicity stands for the ability of the system to react in a human-free way by following self-managing rules. As such, it is one of the most important characteristics to be taken into consideration when designing any emergency management system, so that the system can rapidly self-manage itself without requiring human intervention as, especially in these cases, the latter should be limited. Both characteristics require a high level of reconfigurability of the system, to circumvent obstacles and to react promptly to the disaster. An emergency scenario is characterized by the presence of several users and devices that must collaborate in order to have a ready response to the emergency situation, or to be able to forecast the upcoming emergency situation in time [68]. The coordination among different actors working on emergency management (institutions, local administrators, volunteers, police, etc) is fundamental in order to optimize emergency responses and to reduce disaster consequences on people and things.

The focus of the work in this context is toward the optimization of the communication infrastructure [69, 70, 71] with the aim of supporting emergency prevention and management operations. This requires reliable access to all heterogeneous networks and services in a ubiquitous manner, granted to all to people operating in the disaster area with different mobile devices and terminals (cellular phones, notebooks, smartphones, etc.). The emergency telecommunication infrastructure must be deployed in a simple and effective way in case of disaster and allow functional integration with the survived systems to provide a flexible platform able to satisfy the resilience and autonomicity requirements. One should notice that, nowadays, it is possible to consider an environment where multiple means of communication co-exist. This heterogeneity can be seen as a source of network diversity to be exploited in order to respect the different user requirements typical of an emergency scenario, whenever a disruptive event causes the unavailability of certain network portions.

It is worth noticing that emergency management is also strictly related to modelling the physical/artificial causes and consequences of disastrous situations. Emergency forecasting and management activities are both based on very complex mathematical models, which require high-performance computing to provide clients with prompt and best-effort services [72]. The most up to date trend within this context is to develop a system able to interconnect all operators and citizens within a given emergency area with high-performance computing platforms able to fore-

cast the disaster and/or to monitor its evolution [73]. It is worth noticing that the classical solution of high performance computing is to map the complex models to central processing centres supporting high performance architectures (e.g., clusters), but which are geographically far from the emergency area. An alternative solution is to exploit all locally available processing and communication resources, albeit heterogeneous and with limited computational capabilities [74]. This concept allows a more resilient approach to disaster management, due to the presence of multiple devices near the emergency area, to solve these complex models by exploiting the parallel and distributed computing features. However, this approach requires the development of suitable techniques to manage interconnections among users and computing devices with the timing constraint typical of such applications. The pervasive grid computing paradigm [75] is particularly suited for these applications by allowing the development of distributed applications that can perform parallel computations using heterogeneous devices interconnected by different types of communication technologies. Both computing and communication domains can be seen as a whole. The resources to be managed pertain both systems; these two domains jointly operate in a flexible manner. As shown in the following, this is key to the design of a resilient and autonomous system that can cope with different situations arising in an emergency management scenario. Moreover, an intelligent system, where a pervasive grid infrastructure is employed, can also exploit more efficiently all resources it offers in order to provide a fast solution to any problem. The focus is on the design of a flexible communication infrastructure that can exploit different communication and computing resources within the area in order to create a resilient and autonomic system. The concept of pervasive and cloud computing is introduced; however, attention is given to the communication infrastructure able to interconnect such computing devices and, at the same time, connect the users. The importance of a cooperative scheme to improve the detection performance and the efficiency in exchanging the information between devices is highlighted. Amongst several techniques, the attention has been focused on the cognitive and autonomic approaches that allow to efficiently designing a flexible and resilient communication infrastructure that can cope with the requirements. In particular the attention has been focused on the learning loops of the cognitive and autonomic approaches. It was shown that they can be seen as a single learning loop that can be adapted to the specific scenario that was dealt with. For this purpose the attention has been focused on the adaptation of the learning loop to the emergency management, thus

exploiting the most typical actions done in a cognitive and in an autonomic network for improving some actions done during emergency management operations. This allows to draw a path for the future implementation of emergency management infrastructure able to exploit the most modern techniques derived from the cognitive and autonomic concepts.

4.1.1 ICT Emergency Management Requirements

When faced with an emergency scenario, the nature of the emergency should first and foremost be understood. Emergency scenarios can be divided into three main classes:

- natural disasters;
- artificial disasters;
- homeland security.

The first class belongs to the emergency due to warnings or calamities involving nature: some typical examples for this type of disaster are earthquakes, floods, landslides, avalanches and hurricanes. Artificial disasters are characterized by the presence of man: some typical examples are pollution, means of transport, accidents in energy plants (e.g., nuclear, coal, gas). Finally, the homeland security class is a particular class of emergencies where the security of a nation can be endangered [76]: some typical examples are terrorist raids, wars, as well as border surveillance in particular zones, or the security of some specific areas of national interest (e.g., industrial or tourist sites) and critical infrastructures. The above described emergency scenarios can also be characterized by different timing impact during their management. To this purpose, it is useful to introduce the phases into which an emergency management system can be divided. They are the prevision phase, emergency phase and post-disaster management [68]. Their influence can vary depending on the type of disaster to take into account. However, for a more general analysis, all three phases should be considered:

- prediction and prevention of natural or manmade disasters, leading to the planning of specific monitoring activities and to the analysis of results arising from the monitoring campaign to access some heterogeneous networks;
- efficient handling of emergency activities with the aim of coordinating, designing, and verifying the restoration works;

- carrying out the operations following a natural disaster focused on rapid re-establishment of normal life conditions.

During the prevention of an emergency, the problem of monitoring a given scenario should be faced with the aim of forecasting the evolution of a certain environmental process. The emergency phase, which begins with an emergency warning and continues as long as the emergency lasts, is characterized by the integration of data incoming from the environment (e.g., provided by wireless sensor networks, earth observation) as well as the set-up of interconnections among all those operators that need to work in the emergency area. The communication requirements during this phase are characterized by different priorities, such as strict timing requirements and could have to face with the problem of partial infrastructure damage. The third phase is characterized by the reestablishment of the pre-emergency situation; at this phase emergency operators, as well as civilians, can access to the communication infrastructure until the normal operation re-establishment. It is also worth noticing that emergency management mathematical models have been developed during recent years. They aim of modelling almost all the problems that an emergency management system has to take into consideration. There are predicting models, to estimate an incoming disaster with certain reliability, or others to consider the interactions among humans and devices within an emergency scenario. The models are often very complex to solve, requiring high computational complexity by resorting to the solution of finite difference equations [72]. In [76] a homeland security model has been presented, focusing on the importance of a mutual optimization of communication and computing. The interested reader could refer to [77], where several disaster model are described; It can be noted that all these model are based on complex mathematical equations or even on the presence of distributed computing systems. As a final remark, also the satellite imaging is often used as a basis for the emergency forecasting or monitoring. Even in this case it is needed to resort to efficient computing systems for respect timing constraints [78]. While in the past centralized high performance computing structures have been used, the up to date trend is to exploit pervasive grid principle in order to perform the model computation in a faster way by using multiple devices also in remote areas. This trend is even more interesting to solve some algorithms also in emergency situations where some areas could become isolated. The focus herein is in the Information and Communication Technology (ICT) infrastructure, holding an important role in emergency management because of its ability to interconnect data sources, operators, civilians,

databases and many more resources that can be useful before, during and after a disaster and can help people needing assistance. On the other hand, as mentioned in the introduction, emergency and disaster management have to cope with a huge variety of cases. Hence, it is needed to draw an ICT infrastructure that fulfils all emergency management requirements. The basic requirements of an ICT infrastructure to cope with emergency and disaster management and to respect resilience and autonomicity characteristics can be summarized as follows:

- resilience/robustness;
- self-management;
- decision support system;
- interconnection/interoperability;
- mobility
- power-efficiency;
- broadcasting/multicasting;
- security;
- localization engine.

An emergency management system needs to be resilient in order to react very rapidly to environmental changes. The system here described is composed of several communication links and devices that can be based on different technologies; this heterogeneity is the key for a resilience system because it can be exploited to cope with any requirements incoming from emergency situations. In fact, by exploiting heterogeneity, the system can be reconfigured in order to overcome any infrastructure damage or specific requests of resources. Robustness stands for the ability of withstanding the environmental variations during the emergency. This characteristic allows the communication system to guarantee service continuity even during harsh conditions. This is particularly important when multiple users move in the emergency scenario and need to communicate with each other and with a central operator. The self-management characteristic is strictly related to the resilience because the system needs to self-organize to optimize its behaviour especially during disaster events, in order to respect the resiliency requirements in an autonomous way.

This characteristic increases the request of modelling the communication infrastructure by exploiting the autonomic principle as will be explained in the 4.1.2 section. Furthermore, the disaster management system needs to employ a decision support system with the ability of aiding the operators and the system itself to cope with the emergency situation and help the self-organization of the system. The communication infrastructure depends on the decision support system and has to be able to interconnect such devices composing the decision support system, even if distributed. Interconnection and interoperability refer to the ability of the system to work in a heterogeneous environment. This is one of the most important characteristics that a communication infrastructure needs to have. It is possible to model the system operating in a certain area as composed by multiple technologies with different and heterogeneous users. Furthermore, it is common to have an overlapping coverage of different technologies. At the same time most modern user terminals have the ability of connecting several technologies. On the other hand, many different terminals can communicate with different user requirements to carry voice, video, and data, with different data rate and QoS requirements. Hence, the requirement of the communication infrastructure is towards the exploitation of the multiple technologies present in the disaster area (and having survived the disaster) to interconnect the users, thus allowing a more resilient system. As concerns mobility and power-efficiency requirements, they are more strictly related to the ability of the network of communicating in a wireless way and interconnecting multiple users even when moving. This is a requirement allowing to build up a network composed of multiple devices, each one belonging to citizens or operators and to communicate even during the disaster until normal communication is reestablished. Thus, energy efficiency should be considered in such situations and solutions to reduce energy consumptions should be taken into account, also by taking into account that in an emergency situation each node can be of vital importance due to its relaying or multi-hopping behaviour. One of the most important characteristic of an emergency management infrastructure is to send warning in time to the citizens within the disaster area; this characteristic is well performed by using broadcast or multicast communications that, despite their unidirectional nature, allow a faster warning dispatch to the users. Security is a cross characteristic that, especially when considering disaster, emergency and homeland security scenarios, needs to be considered at the different layers of the system. The security can be considered from a broader point of view, especially in emergency management scenarios, when the paramount aim is to guarantee the secu-

rity to users, devices or, generally speaking, to the environment. However, security needs to be also taken into account by considering secure communications among all the actors, such as secure authentication and transportation of data streams, for the heterogeneous networks scenario. Finally, another important property that an emergency network could have is the localization engine. If operator terminals are able to accurately acquire their position, many operations can be performed in a much more efficient and effective manner: (i) operators can reach and rescue survivors trapped under the rubble faster, and the terminals could even evaluate a safe path from base camp to location in order to avoid further collapses, (ii) homeland security problem can be more easily solved thanks to a better coordination among security operators, (iii) in case of multiple terrorist attack policemen and soldiers can be automatically sent to the nearest treat.

4.1.2 Communication Infrastructure

The main aim of communication infrastructure is to support emergency prevention and management operations by allowing reliable access to heterogeneous networks and services in an ubiquitous manner to people operating in the disaster area with different mobile devices and terminals (i.e., smart phones, notebooks, personal digital assistant (PDA), etc.), as shown in figure 4.1. Attention should be focused on a twofold need: firstly, it is need to define alternative and effective telecommunication and processing means to deploy in a simple, and operative way in case of disaster. Furthermore, the communication infrastructure should guarantee an efficient integration with the existing systems and provide a flexible multimedia services platform in order to satisfy the multiple requirements arising during an emergency.

As already mentioned, one of the keys, when deploying an emergency management system, is reconfigurability. In recent years, CR paradigm [2] and cognitive networking [79] have been acquiring more and more importance: both are characterized by the great importance of the reconfigurability issue. In this section, the focus will be on their principle when designing a reliable and resilient system. In chapter 1 the characteristics of a CR network have been widely presented. As evident in the following, CR ability of using already assigned frequency resources in an opportunistic manner, along with reconfigurability options, is one of the most interesting characteristics for adopting the cognitive paradigm in the emergency management.

An extension toward whole network cognition has been also recently considered by introducing the cognitive networking concept [79]. By extending the cognitive

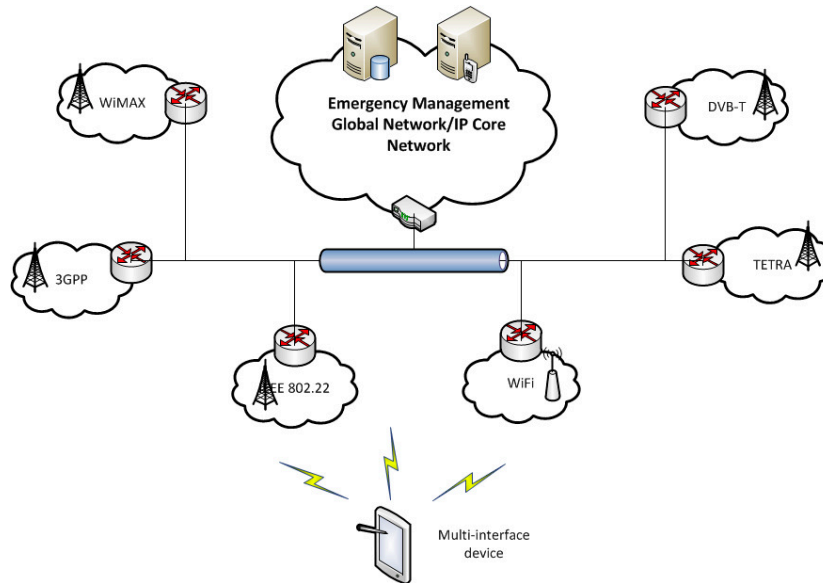


Figure 4.1: Communication Infrastructure.

principle of radio frequency and physical layers introduced by CR systems, cognitive networks aim of exporting the cognition also to the upper layers exploiting network resources (i.e., not only in terms of spectrum resources) to improve performance. Hence, the architecture becomes fully distributed and allows the exploitation of already deployed networks by other secondary networks.

In [80], a cognitive complete knowledge network system is shown. Unlike cognitive radio approach, which mostly focuses on radio proprieties and lower layer performance, a cross layer approach technique spans all layers of the protocol stack and explicitly addresses higher layer performance and adaptation issues. Such concept focuses more directly on the intelligent use of cognitive radio and cognitive networking, coupled with an application CR/user experience and reconfigurable protocol stacks, to make creative use of information that is naturally present and gathered in wireless systems. To achieve this, it also advocates the use of a cross layer paradigm, not only within a single device but also across different devices. A large amount of information gained from the experience of each node can be exploited to improve overall network and user performance. When considering cognitive networking, a similar cognitive loop showed for CRs can be introduced where the four steps are extended from the radio and spectrum parameters towards some higher layer parameters, by considering packets, streams and traffic analysis. Even if the parameters to be monitored and to be reconfigured are different, the learning loop has the same

basic functions.

The most important upgrade consists in the extension from link-to-link behaviour to end-to-end behaviour, which allows performance optimization of the entire network. This includes and extends the characteristics of routing and transport protocols which are able to flexibly redirect traffic towards unused or underused parts of networks. Such an approach needs both the sensing phase, i.e. monitoring of the network to have a map of its behaviour, and reconfigurability techniques that allow adapting a certain protocol in order to exploit such underused resources. The cognitive networking approach is even more interesting when applied to the emergency scenario. As already noticed in figure 4.1, such scenario is formed by several devices, often equipped with more than one technology; they are often referred to as multi-interface devices as characterized by multiple radio interfaces. This allows them to connect with different wireless networks even at the same time. Their main characteristic is to allow the different technologies to supplement each other and not to compete for the bandwidth.

4.1.3 Distributed Computing Infrastructure

As mentioned previously, an ICT infrastructure to be used for emergency management scenarios should also consider a processing layer. In particular, the interaction between distributed computing infrastructure and high performance computing in terms of pervasiveness and resilience should be envisaged. The main paradigms that allow wide-area computing in distributed fashion are represented by grid and cloud computing. Even if originally disjointed, due to the recent developments in terms of communication reliability and data rate, on one hand, and the increasing hardware capabilities even in low-end devices. On the other, the two domains can be considered as overlapping, by thinking of it as a new cloud computing environment realized by using pervasive grid infrastructure [75]. The grid and cloud computing scenario is characterized by fixed and mobile nodes having different computing power and interconnected by heterogeneous wired and wireless links. This implies that different communication technologies with heterogeneous rate and delay profiles need to be evaluated. This is one of the most common scenarios that could be studied when considering an emergency management situation: the goal is to use all resources around the disaster area thus exploiting them independently from their technology [81]. The pervasive grid paradigm is strictly related to the computational grid concept; from this point of view, the computing architecture is composed

of a central computing centre made of clusters of fixed nodes providing a set of services on the outside. A user can exploit them through a pervasive infrastructure allowing a completely transparent access to the end-user at the computing centre. Pervasive infrastructure can be composed by heterogeneous networks, and devices with different computing power and equipped with different software. Pervasive grid computing represents a significant innovation because, in this case, computing resources are "widespread"; for this reason not only a cluster of workstations can take part in a distributed and parallel computing process, but also a mobile device can be used as computing node. The key aspects of distributed application are:

- context-awareness;
- self-adapting;
- QoS-awareness.

In the literature, distributed several computing models are presented trying to address the context-awareness problem [82]. It is important to note that this aspect is strictly related to the self-adaptivity problem. If a change is detected in the computing resource set (e.g., central processing unit CPU is overloaded or personal digital assistant PDA battery is exhausted), the distributed application should react to this change in order to preserve, e.g., the integrity of a result in a distributed problem solving process. QoS problem related to grid paradigm has been addressed in the literature jointly with resource discovery problem and optimal processing task allocation: a processing task should be completed according to the service level agreement between the user and the organization holding the computing infrastructure [83]. A processing task should be mapped in a set of nodes with enough computing power; they can be identified only through efficient resource discovery technique. The pervasive grid concept could to be fully exploited especially in an emergency management scenario where reconfigurability becomes an issue. As mentioned earlier, the focus is on communication infrastructure. The autonomic networking [84] concept has been introduced as an extension of the autonomic computing concept [85] and it is particularly interesting because it allows to define a new infrastructure composed of both communication and computing resources, thus exploiting the pervasive grid potentialities. As highlighted in figure 4.2, the autonomic networking approach can be seen as a further step of the cognitive networking approach toward a fully reconfigurable environment. While in cognitive approach the system adapts

itself to the primary network for exploiting some unused resources, in autonomic one, an environment where all variables can be reconfigured independently from a highest system is considered thus aiming to a global optimization.

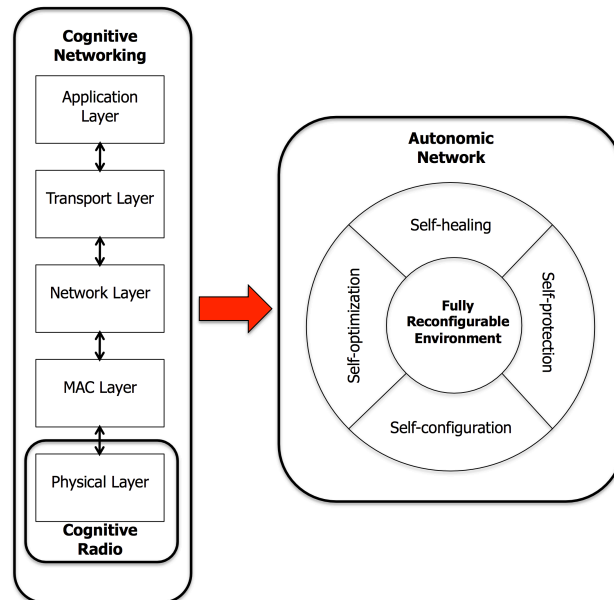


Figure 4.2: The cognitive and autonomic approaches interdependency.

Taking inspiration from the operation of the autonomic nervous system (ANS) in biology, autonomic systems are based on the presence of four main features:

- Self-healing: discover and repair any potential problems to avoid them in the running system.
- Self-protection: identify warning and take countermeasures.
- Self-configuration: automatically maintain the system by installing applications, patches and updates, with the aim of verifying compliance with specified service levels, and optimizing configuration of applications.
- Self-optimization: monitor the goals of the system to ensure that they are pursued.

When applied to communication systems, the four above listed properties must be appropriately interpreted. When considering self-healing, the aim is to consider any communication systems able to autonomously detect, diagnose and repair localized communication problems resulting from software or hardware failures. Self-protection is the need for a communication network to automatically work against

any security failure; this is the case for protection against external attacks, security bugs, viruses, or any other problem that can decrease communication security. As for self-configuration, a system is a self-configuring one if a collection of units coordinates to achieve a goal more efficiently without any explicit human direction. Self-configuration can be defined as the emergence of system-wide adaptive structures and functionalities from simple local interactions between individual entities. Self-optimization is applied to avoid time consuming efforts with hundreds of manually set and non-linear tuning parameters. A self-optimizing network is able to overcome this problem automatically by updating its configuration on the fly to enable optimal behaviour in response to any changes [84]. In order to implement the above mentioned features, an autonomic system needs to be able to have a minimum set of properties allowing to autonomously manage itself without any external intervention. These properties are awareness, adaptivity, and autonomy. Awareness is the ability of monitoring the operational environment and the internal state of any and all entities. Adaptivity exploits the capacity of changing the internal configuration, state and functions to cope with temporal and spatial modifications of the environment, in a wide sense. Autonomy corresponds to the ability of making some independent decisions on adapting to the environment based on the entity's awareness of change. Also the autonomic system can be represented as a learning loop [84]. As shown in figure 4.3, the system collects information from a variety of sources, including environmental sensors, user context, application requirements, network instrumentations as well as feedback from the network. The sensed information includes a large variety of categories mainly related to different characteristics of the network at different protocol layers, as well as concerning environmental information, or network input such as user requirements, QoS requirements, and network status. The main aim of the sensing phase is to acquire knowledge about the surrounding environment to estimate its status.

As better detailed in the following, in case of an emergency management situation the environment should be sensed for possible disaster warning, but also about computing and networking environment in order to be able to know the resources that can be exploited during the decision phase. The output of the sensing phase needs to be analysed to construct a model of the evolving situation faced by the network and its services; this model is then used as a basis for adaptation decisions. For this reason the autonomic loop foresees the presence of multiple algorithms devoted to this phase (e.g., game theory, economic models, inference, rules and policies)

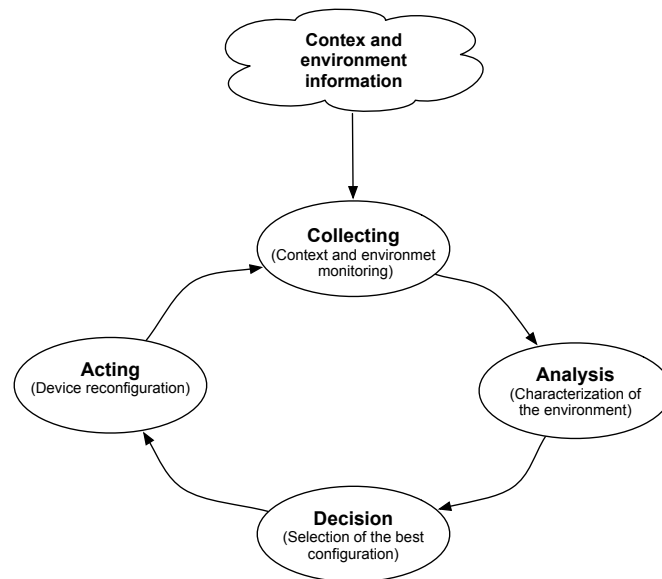


Figure 4.3: The automic learning loop.

[84]. The analysis output is used as input for the decision phase which is performed through the network and will potentially be reported to users or administrators. The decision phase is devoted to control and optimize the system and includes those operations needed to decide which variables, protocols, and resources should be managed. From the communication point of view, the acting phase is the most important aspect. In fact during this phase the communication protocols are used and the resource allocation is enforced: each algorithm and technique within the network performs an action following the analysis of the previous phase in order to fulfil the aim of the automic network. Hence, all system variables are reconfigured in order to optimize the system and, depending on the emergency phase, to prevent possible disaster or manage the operators working within the emergency area. Furthermore, in acting state complex evolutionary models are processed also in emergency areas that are far and disconnected from the rest of the system. It is quite clear how an automic approach, within a fully reconfigurable system, also gives the possibilities to have a more resilient environment able to minimize the detrimental effect of an emergency situation.

4.1.4 Cognitive and Autonomic Approach to Emergency Management

Emergency management refers to the definition of a common framework used by communities to reduce vulnerability to hazards and cope with disasters. The importance of the cognitive and autonomic concepts in designing future networks has been highlighted. In this section the attention is focused on emergency management communication networks based on cognitive and autonomic principles. The reference architecture for emergency management communications has been developed within Project MESA [86]. Following Project MESA statements, the whole network can be seen as composed of several communication networks. On the other hand, large parts of the world are already covered by public communication systems (e.g., UMTS, WiMAX, Wi-Fi) or, in some cases, by institutional communication systems (e.g., TETRA). This leads to the definition of a communication infrastructure that can exploit already deployed resources. At the same time, by focusing on emergency scenarios, several users with different duties are present in the disaster area or nearby. In the 4.1.1 section, the requirements of an emergency management infrastructure have been presented. It becomes clear that, having to interact with such heterogeneous scenario, composed of several users with different requirements both in terms of applications and importance, and with several interacting networks, reconfiguration is the key. Within this field, the latest reconfigurability techniques should be taken into account with particular stress on cognitive and autonomic approaches. These techniques foresee the possibility of reconfiguring the communication infrastructure at different protocol stack layers and adapting the processing layer also in a synergistic way [87]. Their effort can be exploited in function of the different protocols or layers in which it would need to work or by considering different parallelization structures. The focus here is on communication infrastructure reconfigurability, mainly exploiting the methodologies offered by CRs, cognitive networking and autonomic networking approaches to design a more efficient framework for managing emergency situations. Firstly the attention was focused on the management of an emergency scenario at system level by exploiting the concepts of cognitive and autonomic networking, to achieve a global vision on the state of the network: through cognitive networking, it is possible to have knowledge of network elements while the autonomic network manages global optimization of the system. Concerning the cognitive and autonomic networking concept jointly to manage an emergency scenario, the cognition loop showed in figure 4.4 can be taken as ref-

erence. It is composed by four main phases: sensing, analysis, management and reconfigurability. It can be noted that each phase has a wide meaning including functionalities belonging physical as well as upper and even computing layers.

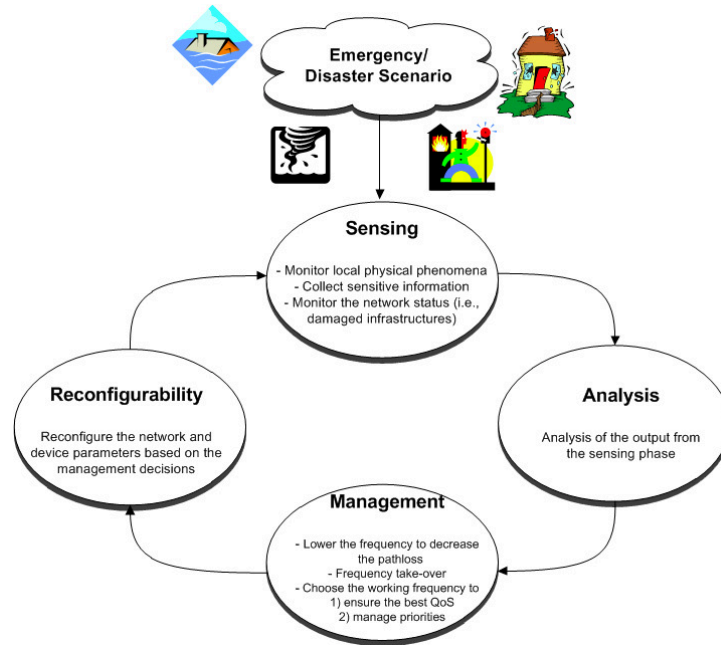


Figure 4.4: Emergency Management learning loop.

The sensing phase is responsible for sensing the network environment. This could be of primary importance when managing an emergency scenario. Let consider the time interval after an emergency warning has been broadcast or when a disaster has occurred. In this scenario, some portions of communication infrastructure can be damaged or some sectors of the network could be congested due to the intensive access request by citizens and operators; a system vision can detect these situations. The cognitive and autonomic sensing phase is fundamental, because it can detect communication infrastructure damage by sensing the under-usage of such network. This information can be used for reconfiguring and optimizing the system, but also as a means to get to know about network damage remotely. Some efficient algorithms are useful during this phase for a more suitable sensing and monitoring of network resources. The designed framework is based on the presence of resources belonging to communication infrastructure as well as to computing infrastructure. Within this context, it is important to develop some suitable resource discovering techniques able to sense and have an updated map of the system. In the literature, there are several resource discovery techniques and several frameworks able

to guarantee specific QoS requirements, within a certain path between source and destination nodes. This leads to complexity of the distributed application and to an increasing in the signalling traffic that could decrease the performance of the network. Hence, integration between resource discovery and routing becomes convenient. Such designing scheme allows to avoid specific framework for QoS management: each node can fill its own network resource map. After a disaster warning or during the disaster itself, the whole network should respect users and QoS requirements to allow faster communications among operators and citizens. This requires fast reconfiguration of network elements that can be achieved during the cognitive and autonomic networking reconfigurability phase where a reconfiguration of communication protocols from an end-to-end point of view is performed. In that sense, it will be considered a scenario where multiple wireless communication technologies coexist, allowing the choice of different paths with different link layer technologies among the nodes. At network layer, reconfiguration techniques need to be taken into account with the aim of updating the routing tables by considering flat, hierarchical, cluster, or mixed architectures, based on the emergency scenario. The routing protocol requires a periodic exchange of messages in the network bearing the information on the nodes and links status. Hence, it follows that on demand routing approach is not the best option; in this case the routing messages are exchanged among nodes only when a packet is ready to be sent to a certain destination, and its definition has a specific rule in the choice of scheduling and mapping policies, aided by the information routed through the routing messages. On the other hand, proactive or link state protocols, meet the requirements. QoS-driven routing policy aims not only at identifying the route between a source and a destination node, but also at selecting the route able to respect QoS requisites globally. The development of an autonomic routing algorithm should be considered by integrating both the information deriving from communication and computing points of view. In that sense, the network layer should consider the communication and computing resources as integrated, when searching for a certain path. As mentioned before, the emergency environment is often composed of several overlapping wireless networks and with multi-interface terminals that can connect different technologies. The main characteristic of these devices is to allow the different technologies to support each other and not to compete for the bandwidth. A typical example is 3G technology that has a broad coverage, medium bandwidth and higher access cost, and IEEE 802.11x technologies that are broadband, low cost, but with low coverage area. This

heterogeneity can be an advantage for the mobile devices, especially in emergency scenarios, thanks to the exploitation of multi-interface solutions, by selecting the best interface to optimize the system. The recently approved IEEE 802.21 standard allows a rapid and seamless vertical handover by lowering out-of-service time interval and better exploitation of device interfaces [88]. The global vision given by cognitive networking and autonomic network about the state of the entire system can help the management of single critical situations by CR devices. As described in 4.1.2 section, CRs are able to sense and detect radio signals, find available channels on which to roam from band to band and network to network. Users would dynamically access spectrum and shared infrastructures. CR characteristics (e.g., spectrum sensing, policy-based operation and ability to rapidly change frequencies, power, bandwidth, and waveform) together with the information given by a higher level point of view would ultimately empower a much more robust communications paradigm for public safety. The idea of applying CR to emergency networks also tries to compensate limited availability and inefficiency in spectrum usage. Indeed, today's spectrum scarcity problem in wireless networks affects emergency networks as well. By dynamically accessing free spectrum resources, CRs are able to communicate in shared channels, work in multi-band, combine frequency bands, cope with various wireless channels and support various services. From an emergency management point of view, the cognitive radio loop can be exploited as described in the following. Through spectrum sensing and spectrum analysis, CR monitors the available spectrum bands, captures their information, detects and estimates the characteristics of spectrum holes. Hence, thanks to the capability of using or sharing the spectrum in an opportunistic way and the ability of capturing the temporal and spatial variations in radio environment, CR can be exploited to exchange data between Wireless Sensor Network (WSN) components. In fact, in each phase of an emergency, WSN and mobile ad hoc network (MANET) are employed to monitor local physical phenomena and collect sensitive information (e.g., the water level of a river or the pollution in a city). Usually, the communication between sensor nodes (in a multi-hop configuration) between sensor nodes and sink nodes and between sink nodes and local monitoring centre occurs through a dedicated channel. So CR techniques can be used in WSN to exchange data with the advantage that a dedicated frequency range for communication is not needed. Furthermore, during the sensing phase, CRs are able to monitor primary infrastructure activity. Considering a critical area prone to environmental calamity, the monitoring of BSs activity, by

deploying CR devices in the area, could be useful. Each device compares periodically the received pilot power with a predefined threshold. Through centralized cooperative sensing, a central unit collects sensing information from cognitive devices and decides if a BS can be considered active. If the central unit reveals the inactivity of a BS, it alerts a special centre that, if needed, starts the emergency management. Management and reconfigurability phases of the cognition loop allow CR devices to select the best frequency band and adjust operating parameters for transmission on the fly so that they can adapt easily to the dynamic radio environment. Referring to figure 4.5, a framework of wireless emergency communications is proposed for communications in disaster scenarios based on relaying and CR. After the damaging of a BS, an Emergency communications car (Ecc) could be employed to temporarily substitute the BS. Due to the poor capability of the Ecc to cover the needs of throughput and coverage of the original network, uncovered areas are still present. So, if a Mobile Terminal (MT) is not able to access the BS, it will try to work in a relay mode exploiting a MT closer to the Ecc. If MT3 with cognitive skills is considered, which still cannot access the network by relaying, it will lower its frequency in order to decrease pathloss effect. This can be done by exploiting CR functions. In fact, during the sensing phase, the CR could find a set of available frequencies, select the lower to enhance coverage, according to the signalling from the adjacent BS, and communicate it to MT3. An extension of this framework is the use of CR devices as relays. Let us consider the emergency scenario in which the operators of each network (e.g., TV or WiMAX operators) can decide to limit their primary services in order to leave their frequencies free for emergency communications. This function that can be called *frequency take-over* can allow CR devices to detect the unused spectrum through sensing. Thus, they communicate the revealed free frequency range to an operational centre and, if it does not correspond to a damaged BS, they are allowed to transmit on these frequencies. As shown in figure 4.5, when the CR device receives the information from MT3, it can decide to forward the signal to Ecc or directly to primary BS (e.g., WiMAX BS). This could be an effective scenario because in the emergency phase, a communication among the operators is preferable to ensure DVB-T or Wireless Metropolitan Area Network (WMAN) communication link. This scenario corresponds to consider a CR as the primary user of that frequency range. In this phase CR devices acquire a very important role becoming the only one system to transmit on that frequency. During this phase, CR devices should not worry about interfering with other primary users

in the frequencies that they are using. As soon as the emergency phase is over, they should leave the frequencies and return to sensing the electromagnetic environment to find other spectrum holes to transmit on.

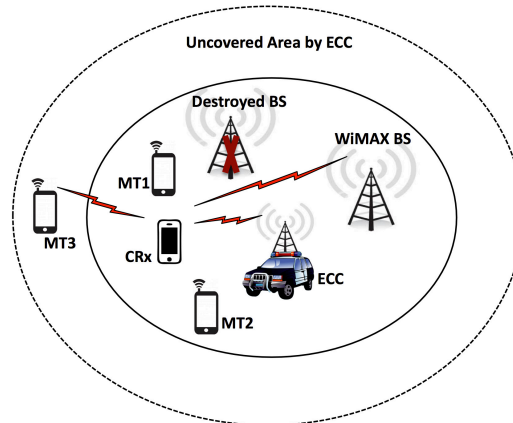


Figure 4.5: The relaying cognitive scenario.

Another issue to be considered is that, in order to maintain communications, the emergency communication network must provide enough capacity to guarantee QoS for multiple services. Thanks to the ability of CR systems to operate over a wide frequency range and switch between them in real time, they can choose the best working frequency to transmit on in order to guarantee the best quality for a communication link. On the other hand, in an emergency scenario, the network should be able to manage different priority: terminals that communicate with different user requirements to carry voice, video, and data, with different data rate and QoS requirements. CR systems can be used to support wideband or broadband voice or data applications and different user requirements by exploiting reconfigurable architecture, supporting multiband and adaptive operations. Furthermore, taking advantage by combining non contiguous channels, it is possible to properly allocate network resources to assign priority to critical applications, such as real-time applications or video services that have more stringent band requirements. For example, two communicating radios might support a wideband data service by selecting several channels flanking both ends of spectrum supporting a single priority narrowband voice session. The learning cycle can be specialized for the specific interests of emergency management.

4.2 CR in Hybrid Satellite-Terrestrial System

As highlighted in previous chapter, the main advantage of the cognitive approach is to allow the coexistence of multiple networks on the same transmission resources. The essential condition is that secondary users do not generate harmful interference towards the so called primary users. In order to fulfil these requirements, the CR systems are based on sensing and reconfigurability characteristics aiming at obtaining a knowledge of the surrounding environment and adapting to it.

One of the most important issue that has been recently highlighted in the cognitive radio community is to consider also those spectrum resources already occupied. While in the past we were talking about white spaces as those spectrum resource free of any other communications and black spaces as those occupied, it has been recently introduced the gray spaces concept as those spectrum resources occupied by the primary network [89]. The advantage of the gray spaces is that they can be exploited by cognitive devices, only after an accurate transmission power tuning, able to minimize the interference toward the primary network.

Differently from other approaches, hybrid satellite and terrestrial communications have been considered by taking into account both scenarios where terrestrial communications and satellite communications are, in turn, the primary or the secondary networks. The idea of such hybrid system is not new [90], however it is not been explored sufficiently in the literature.

The gray space concept is particularly important in such hybrid context mainly due to the broadcasting nature of the satellite communications. Main challenges of such scenario is that the satellite component has less degree of reconfigurability due to the higher requirements on terms of network planning and due also the higher round trip delays involved. Moreover, when considering a satellite communications, the problem that most of the services cover a very huge area, even a whole continent has to be considered.

The aim of this work is to evaluate a hybrid cognitive scenario where the terrestrial component is seen as secondary. In order to evaluate the interference caused by the terrestrial transmission, an appropriate statistical model has been exploited allowing us to estimate with a stochastic approach the total amount of interference caused by the terrestrial cognitive devices. Numerical results obtained through computer simulations show that the transmission is possible, given a certain threshold. In particular, the performance has been evaluated in terms of outage probability.

4.2.1 Hybrid Cognitive Terrestrial-Satellite Scenarios

Cognitive Radio strategies are strictly related to their operating environment. In this section, two hybrid satellite-terrestrial scenarios are taken into account, which differ in the role played by the two systems within the overall Cognitive Radio system.

In the first case, the satellite network is assumed to be the secondary system which exploits the spectrum holes left by the terrestrial system which acts as primary network and, therefore, has the license to operate in a certain area by occupying a specified spectrum band. As it is well-known, the secondary system does not have a license to work in a desired band but, being "cognitive", it can exploit the unused resources of the licensed system. This can happen if the cognitive devices are able to use efficiently the radio spectrum, without interfering with the licensed communication service.

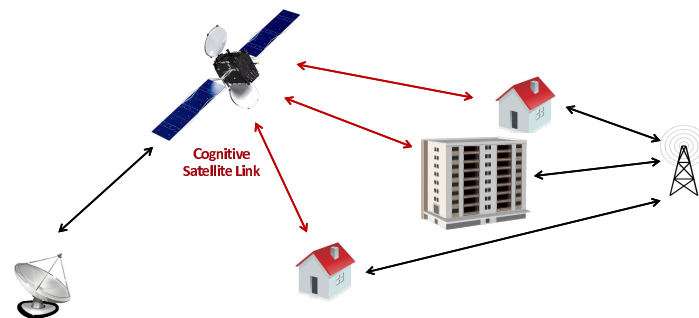


Figure 4.6: Example of cognitive satellite system.

An example of such scenario is reported in figure 4.6 where both satellite down-links and up-links can be considered cognitive links whereas the satellite feeder link is assumed to have a dedicated spectrum portion.

A critical issue is the assumption that satellite down-links are cognitive links. In fact, in this case, the large coverage area provided by the satellite and the potential high interference that it could cause to the primary system, can make hard to perform dynamic spectrum sharing, [90] so it could be reasonable to consider the adoption of CR strategies in conjunction with traditional spectrum band alloca-

tion strategies in order to guarantee the satellite transmission and to exploit unused frequency bands only for extending network capacity.

Differently from the previous case, the second scenario is characterized by a licensed primary satellite system and a secondary terrestrial wireless system. Both systems work in the same band and exploit a context of coexistence in which the secondary network is allowed taking resources from the other system without interfering in its normal operations. In particular, the secondary system can select resources among the frequencies unused by the primary system in a given time interval and in a given location but also exploiting the gray spaces taking under control its interference toward the licensed system.

In this latter scenario it is important to investigate the impact of the overall interference produced by cognitive network on the satellite system. The model proposed in the next section aims at evaluating and modelling such interference in order to perform an assessment of the capability of the cognitive system.

4.2.2 The stochastic geometry interference model

In this Section, a simple model which allows to take into account the interference generated by terrestrial cognitive devices on the uplink of a satellite-terrestrial system when considering a co-channel cognitive radio network is provided. Due to the huge dimension of the footprint of a typical satellite link, the analysis of the interference cannot be done by considering a deterministic approach.

The proposed model is based on stochastic geometry, which is a powerful and flexible tool as it allows to take into account the randomness of the spatial positions of the cognitive device. The considered scenario in the following is shown in figure 4.7.

Ground Station (GS) transmitting with Effective Radiated Power (ERP) P_0G_0 is considered, where P_0 and G_0 are the transmitted power and the antenna gain respectively, and a satellite receiving with antenna gain equal to G_S . The satellite is on a Geostationary orbit, thus, the distance between the GS and the satellite is around $L=36000$ km. In the proximity of the GS there is an interfering network spatially deployed as a 2D Poisson Point Process Φ with density λ_{int} , in which each interfering terminal transmits an ERP equal to $P_I G_I$, with P_I and G_I being respectively the transmitted power and the antenna gain of the cognitive devices.

The aim is to evaluate the outage probability, defined as the probability that the cognitive device power is higher than a certain threshold, as a function of the

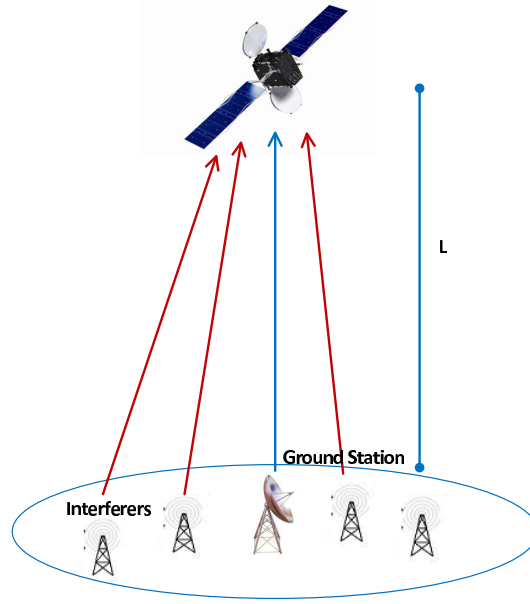


Figure 4.7: Cognitive terrestrial system.

aggregate interference generated by the 2D Poisson Point Process Φ , which is given by:

$$\mathcal{I}_{\Phi} = \sum_{i \in \Phi} |\tilde{h}_i|^2 R_i^{-\alpha} \quad (4.1)$$

where $|\tilde{h}_i|^2$ are the normalized channel gains on the interfering links, $R_i^{-\alpha}$ is the distance between the i -th interferer and the satellite, α is the path-loss exponent of the exponential-decaying propagation model, with $\alpha > 2$, and the summation is performed over all the cognitive devices belonging to the process Φ . Please note that (4.1) shows the normalized aggregate interference.

The interfering links have been assumed affected by Rayleigh fading, thus, the PDF of the normalized channel gains is given by $f_{|\tilde{h}_i|^2}(\xi) = \exp(-\xi)$. Moreover, considering that the distance from the ground to the satellite is significantly greater than the interfering area radius, all the cognitive devices are assumed to be at a distance L , i.e., $R_i^{-\alpha} = L$, $\forall i \in \Phi$. Thus, for the interfering links, the following simplified propagation behaviour has been assumed: at the beginning (i.e., as long as the interfering signals do not get over the foliage), an exponential-decaying path loss model with $\alpha \sim 2$ is present, and then an almost free space propagation from the ground to the satellite, i.e. a path loss given by L^{-2} for all the cognitive devices.

Under these assumptions, the outage probability can be written as:

$$P_{out} = 1 - \mathbb{P}[\text{SINR} > T] = \mathbb{P}\left[\frac{P_0 G_0 G_S L^{-2}}{\sigma_N^2 + P_I G_I G_S L^{-2} \mathcal{I}_\Phi}\right] \quad (4.2)$$

where SINR is the Signal-to-Interference plus Noise-Ratio, σ_N^2 is the Additive White Gaussian Noise power and T is the SINR threshold above which the useful link is considered to be still working.

Under the assumptions of this work, the useful link is deterministic and thus in the (4.2) the only source of randomness is given by the aggregate interference. The outage probability can be written as:

$$\mathbb{P}[\mathcal{I}_\Phi > T_I] = 1 - F_{\mathcal{I}_\Phi}(T_I) \quad (4.3)$$

where $F_{\mathcal{I}_\Phi}(x)$ is the cumulative distribution function (CDF) of the aggregate interference, and T_I is the interference level above which the useful link is not working anymore, i.e., evaluating the outage probability as the probability that the interference exceeds a given maximum level

$$T_I = \frac{P_0 G_0 G_S L^{-2} - T \sigma_N^2}{T P_I G_I G_S L^{-2}} \quad (4.4)$$

In [91], it was shown that the CDF of a positive random variable can be obtained through numerical inversion of its Laplace transform. In this case, the Laplace transform of the CDF of \mathcal{I}_Φ can be written in terms of its Moment Generating Function (MGF), as

$$\widehat{F}_{\mathcal{I}_\Phi}(s) = \mathcal{M}_{\mathcal{I}_\Phi}(s)/s$$

where $\mathcal{M}_{\mathcal{I}_\Phi}(s)$ and $\widehat{F}_{\mathcal{I}_\Phi}(s)$ are the MGF and the CDF Laplace transform of \mathcal{I}_Φ .

The MGF of the aggregate interference was found in [92] for a cellular network over Rayleigh fading channels, where the cognitive devices were deployed outside a given radius (exclusion region) r equal to the distance between the intended Mobile Station and its closest Base Station. By setting the radius of the exclusion region to a small enough value, as the cognitive devices deployed on the whole area around the GS, the same MGF by simply setting $r = R$ can be considered:

$$\begin{aligned} \mathcal{M}_{\mathcal{I}_\Phi}(s) = & \exp[\pi \lambda_{int} R^2] \times \exp\left[-\frac{\pi \lambda_{int} R^2}{1 + s R^{-\alpha}}\right] \times \\ & \times \exp\left[-\frac{\pi \lambda_{int} s R^{2-\alpha} {}_2F_1\left(2; 1; 2 - \frac{2}{\alpha}; \frac{s}{s + R^\alpha}\right)}{\left(1 - \frac{2}{\alpha}\right) (1 + s R^{-\alpha})^2}\right] \end{aligned} \quad (4.5)$$

By applying the numerical inversion of the MGF of the aggregate interference provided in (4.5), it is possible to estimate its CDF, and, thus, the outage probability. It is important to notice that this model is not a function of the cognitive devices area dimension, but only of their density λ_{int} . This behaviour is due to the computation of the MGF proposed in [92], as for large enough radius of the cellular network, the interference behaviour is the same as that of an infinite cognitive device area.

The radius above which the aggregate interference in a finite area can be considered equivalent to that of an infinite area can be easily obtained with the procedure provided in [93]. In this scenario, considering the dimensions of a satellite ground spot, the aggregate interference can indeed be compared to the infinite area case.

4.2.3 Numerical Results

This section presents numerical results obtained through computer simulations when applying the proposed statistical interference model. As stated above, a small enough value of the exclusion region radius R and a path-loss exponent α close to 2 have been selected, since the model provided in [92] is valid for $\alpha > 2$.

It was set α equal to 2.1, while R was set equal to 0.1 m. For the satellite-terrestrial system, some typical values for the C Band have been chosen: the useful link ERP is $P_0G_0 = 77.83$ dBW, the satellite antenna gain is $G_S = 34.65$ dBi and the noise power over a 36 MHz channel is given by $\sigma_N^2 = N_0B = -128.44$ dBW, with $N_0 = -204$ dBm.

Figures 4.8 -4.10 show the outage probability for different values of the cognitive devices density and their transmitted ERP, in particular $\lambda_{int} = 10^{-2}, 10^{-4}, 10^{-6}$ m⁻² and $P_I G_I = 60, 70, 80$ dBW.

The results are focused on the outage probability as a function of the SINR threshold T , but it is worthwhile highlighting that the variability on the performance is completely given by the aggregate interference through the modified threshold T_I (which is a function of T as well as of the other simulation parameters).

It can be noticed that, increasing the cognitive devices ERP value, it is generated more interference, and thus the outage probability increases correspondingly. A higher value of the threshold also causes an increase in outage probability as it corresponds to more demanding SINR performance.

The outage probability also increases for higher values of the cognitive devices density λ_{int} , but the outage probability takes significant values only for $\lambda_{int} = 10^{-2}$ or 10^{-4} m⁻², while for $\lambda_{int} = 10^{-6}$ m⁻² the effect of the interference is negligible

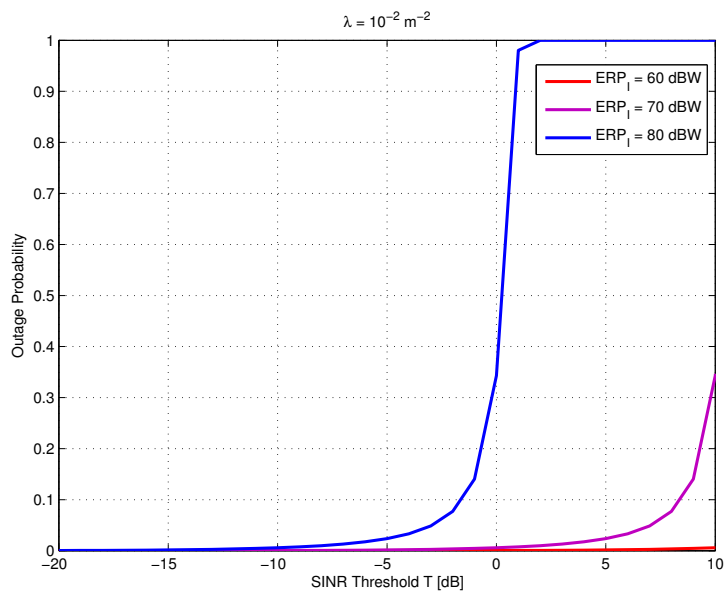


Figure 4.8: Outage probability with $\lambda_{int} = 10^{-2} \text{ m}^{-2}$.

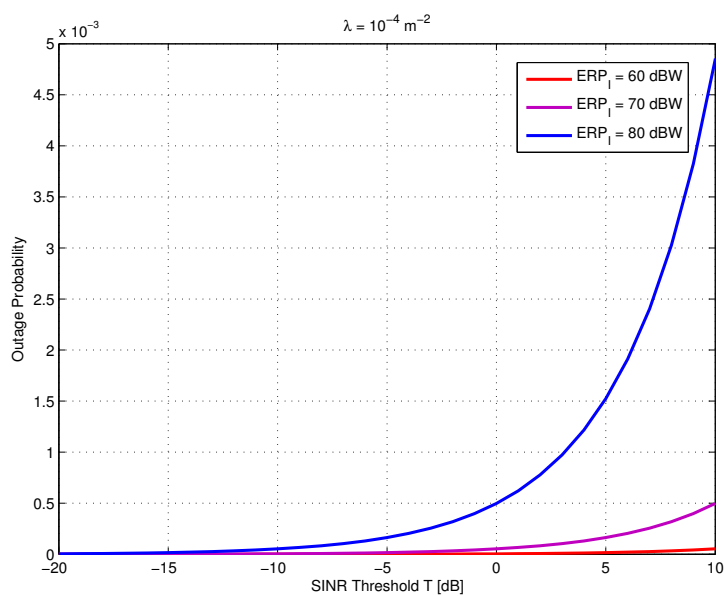


Figure 4.9: Outage probability with $\lambda_{int} = 10^{-4} \text{ m}^{-2}$.

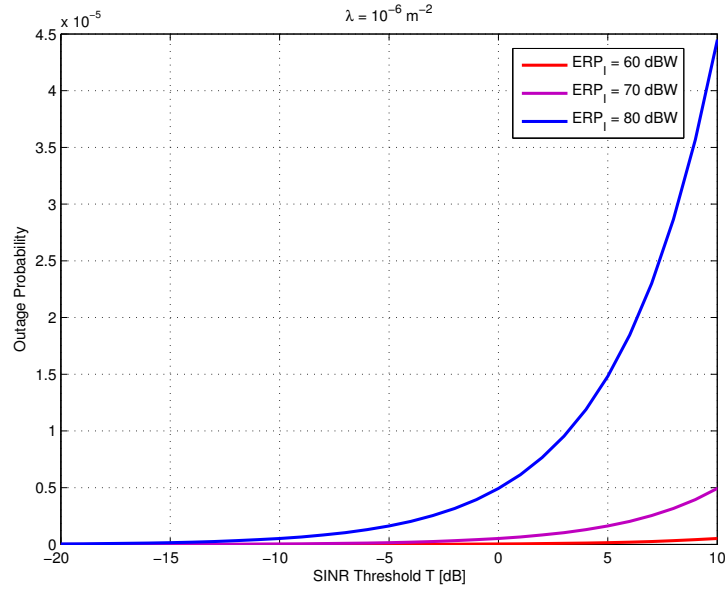


Figure 4.10: Outage probability with $\lambda_{int} = 10^{-6} \text{ m}^{-2}$.

($5 \cdot 10^{-3} \%$ for a 10 dB threshold T).

This is probably due to the simple propagation model considered in this work: as a matter of fact, by applying the MGF-based approach it is equivalent to consider the MGF of the aggregate interference as if it was evaluated at the GS position, scaled of a L^2 factor in order to take into account the uplink to the satellite.

This is an assumption which allowed to compute the outage probability in a very simple way, but actually it introduces some errors. Future works will include the evaluation of the PDF of the distances between the cognitive devices on the ground and the satellite, and the averaging of the SINR on this statistic, in order to correctly model the randomness in their positions and to fully exploit the stochastic geometry properties.

Conclusions

This thesis has addressed the main issues of cognitive radio specifically related to white spaces identification and WSD emission levels. Two applications of cognitive radio technology at different scenarios, i.e. emergency management and satellite-terrestrial systems, have been considered.

The dissertation was focused on cognitive radio systems in the white spaces of frequency band 470-790 MHz with particular attention at the protection of TV broadcasting systems. An overview of cognitive radio technology is firstly presented, highlighting the motivations that led to the great interest on this kind of technology for the development of future wireless systems. The technical capabilities, i.e. adaptive modulation, transmit power control, geo-localization and negotiation, that could be incorporated into cognitive radio systems are analysed. The behaviour of a cognitive radio can be modelled by a loop i.e. the cognitive radio learning loop, that contains four main steps: (1) sensing of the surrounding environment, (2) analysis of available resources, (3) management to determinate the best frequency band and (3) reconfigurability of parameters. Then, an overall description of a reference cognitive radio network is provided.

In chapter two, two cognitive techniques, i.e. sensing and geo-location database, are considered in order to identify potentially available unoccupied channels. With spectrum sensing, WSDs try to detect autonomously the presence of the protected incumbent services in each of the potentially available channels. Three main spectrum sensing techniques, i.e. energy detection, cyclostationary feature detection and matched filter detection, are compared. Energy detection is the most common type of spectrum sensing: it has low complexity and requires no prior knowledge about the primary signal. Feature detectors are a more sophisticated class of spectrum sensing algorithms that exploit some known features of the primary signal. If the complete structure of the primary signal is known, the optimal detector in additive white Gaussian noise is the matched filter.

Due to their high complexity of implementation, feature detectors and matched filter detectors are not considered in this first stage of study by international groups working on this field.

The energy detector is simple to implement and flexible because it is independent from the radio system to be detected. A disadvantage of this detector is the required low sensitivity due to the noise floor. In case of very low required detection thresholds, an energy detector alone might not be a feasible solution.

An alternative technique to identify the available spectrum is the use of geo-location database. Geo-location database can assist the WSDs to identify the available spectrum. A WSD, which intends to operate in a specific location, sends its information to the geo-location database and receives information on the available frequencies with the associated values of maximum permitted EIRP.

Specifically, the analysis carried out in this work was focused mainly on two aspects related to cognitive radios: study of different cognitive methods to identify potentially available white spaces and study of algorithms to be implemented in geo-location database for the calculation of maximum permitted WSD EIRP.

Concerning the first aspect, different methodologies based on the geo-location database approach to identify white spaces potentially available in the 470-790 MHz band in Italian scenarios have been investigated. Using a proprietary software tool, DTT coverage simulations have been performed for channels 21-60 in different Italian regions. Based on this information, occupied and vacant DTT channels are calculated according to different levels of protection. Subsequently channel occupancy in several specific locations has been investigated through measurements using a portable Narda SRM 3000 spectrum analyzer. Both simulations and measurements confirm that the 470-790 MHz band is densely occupied in the considered Italian scenario.

Some general considerations and remarks can be derived from the obtained results. In particular, the analysis confirms that a combined geo-location and sensing approach may give higher protection to incumbent services, provided that a proper detection threshold is applied. In this specific case study, the sensing threshold has been relaxed with respect to the case of sensing alone (-120.71 dBm for the scenario of interest). With a sensing threshold as high as -105 dBm the combined approach gives higher protection to the incumbent broadcasting service, whereas no further protection is gained with the sensing threshold set to -80 dBm.

Furthermore, the calculations which a geo-location database would need to per-

form in order to derive location-specific maximum permitted WSD EIRP are presented. Two specific numerical issues, the estimation of the DTT location probability and the calculation of the maximum permitted white space device EIRP for the protection of the DTT service are addressed. Two new approaches for improving the accuracy of the above calculations have been proposed, and their performance have been compared with results derived via Monte Carlo simulations. The results indicate that the proposed numerical approaches provide accurate and repeatable estimates at a fraction of the computational effort of Monte Carlo simulations.

Then this methodology is extended to other scenarios. In particular considerations, supported by calculation examples are provided (1) regarding the approach when the location probability degradation is set to a fixed value, (2) regarding the approach that consider the location probability degradation varying across the coverage area, (3) regarding a co-channel analysis considering both fixed value of location probability degradation and the case that it varies across the coverage area and (4) regarding an analysis on variation of DTT self-interference.

Concerning the analysis on different values of fixed location probability degradation, results indicate that if the admitted degradation is fairly high i.e. 3%, a small increase in WSD EIRP is enough to increase the degradation of 1%, while greater values of WSD EIRP are needed to pass, for example from 1% of location probability degradation to 2%.

It is pointed out the importance of setting properly the value of maximum location probability degradation, in order to accomplish a fair treatment for all DTT service conditions. Considering that very well covered areas should have stricter protection than areas with poor coverage (also because the marginal implementation costs for increasing quality of a DTT network could be very high), two possible trends for the allowed degradation of location probability as functions of the local DTT coverage quality have been analysed. The considered degradations led to obtain higher values of maximum permitted WSD EIRP in respect to the fixed location probability degradation of 1%, in areas where the location probability in absence of WSD interferer is low, while lesser admissible WSD EIRP values have been obtained for high location probability values.

Then, the co-channel analysis has been performed considering the WSD interferer and the DTT victim receiver, some pixels apart. Both free-space and dual-slope models are considered to describe the propagation path. Different fixed values of maximum permitted WSD EIRP have been considered and the minimum distance

between the WSD and the DTT receiver that guarantees a location probability degradation of 1% is evaluated. As could be expected the minimum separation is smaller in case of considering dual-slope model.

Finally the location probability and the maximum permitted WSD EIRP have been examined in relation to the DTT self-interference, considering different values of wanted DTT signal. The results show that the permitted WSD EIRP is constant in noise-limited environment and start to decrease while the DTT self-interference increase. In interference-limited scenarios, i.e. where the DTT self-interference is high, the permitted WSD EIRP increases.

Then different examples are provided in order to study the WSDs transmit opportunities in different network plans. Maximum permitted WSD emission levels are computed considering real transmitters data of the Italian region of Friuli-Venezia Giulia. The same network composed by the same DTT installations is considered for three strategies of network planning, i.e. SFN, MFN and k-SFN. Analysis on location probability and maximum permitted WSD EIRP distribution over the territory has been carried out. The results show that the three planning strategies provide good coverage in most populated areas while mountain areas and valleys are not covered by DTT broadcasting service. This translates in high maximum permitted WSD EIRP values in mountain areas and valleys. Then it is shown that k-SFN plan is more robust to the interference. The robustness of the SFN technique, in fact, results in considerable increase of the zones where a WSD can be allowed to transmit with power levels of practical interest.

In the forth chapter two possible cognitive radio deployment scenarios have been analysed. The first considered application is the emergency management. The attention was focused on the consideration of both cognitive and autonomic networking approaches when deploying an emergency management system. The cognitive approach was initially considered specifically for wireless communications, while the autonomic approach was initially introduced for managing complex computing systems; however, they share several similarities in dealing with fully reconfigurable systems. It is shown how the future trend could be to expand their influence toward the global optimization of the Information and Communication Technology (ICT) infrastructure for the specific case of emergency management systems.

The cognitive radio technology has been then considered in applications related to satellite systems. In particular hybrid cognitive satellite-terrestrial system has been introduced. Analysis of coexistence between terrestrial and satellite networks

by considering a cognitive approach has been performed. A statistical interference model that aims at evaluating the mutual interference among the two system has been presented. The considered model allowed to evaluate the interference generated by terrestrial cognitive devices toward the satellite communication link. In particular the outage probability for different thresholds has been considered as merit figure for the hybrid scenario.

Future work concerning the white space device emission levels could be mainly devoted to widen the analysis of real DTT networks and to further investigate the practical impact of the choices involved in the proposed model. Furthermore the model to calculate the WSD maximum allowed power levels could be extended to better characterise the multiple WSD interference. In particular, instead of considering the safety margin introduced in the proposed model to take account of multiple WSD interference, future studies could be focused on the issue of how to manage mutual interference between different WSDs.

Another issue that could be examined is integration of the information provided by the geo-location database and sensing techniques in order to asses the WSD emission levels. In particular, it could be interesting to investigate if a cooperative approach complementing the information available to the geo-location database with a proper set of sensing measurements should be useful to better characterize the realistic power distribution of the WSD interference and hence identify WSD permitted power levels also as a function of the environment topology.

Appendices

Appendix A

Energy Efficiency in Mobile Systems

In Europe the telecommunications market accounts for 8% of the total energy consumption and for the 4% of CO_2 emission. The problem of increasing energy consumption and CO_2 emissions in different industrial sectors led the European Commission to identify the so-called 2020 objectives which foresee to reach the 20% of renewable energy production, to improve energy efficiency by 20% and to decrease by 20% CO_2 emissions by the end of the year 2020.

In both fixed and mobile telecommunication sectors, the access network is responsible of a large part of the energy consumption. As an example, in a typical mobile radio network, up to about 80% of total power consumption occurs at base stations. It is worth noting that the power consumption in cellular networks is steadily increasing due to growing demand of broadband wireless internet access through the usage of new mobile terminals such as smartphones, tablets and other high-end terminal devices, as well as laptops with cellular connectivity. On the other hand, the cost of energy production is increasing due to the larger demand experienced particularly in emerging markets, which causes an increased price of natural resources such as gas and oil. The combined effect of these two trends is causing an augmented cost for operators, which also have to face a reduction of Average Revenue Per Unit (ARPU) in most markets. As a consequence, the effect of energy consumption on operators bottom lines may become excessive and, in some cases, even unbearable.

In order to attain a significant reduction in the energy balance (and hence both in the carbon footprint and in the OPERating EXpenditure (OPEX)) of mobile radio

networks, different strategies such as a smart cellular coverage, the usage of new base station equipment (single Radio Access Network (RAN): UMTS and GSM) and MIMO smart antennas can be envisaged.

As already stated in [96], an optimum planning should be able to maximize the overall system efficiency, which requires a trade-off between the bandwidth and power efficiencies, where the former η_B is the ratio between the achievable bit rate and the available bandwidth and the latter η_P is the number of bits per thermal energy unit.

One more aspect has to be considered in this evaluation and it is the fact that cellular structure allows to reuse the spectral resources over the service area, thus introducing a third dimension to the problem, i.e. the spatial efficiency that gives account of how the spectral resources are reused over the territory. As it is well known, the received power S decreases with distance from the Base Station according to different path loss factors which depend on cell size and on the propagation environment (e.g. urban, suburban).

The cellular layout of a mobile radio system has an impact on its performance (in terms of both coverage and capacity) as well as on its economical and environmental sustainability in terms of power consumption and of exposure of population to electromagnetic field.

In this annex, different coverage solutions (e.g. macrocellular and microcellular BSs) have been compared in order to identify the best configuration which guarantees an appropriate trade-off between spectral and power efficiencies [15, 14].

Of course, for a complete network planning analysis, it is very important to consider jointly all aspects. In [97] a study of different coverage strategies for a mobile radio system in a real urban area is presented.

Focusing on the indoor coverage analysis, in this annex, it is shown that macrocellular coverage guarantees high signal levels at higher floors, but extremely poor at ground floor, while the opposite occurs with the pure microcellular deployment, where the covered fraction sharply decreases at higher floors. Furthermore, in the former case increasing the transmitter power is not sufficient to cover lower floors, while in the latter case in order to increase the percentage to 90% and 95% the transmitter power should be increased by 11 dB and 14 dB respectively. Apart from exposure levels concerns, this would imply an extremely high increase of energy consumption.

A combined use of both cellular layers was therefore suggested to guarantee the

required coverage while keeping the field exposure levels within the values imposed by law: this idea is further developed in this work with the help of a 3D ray tracing tool.

Moreover, a theoretical investigation is carried out on an idealized cellular layout case with a dual slope propagation model to determine the dependence of emitted power spatial-density on cell radius.

A.1 Single Cell Layout

A single cellular layout coverage is addressed assuming a circular coverage area. A minimum received signal level P_R of -90 dBm is imposed in order to guarantee service coverage at the cell border. Similarly to what done in [98], the BTS transmitted power P_T is calculated as a function of the cell radius R based on a "dual-slope model":

$$P_T = P_R \left(\frac{\pi d_0}{\lambda} \right)^2 \frac{G_{T,max}}{G_m} \left(\frac{R}{d_0} \right)^\alpha \quad (\text{A.1})$$

where P_r is the minimum received signal strength at the cell edge (-90 dBm), R is cell radius, α is the power-decay exponent after the reference distance d_0 , G_T and G_m are respectively the transmitter and the receiver gains, and λ the wave length. According to this propagation model, if the cell radius R is lower or equal to the reference distance d_0 a free-space ($\alpha = 2$) propagation applies, otherwise a stronger attenuation law with $\alpha > 2$ is considered. The transition distance d_0 depends on transmitter and receiver heights and on other parameters according to the expression identified in [98].

A typical BS antenna diagram and gain have been adopted [98] and an empirical law has been assumed to identify suitable BS heights h as a function of the cell radius:

$$R = 0.0257h^3 + 11.5h^2 - 40.4 \quad (\text{A.2})$$

In table A.1 the parameter values adopted for the single cell case are shown.

The power P_T emitted by a single BTS cell for one single carrier is assumed to be equal to the power $P_{T,min}$ which guarantees the minimum received power $P_{Rmin} = -90$ dBm on cell border. $P_{T,min}$ is evaluated for different cell radius R and as a function of the path loss exponent. Energy consumption is then assessed as

Table A.1: SINGLE CELL LAYOUT PARAMETERS

Single Cell layout parameters	
λ	0.16
R	150 m - 6 Km
G_T	20 dB
G_R	1 dB
α	2-6

the emitted power density [W/km^2], i.e. the emitted power per square kilometre obtained by dividing the obtained $P_{T,min}$ values by the coverage area, πR^2 .

A.2 Regular Manhattan Layout

Figure show the regular Manhattan-like scenario tha has been considered.

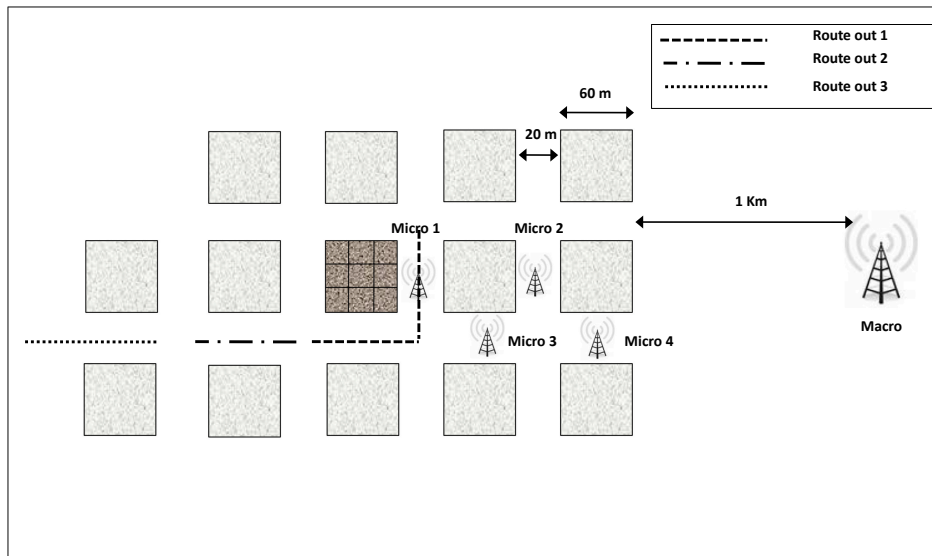


Figure A.1: Manhattan cellular layout.

The city is composed of a regular grid of square building blocks, with side equal to 60 m, separated by 20 m wide streets. The buildings have a random number of floors, which can be 9 or 11 with equal probability; as each floor is supposed 3 m high, the building height can be 27 or 33 m.

The figure also shows the simulated routes along which the terminal moves. Indoor coverage within the building highlighted in dark grey was also evaluated.

Field prediction is made by a full 3D ray-tracing model developed in our laboratory [99, 100]. One macrocellular base station, 40 m high and is located 1 Km away from the considered area has been simulated. Furthermore, 3 m high microcellular base stations in various positions with a transmitted power of 200 mW were considered.

In this analysis the macrocellular power necessary to guarantee 75% of locations in outdoors environment, and 50% for indoor locations, above the threshold of -90 dBm has been evaluated. This value was imposed assuming that the simulated area lies at the cell border. For microcells, a coverage probability of 90% was imposed over the whole cell area in outdoors and 50% in indoors. In order to determine cell shape and size in the microcellular case, different BS positions and receiver routes are considered. Base stations have been placed along the city block side (in the centre of the street), as this solution maximizes inter-cell isolation and therefore overall system capacity. In both the macro- and micro-cellular cases the emitted power density is then computed as the ratio between BS's emitted power and cell area

A.3 Simulation Results

Simulations results are shown for the first theoretical single cell scenario, as a function of the cell radius.

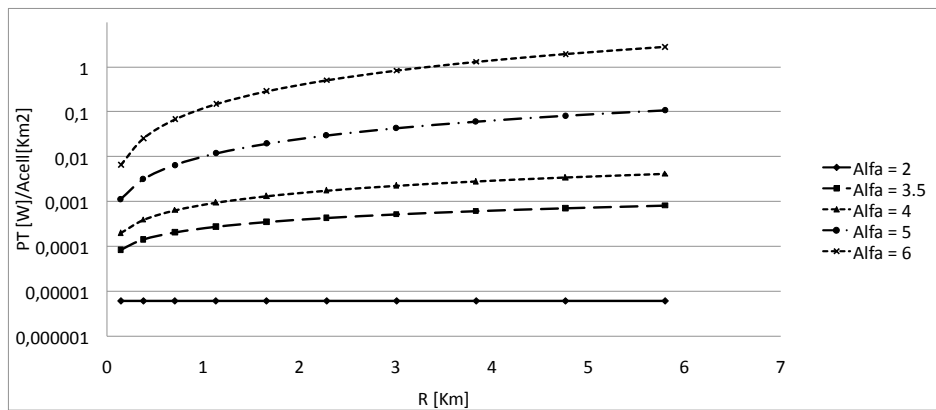


Figure A.2: Single cell BS transmitted power density as a function of the cell radius.

In figure A.2 the emitted power density is plotted as a function of cell radius and path loss exponent, for various propagation conditions varying from LOS ($\alpha = 2$) to high NLOS ($\alpha = 6$). The higher the α , the more substantial is the reduction of total

Table A.2: POWER DENSITY AND PERCENTAGE OF COVERED LOCATIONS

Power Density(W/Km ²)	Percentage of covered locations
0.8	75% outdoor
	0% indoor 1 st floor
	8.8% indoor 9 th floor
2	88% outdoor
	0% indoor 1 st floor
	50% indoor 9 th floor
81.4	98.5% outdoor
	50% indoor 1 st floor
	98.2% indoor 9 th floor

power owing to the introduction of microcells (small radius) in this very simple scenario. In order to analyze the effect of cellular layout in spectral and power efficiency a regular Manhattan-like scenario has been then considered, described in section A.2.

In macrocellular scenario, if only outdoor coverage requirements are considered (75% of locations above the -90 dBm threshold) the needed power density is of 0.8 W/Km², but in this case only 8.8% of indoor location at the 9th floor are above the -90 dBm threshold and the percentage of covered indoor locations at 1st floor falls to 0%. In order to reach at least a 50% covered indoor locations at 9th floor the power level was increased to 2 W/Km², in this case the percentage of outdoor covered locations reaches 88%, but is not sufficient to increase the number of covered indoor locations at 1st floor, which remain at 0%. To increase the percentage of indoor covered locations at 1st floor up to 50%, it was needed to augment the transmit power up to 81.4 W/Km², which is a quite high value. Table A.2 summarises the power density and the corresponding percentage of covered locations.

As the power density needed to reach a 50% of indoor covered locations at 1st floor is not achievable, a microcellular layout to cover the same Manhattan-like scenario is analysed. In table A.3 the indoor coverage percentages evaluated at the 1st and 9th floor of the central Manhattan building are shown for each different microcell location, assuming the same transmitted power P_T equal to 200 mW.

As it can expected, a good coverage is obtained at the first floor especially for microcells 1 and 3 which are located near the building while in the higher floors

Table A.3: INDOOR COVERAGE PERCENTAGE

Indoor microcellular coverage ($P_T = 200$ mW)		
<i>Microcell</i>	1 st floor	9 th floor
1	100 %	75.4 %
2	8.7 %	0 %
3	70.1 %	35 %
4	24.5 %	8.7 %

Table A.4: OUTDOOR COVERAGE PERCENTAGE

Outdoor microcellular coverage ($P_T = 200$ mW)			
<i>Microcell</i>	Route 1	Route 2	Route 3
1	100 %	100 %	56.5 %
2	52.5 %	0 %	0 %
3	100 %	100 %	100 %
4	82 %	100 %	100 %

(9th floor) only microcell 1 provides a significant percentage of covered points. Less critical coverage situations occur in the outdoor microcellular environment as shown in A.4. In this case, apart from microcell 2, microcells 1, 3 and 4 guarantee high coverage percentages in the 3 different routes.

If it is assumed an outdoor microcellular coverage requirement of 90% and a minimum indoor coverage of 50%, it is possible to evaluate the microcell coverage area and calculate the corresponding power density. The extension of the coverage area is equal to about a square area of $0.22 \times 0.22 \text{ Km}^2$ and the power density is 4.13 W/Km^2 . In this case only in the central building coverage at the last floor is higher than 50%. In order to serve the higher floors also for the other buildings of the square area $0.22 \times 0.22 \text{ Km}^2$, the microcell 1 transmitted power should be increased by 18 dB which corresponds to an unacceptable power density of 260.7 W/ Km^2 .

Appendix B

Methods for the Summation of Log-normal Distributions

B.1 Schwartz and Yeh Method

The Schwartz and Yeh (SY) method is an iterative method for calculation of the characteristics of the resultant of n fields. It make the assumption that the combination of two log-normal variables also has a log-normal distribution and it gives the formulas to calculate the resultant of two variables. For more than two signals an iterative process is applied. Originally, the SY method was developed for the sum of independent log-normal random variables [56]. However, it can be extended to the case of correlated log-normal random variables with some modifications [57]. Assuming that $L_i = e^{Y_i}$ ($i = 1, \dots, n$) are correlated log-normal random variables such that Y_i ($i = 1, \dots, n$) are jointly correlated Gaussian random variables, each with mean (m_{y_i}) and variance ($\sigma_{y_i}^2$). To estimate the distribution of $L = L_1 + L_2 + \dots + L_n$ let $Z_k = \ln(L_1 + \dots + L_k)$. According with [56], the exact mean and standard deviation of Z_2 are given by:

$$m_{z_2} = m_{y_1} + G_1(\sigma_w, m_w) \quad (\text{B.1})$$

and

$$\sigma_{z_2}^2 = \sigma_{y_1}^2 - G_1^2(\sigma_w, m_w) + \frac{2(r_{12}\sigma_{y_2} - \sigma_{y_1})\sigma_{y_1}}{\sigma_w^2} G_3(\sigma_w, m_w) + G_2(\sigma_w, m_w) \quad (\text{B.2})$$

where m_w and σ_w are the mean and standard deviation of $W = Y_2 - Y_1$, respectively.

Function $G_1(\cdot)$, $G_2(\cdot)$ and $G_3(\cdot)$ are defined in the following according to [57]. Parameters m_w and σ_w are defined as:

$$m_w = m_{y_2} - m_{y_1} \quad (\text{B.3})$$

and

$$\sigma_w^2 = \sigma_{y_1}^2 + \sigma_{y_2}^2 - 2r_{12}\sigma_{y_1}\sigma_{y_2} \quad (\text{B.4})$$

where r_{ij} is the correlation coefficient of the jointly Gaussian random variables Y_i and Y_j defined as:

$$r_{ij} = \frac{E[(Y_i - m_i)(Y_j - m_j)]}{\sigma_{y_i}\sigma_{y_j}} \quad (\text{B.5})$$

To find the distribution of the random variable Z_2 , it is assumed to be B.1 and B.2.

In the following, the analytical expressions for $G_1(\cdot)$, $G_2(\cdot)$ and $G_3(\cdot)$ are presented.

$$G_1(\sigma w_k, m_{w_k}) = m_{w_k} \Phi\left(\frac{m_{w_k}}{\sigma_{w_k}}\right) + \frac{\sigma_{w_k}}{\sqrt{2\pi}} e^{\frac{m_{w_k}^2}{2\sigma_{w_k}^2}} + \sum_{k=1}^{\infty} c_k e^{\frac{\sigma_{w_k}^2 k^2}{2}} \left[e^{km_{w_k}} \Phi\left(\frac{-m_{w_k} - k\sigma_{w_k}^2}{\sigma_{w_k}}\right) + T_1 \right] \quad (\text{B.6})$$

where

$$c_k = \frac{(-1)^{k+1}}{k},$$

$$T_1 = e^{-km_{w_k}} \Phi\left(\frac{m_{w_k} - k\sigma_{w_k}^2}{\sigma_{w_k}}\right)$$

and

$$\Phi(X) = \frac{1}{\sqrt{2\pi}} \int_{-\infty}^X e^{-\frac{t^2}{2}} dt$$

The function $\Phi(X)$ is related to the error function by:

$$\text{erf}(x) = \frac{2}{\sqrt{\pi}} \int_0^x e^{-t^2} dt$$

$$\Phi(x) = \frac{1}{2} + \frac{1}{2} \operatorname{erf}\left(\frac{x}{\sqrt{2}}\right)$$

$$\begin{aligned} G_2(\sigma w_k, m_{w_k}) &= \sum_{k=1}^{\infty} b_k T_2 + \left[1 - \Phi\left(-\frac{m_{w_k}}{\sigma w_k}\right)\right] (m_{w_k}^2 + \sigma_{w_k}^2) + \\ &+ \frac{m_{w_k} \sigma_{w_k}}{\sqrt{2\pi}} e^{-\frac{m_{w_k}^2}{2\sigma_{w_k}^2}} + \\ &+ \sum_{k=1}^{\infty} b_k e^{-(k+1)m_{k_w} + \frac{(k+1)^2 \sigma_{k_w}^2}{2}} \Phi\left(\frac{m_{w_k} - \sigma_{w_k}^2 (k+1)}{\sigma_{w_k}}\right) + \\ &- 2 \sum_{k=1}^{\infty} c_k e^{-m_{k_w} k + \frac{k^2 \sigma_{k_w}^2}{2}} \left[m_{w_k} \Phi\left(\frac{-m_{w_k}}{\sigma_{w_k}}\right) - \frac{-\sigma_{w_k}}{\sqrt{2\pi}} e^{\frac{m_{w_k}^2}{2\sigma_{w_k}^2}} \right] \end{aligned} \quad (\text{B.7})$$

$$G_3(\sigma w_k, m_{w_k}) = \sigma_{k_w}^2 \sum_{k=0}^{\infty} (-1)^k e^{\frac{k^2 \sigma_{k_w}^2}{2}} T_1 + \sum_{k=0}^{\infty} (-1)^k T_2 \quad (\text{B.8})$$

where

$$T_2 = e^{(k+1)m_{k_w} + \frac{(k+1)^2 \sigma_{k_w}^2}{2}} \Phi\left(\frac{-m_{w_k} - \sigma_{w_k}^2 (k+1)}{\sigma_{w_k}}\right),$$

$$b_k = \frac{2(-1)^{k+1}}{k+1} \sum_{j=1}^k j^{-1}$$

and

$$m_k = -m_{k_w} + k\sigma_{k_w}^2$$

B.2 k-LNM Method

The log-normal method (LNM) is an approximation method for the statistical computation of the sum distribution of several log-normally distributed random variables. The method is based on the assumption that the resulting sum distributions is also log-normal.

The k-LNM method is identical to the standard LNM [54] but with a correction factor k to improve the accuracy.

The approximation is based on the fact that for all kind of distributions mean value and standard deviation of the distribution of the sum of the individual statistical variables are given by the sums of the mean values and the standard deviations of the individual statistical variables.

Consider M log-normally distributed random variables x_i with mean value m_i and standard deviation σ_i ($i = 1, \dots, M-1$). The procedure to asses the moments of the resultant log-normal distribution z , defined as:

$$z = \sum_{i=0}^M x_i,$$

can be summarized in five points:

1. Usually m_i and σ_i are expressed in dB. The first step is to transform m_i^{dB} and σ_i^{dB} from dB scale to Neper scale:

$$m_i = \frac{1}{10 \log_{10}(e)} m_i^{dB} = 0.23 m_i^{dB}$$

and

$$\sigma_i = \frac{1}{10 \log_{10}(e)} \sigma_i^{dB} = 0.23 \sigma_i^{dB}$$

2. Starting from the moments of the variable $y_i = \ln(x_i)$, normal variable, the mean and the standard deviation of the related log-normal variables are:

$$\mu_i = e^{m_i + \frac{\sigma_i^2}{2}} \quad i = 1, \dots, M$$

$$S_i^2 = e^{2m_i + \sigma_i^2} (e^{\sigma_i^2} - 1) \quad i = 1, \dots, M$$

3. Mean value, m_z , and variance, S_z^2 , of the sum variable z , can be obtained from the sum of M different log-normal variables, respectively:

$$\mu_z = \sum_{i=0}^M \mu_i$$

$$S_z^2 = \sum_{i=0}^M S_i^2$$

The second equation is true only if the M variables are statistically independent.

4. From μ_z and S_z , the mean value m_z and the variance σ_z of the normal variable z , can be obtained as:

$$\sigma_z^2 = \ln \left(1 + K \frac{S_z^2}{\mu_z^2} \right)$$

$$m_z = \ln(\mu_z) - \frac{\sigma_z^2}{2}$$

5. The last step is the transformation of m_z and σ_z^2 from Neper to dB scale

k-LNM suffers from the drawback that the appropriate correction factor K depends on the number, the means and the variance of the variables being summed. To obtain optimal results, an interpolation table for the derivation of the value of K would be necessary, which is not suitable for a heuristic approach like k-LNM. Therefore, to keep the simple and analytic character of the approximation, an average value of K is chosen. For the summation of fields with standard deviations σ_i^{dB} between 6 and 10 dB the value $K = 0.5$ seems to represent a fair compromise. For values between 4 and 6 dB, K is chosen equal to 0.7 and for σ_i^{dB} between 0 and 4 K is chosen equal to 1. If K is set to 1, k-LNM is identical to the standard LNM approach.

Appendix C

Property of Log-Normal Distribution

This annex has the objective of demonstrating that *the sum of a log-normal random variable and a deterministic variable is not longer log-normal distributed*. Let consider a log-normal random variable X with mean value μ and standard deviation σ , whose *Probability Density Function* PDF is:

$$f_X(x) = \begin{cases} \frac{1}{x\sigma\sqrt{2\pi}} e^{-\frac{\ln(x-\mu)^2}{2\sigma^2}}, & \text{if } x \geq 0 \\ 0, & \text{otherwise} \end{cases} \quad (\text{C.1})$$

where \ln represents the natural logarithm.

The objective is to determinate the PDF of $y = g(x) = \ln(x + c)$.

1. Some statistical concepts are introduced as follows:

The PDF of a random variable which is function of a random variable is given by:

$$f_Y(y) = \frac{f_X(x_1)}{|g'(x_1)|} + \frac{f_X(x_2)}{|g'(x_2)|} + \dots + \frac{f_X(x_n)}{|g'(x_n)|}$$

where x_n is the n^{th} solution of the equation $y = g(x)$ solved respect to x .

2. To demonstrate the validity of the previous expression, the following example is considered. Suppose to look for the PDF of $y = \ln(x)$. This implies that:
 - The resolution of the equation respect to x admits only a solution: $x_1 = e^y$.

- $|g'(x)| = \frac{1}{x}$.

So, it results:

$$f_Y(y) = \frac{f_X(x_1)}{|g'(x_1)|} = \frac{1}{1/x_1} \frac{1}{\sqrt{2\pi}\sigma x_1} e^{-\frac{(\ln(x_1)-\mu)^2}{2\sigma^2}} = \frac{1}{\sqrt{2\pi}\sigma} e^{-\frac{(y-\mu)^2}{2\sigma^2}} \quad Q.E.D$$

3. Analysing the case: $y = \ln(x + c)$ we have:

- $x_1 = e^y - c$.
- $|g'(x)| = \frac{1}{|x+c|}$.

and

$$f_Y(y) = \frac{f_X(x_1)}{|g'(x_1)|} = \frac{1}{1/|x_1 + c|} \frac{1}{\sqrt{2\pi}\sigma x_1} e^{-\frac{(\ln(x_1)-\mu)^2}{2\sigma^2}} = \frac{e^y}{(e^y - c)} \frac{1}{\sqrt{2\pi}\sigma} e^{-\frac{[\ln(e^y - c) - \mu]^2}{2\sigma^2}}$$

This expression is not the PDF of a Gaussian random variable for all c values but only for $c \rightarrow 0$

In particular it has to be noted that if x is log-normal distributed, it can assume only positive values ($x > 0$). So the values of y are greater than $\ln(c)$ ($y > \ln(c)$) and the result is:

$$f_Y(y) = \begin{cases} \frac{e^y}{(e^y - c)} \frac{1}{\sqrt{2\pi}\sigma} e^{-\frac{[\ln(e^y - c) - \mu]^2}{2\sigma^2}} & \text{if } y \geq \ln(c) \\ 0, & \text{otherwise} \end{cases} \quad (C.2)$$

Appendix D

Computation of Carrier to Interference-plus-Noise Ratio

A common issue in computing the coverage probability at a specific location, is the estimation of the statistics of the Carrier to Interference-plus-Noise Ratio:

$$A = \frac{C}{I + N} \quad (\text{D.1})$$

Where:

- C is the Field Strength of the wanted signal, which can be modeled as log-normal variable.
- I is the sum of the protected field strengths of all interferers. Since the contribution of each interferer can be modeled as a log-normal variable, their sum can also be approximated by a log-normal.
- N is the minimum field strength. It is a constant.

Equation D.1 can be written as:

$$A = \frac{1}{\frac{I}{C} + \frac{N}{C}} \quad (\text{D.2})$$

It can be set:

$$X = \frac{1}{C} \quad Y = \frac{N}{C} \quad (\text{D.3})$$

Then:

$$A = \frac{1}{X + Y} \quad (\text{D.4})$$

X and Y are log-normals, so taking their sum to be a log-normal is a valid approximation. The issue however is that X and Y are partially correlated. The Schwartz and Yeh approach allows the addition of correlated log-normal, however the cross correlation ρ_{xy} of the corresponding Gaussians $x = 10\log(X)$ and $y = 10\log(Y)$ needs to be computed.

Computing the cross-correlation coefficient

By definition:

$$\rho_{xy} = \frac{\text{cov}(x, y)}{\sqrt{[\text{var}(x)\text{var}(y)]}} \quad (\text{D.5})$$

Where:

- $\text{cov}(x, y)$ is the co-variance of the Gaussians x and y
- $\text{var}(x)$ and $\text{var}(y)$ are variances of the Gaussians x and y

If $c = 10\log(C)$, $i = 10\log(I)$ and $n = 10\log(N)$:

$$x = i - c \quad y = n - c \quad (\text{D.6})$$

Assuming that the wanted and interfering signals are independent, c and i are independent random variables, the numerator of equation D.5 can be written as:

$$\begin{aligned} \text{cov}(x, y) &= \text{E}[(x - \text{E}[x])(y - \text{E}[y])] \quad (\text{D.7}) \\ &= \text{E}[xy] - \text{E}[x]\text{E}[y] \\ &= \text{E}[(i - c)(n - c)] - \text{E}[(i - c)]\text{E}[(n - c)] \\ &= \text{E}[(in - ic - cn + c^2)] - \text{E}[i]\text{E}[n] + \text{E}[i]\text{E}[c] + \text{E}[c]\text{E}[n] - \text{E}[c]^2 \\ &= \text{E}[(in)] - \text{E}[(ic)] - \text{E}[(cn)] + \text{E}[c^2] - \text{E}[i]\text{E}[n] + \text{E}[i]\text{E}[c] + \text{E}[c]\text{E}[n] - \text{E}[c]^2 \\ &= n\text{E}[i] - \text{E}[(ic)] - n\text{E}[c] + \text{E}[c^2] - n\text{E}[i] + \text{E}[i]\text{E}[c] + n\text{E}[c] - \text{E}[c]^2 \\ &= -\text{E}[(ic)] + \text{E}[c^2] + \text{E}[i]\text{E}[c] - \text{E}[c]^2 \\ &= \text{E}[c^2] - \text{E}[c]^2 - \{\text{E}[(ic)] - \text{E}[i]\text{E}[c]\} \\ &= \text{E}[c^2] - \text{E}[c]^2 \quad [\text{since } i \text{ and } c \text{ are independent}] \\ &= \text{var}(c) \end{aligned}$$

The quantity within square root in denominator of equation D.5 can be written as:

$$\begin{aligned}
\text{var}(x) &= \text{E}[x^2] - \text{E}[x]^2 && \text{(D.8)} \\
&= \text{E}[(i - c)^2] - \text{E}[(i - c)]^2 \\
&= \text{E}[i^2] + \text{E}[c^2] - 2\text{E}[(ic)] - \text{E}[i]^2 - \text{E}[c]^2 + 2\text{E}[i]\text{E}[c] \\
&= \text{E}[i^2] - \text{E}[i]^2 + \text{E}[c^2] - \text{E}[c]^2 && \text{[since } i \text{ and } c \text{ are independent]} \\
&= \text{var}(i) + \text{var}(c)
\end{aligned}$$

And:

$$\begin{aligned}
\text{var}(y) &= \text{E}[y^2] - \text{E}[y]^2 && \text{(D.9)} \\
&= \text{E}[(n - c)^2] - \text{E}[(n - c)]^2 \\
&= \text{E}[n^2] + \text{E}[c^2] - 2\text{E}[(nc)] - \text{E}[n]^2 - \text{E}[c]^2 + 2\text{E}[n]\text{E}[c] \\
&= n^2 + \text{E}[c^2] - 2n\text{E}[c] - n^2 - \text{E}[c]^2 + 2n\text{E}[c] && \text{[since } n \text{ is deterministic]} \\
&= \text{E}[c^2] - \text{E}[c]^2 \\
&= \text{var}(c)
\end{aligned}$$

Equation D.5 becomes:

$$\begin{aligned}
\text{cov}(x, y) &= \frac{\text{cov}(x, y)}{\sqrt{[\text{var}(x)\text{var}(y)]}} && \text{(D.10)} \\
&= \frac{\text{var}(c)}{\sqrt{\{[\text{var}(i) + \text{var}(c)] \text{var}(c)\}}} \\
&= \frac{\sqrt{\text{var}(c)}}{\sqrt{[\text{var}(i) + \text{var}(c)]}} \\
&= \frac{\sigma_c}{\sqrt{\sigma_c^2 + \sigma_i^2}}
\end{aligned}$$

Bibliography

- [1] Shared Spectrum Company (SSC), *General Survey of Radio Frequency Bands (30 MHz to 3 GHz): Vienna, Virginia, September 1-5, 2009*.
- [2] Ian F. Akyildiz, Won-Yeol Lee, Mehmet C. Vuran, and Shantidev Mohanty, "Next generation/dynamic spectrum access/cognitive radio wireless networks: A survey," *Computer Networks*, vol. 50, no. 13, pp. 2127–2159, Sept. 2006.
- [3] A. M. Wyglinski, M. Nekovee, and T. Hou, *Cognitive radio communications and networks: principles and practice*, Academic Press., 2010.
- [4] "Technical considerations regarding harmonizations options for the digital dividend - a preliminary assessment of the feasibility of fitting new/future applications/services into non-harmonised spectrum of the digital dividend (namely the so-called "white spaces" between allotments)," Report 24, CEPT, June 2008.
- [5] *Establishing a multiannual radio spectrum policy programme*, web site: <http://eur-lex.europa.eu/LexUriServ/LexUriServ.do?uri=CELEX:32012D0243:EN:NOT>, 2012.
- [6] European Commission, *Digital Agenda for Europe*, web site: <http://ec.europa.eu/digital-agenda/>.
- [7] CEPT, *WG SE 43 - White Space - cognitive radio systems*, web site: <http://www.cept.org/ecc/groups/ecc/wg-se/se-43>.
- [8] European Cooperation in Science COST and Technology, *COST Action 2100 - Pervasive Mobile & Ambient Wireless Communications*, web site: <http://www.cost2100.org/>.

- [9] European Cooperation in Science COST and Technology, *COST Action 1004 - Cooperative Radio Communications for Green Smart Environments*, web site: <http://www.ic1004.org/>.
- [10] V. Petrini and H.R. Karimi, "Tv white space database: Algorithms for the calculation of maximum permitted radiated power levels," *IEEE Symposium on new Frontiers in Dynamic Spectrum Access Networks (DySPAN)*, 2012., pp. 529–537, October 2012.
- [11] M. Barbiroli, C. Carciofi, D. Guiducci, and V. Petrini, "White spaces potentially available in italian scenarios based on the geo-location database approach," *IEEE Symposium on new Frontiers in Dynamic Spectrum Access Networks (DySPAN)*, 2012., pp. 393–398, October 2012.
- [12] R. Suffritti, G.E. Corazza, A. Guidotti, V. Petrini, D. Tarchi, A. Vanelli-Coralli, and M. Di Renzo, "Cognitive hybrid satellite-terrestrial systems," in *CogART'11*, 2011, pp. 64–64.
- [13] D. Tarchi, V. Petrini, and G.E. Corazza, "A fully reconfigurable approach to emergency management," vol. 3, no. 3, Jan. 2012.
- [14] M. Barbiroli, C. Carciofi, P. Grazioso, D. Guiducci, V. Petrini, and G. Riva, "Planning criteria to improve energy efficiency of mobile radio systems," *IEEE-APS Topical Conference on Antennas and Propagation in Wireless Communications (APWC)*, 2011., September 2011.
- [15] M. Barbiroli, C. Carciofi, D. Guiducci, and V. Petrini, "A study on the energy efficiency of urban cellular radio deployment solution," *IEEE International Symposium on Antennas and Propagation and USNC/URSI National Radio Science Meeting*, 2012., July 2012.
- [16] D. Robalo, J. Oliveira, F.J. Velez, V. Petrini, M. Barbiroli, C. Carciofi, P. Grazioso, and F. Fuschini, "Experimental characterization of wimax propagation in different environments," *EUROCON - International Conference on Computer as a Tool (EUROCON)*, 2011 IEEE., April 2011.
- [17] "Technical and operational requirements for the possible operation of cognitive radio systems in the "white spaces" of the frequency band 470-790 mhz," Report 159, ECC, Nov. 2010.

- [18] V. Valenta, R. Marsalek, G. Baudin, M. Villegas, M. Suarez, and F. Robert, "Survey on spectrum utilization in europe: Measurements, analyses and observations," *Proceeding of the Fifth International Conference on Cognitive Radio Oriented Wireless Networks & Communications (CROWNCOM)*., pp. 1–5, June 2010.
- [19] "Secondary markets initiative.," Tech. Rep., FCC.
- [20] "Facilitating opportunities for flexible, efficient, and reliable spectrum use employing cognitive radio technologies.," Tech. Rep. ET docket no. 03-108, FCC, 2003.
- [21] J. Mitola III and G.Q. Maguire Jr, "Cognitive radio: making software radios more personal," vol. 6, no. 4, pp. 13–18, Aug. 1999.
- [22] "Unlicensed operations in the tv broadcast bands, second memorandum opinion and order," Tech. Rep. 10-174, FCC, 2010.
- [23] "In the matter of unlicensed operation in the TV broadcast bands, additional spectrum for unlicensed devices below 900 MHz and in the 3 GHz band," Tech. Rep. 08-260, FCC, Nov. 2008.
- [24] "Cognitive radio systems: White spaces," Tech. Rep., ECC, Spectrum Engineering Working Group SE43.
- [25] IEEE 802.22 WG, web site: <http://www.ieee802.org/22/>.
- [26] C. Cordeiro, K. Challapali, D. Birru, and N. Sai Shankar, "Ieee 802.22: the first worldwide wireless standard based on cognitive radios," in *New Frontiers in Dynamic Spectrum Access Networks, 2005. DySPAN 2005. 2005 First IEEE International Symposium on*, Nov. 2005, pp. 328 –337.
- [27] B. Wang and K. J. R. Liu, "Advances in cognitive radio networks: A survey," vol. 5, no. 1, pp. 5–23, Feb. 2011.
- [28] H. Olland, L. De Nardis, K. Nolan, A. Medeisis, P. Anker, L.F. Minervini, F. Velez, M. Matinmikko, and J. Sydor, "Pluralistic licensing," *IEEE Symposium on new Frontiers in Dynamic Spectrum Access Networks (DySPAN), 2012.*, October 2012.
- [29] I.F. Akyildiz, W-Y Lee, and R. Chowdhury, "CRAHNs: Cognitive radio ad hoc networks," *Ad Hoc Networks*, , no. 7, pp. 810–836, 2009.

- [30] I.F. Akyildiz, W-Y Lee, and R. Chowdhury, "Spectrum Management in Cognitive Radio Ad Hoc Networks," *IEEE Network*, Jul 2009.
- [31] D. Niyato and E. Hossain, "Cognitive Radio for Next-Generation Wireless Networks: An Approach to Opportunistic Channel Selection in IEEE 802.11 - Based Wireless Mesh," *Wireless Communications, IEEE*, vol. 16, no. 1, pp. 46–54, Feb 2009.
- [32] E. Axell, G. Leus, E. Larsson, and H. Poor, "Spectrum sensing for cognitive radio: State-of-the-art and recent advances," *IEEE Signal Processing Magazine*, vol. 29, no. 5, pp. 101–116, May 2012.
- [33] R. Tandra and A. Sahai, "Spectrum sensing for cognitive radio: State-of-the-art and recent advances," *IEEE Journal of selected topics in signal processing*, vol. 2, no. 1, pp. 4–17, Feb 2008.
- [34] "Radio noise measurements (s.m.2055)," Report, ITU, 2006.
- [35] A. Ghasemi and E.S. Sousa, "Spectrum sensing in cognitive radio networks: requirements, challenges and design trade-offs," *Communications Magazine, IEEE*, vol. 46, no. 4, pp. 32–39, Apr. 2008.
- [36] T. Yucek and H. Arslan, "A survey of spectrum sensing algorithms for cognitive radio applications.," *IEEE Communications Surveys & Tutorials*, vol. 11, pp. 116–130, 2009.
- [37] Wendong Hu, D. Willkomm, M. Abusubaih, J. Gross, G. Vrantis, M. Gerla, and A. Wolisz, "Cognitive radios for dynamic spectrum access - dynamic frequency hopping communities for efficient ieee 802.22 operation," *Communications Magazine, IEEE*, vol. 45, no. 5, pp. 80–87, May 2007.
- [38] F. Weidling, D. Datla, V. Petty, P. Krishnan, and G.J. Minden, "A framework for r.f. spectrum measurements and analysis," in *New Frontiers in Dynamic Spectrum Access Networks, 2005. DySPAN 2005. 2005 First IEEE International Symposium on*, Nov. 2005, pp. 573–576.
- [39] M. Nekovee, "A survey of cognitive radio access to tv white spaces," in *Ultra Modern Telecommunications Workshops, 2009. ICUMT '09. International Conference on*, Oct. 2009, pp. 1–8.

- [40] Hou-Shin Chen, Wen Gao, and D.G. Daut, "Spectrum sensing for ofdm systems employing pilot tones and application to dvb-t ofdm," in *Communications, 2008. ICC '08. IEEE International Conference on*, May 2008, pp. 3421–3426.
- [41] F.-X. Socheleau, P. Ciblat, and S. Houcke, "Ofdm system identification for cognitive radio based on pilot-induced cyclostationarity," in *Wireless Communications and Networking Conference, 2009. WCNC 2009. IEEE*, Apr. 2009.
- [42] K. Ben Letaief and Wei Zhang, "Cooperative communications for cognitive radio networks," *Proceedings of the IEEE*, vol. 97, no. 5, pp. 878–893, May 2009.
- [43] F. I. Akyldiz, Brandon F. L., and R. Balakrishnan, , " *Physical Communication*, , no. 4, pp. 40–62, 2010.
- [44] "Method for point-to-area predictions for terrestrial services in the frequency range 30 mhz to 3000 mhz," Recommendation p. 1546-2, ITU-R, Oct. 2009.
- [45] H.R. Karimi, "Geo-location databases for white space devices in the uhf tv bands: Specification of maximum permitted emission levels," *IEEE Symposium on new Frontiers in Dynamic Spectrum Access Networks (DySPAN), 2011.*, May 2011.
- [46] "Final acts of geneva," Tech. Rep., ITU, 2006.
- [47] M. Mishra and A. Sahai, "How much white space is there?," Technical report, EECS Department, University of California, Berkeley, Jan. 2009.
- [48] K. Harrison, S. Mishra, and A. Sahai, "How much white-space capacity is there?," *IEEE Symposium on new Frontiers in Dynamic Spectrum Access Networks (DySPAN), 2010.*
- [49] J. Van de Beek, J. Riihijarvi, A. achtzehn, and P. Mahonen, "Tv white space in europe," *IEEE Transactions on Mobile Computing*, vol. 11, pp. 178–188, 2012.
- [50] T. Dudda and T. Irnich, "Capacity of cellular networks deployed in tv white space," *IEEE Symposium on new Frontiers in Dynamic Spectrum Access Networks (DySPAN), 2012.*, pp. 554–565, October 2012.

- [51] “Propagation by diffraction,” Recommendation p. 526, ITU-R, Feb. 2012.
- [52] “The shuttle radar topography mission,” Tech. Rep., NASA.
- [53] “Digital video broadcasting (dvb); implementation guidelines for dvb terrestrial services; transmission aspects,” Tech. Rep. ETSI TR 101 190, European Broadcasting Union, EBU, 2010.
- [54] “Guide on sfn frequency planning and network implementation with regard to t-dab and dvb-t,” Tech. Rep., European Broadcasting Union, EBU, 2005.
- [55] K.L. Beeke, “Spectrum planning-analysis of methods for the summation of log-normal distribution,” *EBU TECHNICAL REVIEW*, Oct. 2007.
- [56] S. Schwartz and Y. S. Yeh, “On the distribution function and moments of power sums with log-normal components,” *Bell System Technical Journal*, vol. 61, pp. 1441–1462, 1982.
- [57] A. Safak, “Statistical analysis of the power sum of multiple correlated log-normal components,” *IEEE Transaction on Vehicular Technology*, vol. 42, no. 1, pp. 58–61, Feb. 1993.
- [58] “Technical analysis of interference from mobile network base stations in the 800 mhz band to digital terrestrial television,” Tech. Rep., Ofcom, 2011.
- [59] “Technical analysis of interference from mobile network base stations in the 800 mhz band to digital terrestrial television: Further modelling,” Tech. Rep., Ofcom, 2012.
- [60] L. Shi, K.W. Sung, and J. Zander, “On the permissible transmit power for secondary user in tv white spaces,” *Cognitive Radio Oriented Wireless Networks and Communications (CROWNCOM), 2012*, pp. 13–17, 2012.
- [61] P.G. Brown, K. Tsioumparakis, Jordan M., and A. Chong, “R&d white paper:uk planning model for digital terrestrial television coverage,” Tech. Rep., BBC, 2002.
- [62] contribution to CEPT SE43, “Measured dvb-t protection ratios in the presence of interference from white space devices,” Tech. Rep., BBC, 2011.
- [63] ETSI TR 102 831, Implementation guidelines for a second generation digital terrestrial television broadcasting system (DVB-T2), 2006.

- [64] J. Wang, M. Ghosh, and K. Challapali, "Emerging cognitive radio applications: A survey," *IEEE Communications Magazine*, vol. 49, pp. 74–81, 2011.
- [65] G. D. Haddow, J. A. Bullock, and D. P. Coppola, "Introduction to emergency management.," *Burlington, MA, USA: Elsevier.*, 2008.
- [66] A. Boin and A. McConnell, "Preparing for critical infrastructure breakdowns: The limits of crisis management and the need for resilience.," *Journal of Contingencies and Crisis Management.*, vol. 15, pp. 50–59, March 2007.
- [67] S. M. Rinaldi, J. P. Peerenboom, and T. K. Kelly, "Identifying, understanding, and analyzing critical infrastructure interdependencies.," *IEEE Control Systems*, vol. 21, pp. 11–25, Dec. 2001.
- [68] F. Chiti, R. Fantacci, L. Maccari, D. Marabissi, and D. Tarchi, "A broadband wireless communications system for emergency management.," *IEEE Wireless Communications Magazine.*, vol. 15, pp. 8–14, June 2008.
- [69] I. Gucenc, U. C. Kozat, M.-R. Jeong, F. Watanabe, and C.-C. Chong, "Reliable multicast and broadcast services in relay-based emergency communications.," *IEEE Wireless Communications*, vol. 15, pp. 40–47, June 2008.
- [70] I. Habib and F. Mazzenga, "Wireless technologies advances for emergency and rural communications.," *Wireless Communications and Mobile Computing*, vol. 10, pp. 1159–1161, Sept. 2010.
- [71] B. Manoj and A. H. Baker, "Communication challenges in emergency response.," *Communications of the ACM*, vol. 50, pp. 51–53, Mar. 2007.
- [72] J. R. Thompson, H. Refstrup Sørensen, H. Gavina, and A. Refsgaard, "Application of the coupled mike she/mike 11 modelling system to a lowland wet grassland in southeast england.," *Journal of Hydrology*, vol. 293, pp. 151–179, June 2004.
- [73] R. Fantacci, M. Vanneschi, C. Bertolli, G. Mencagli, and D. Tarchi, "Next generation grids and wireless communication networks: towards a novel integrated approach.," *Wireless Communications and Mobile Computing*, vol. 9, pp. 445–467, April 2009.

- [74] C. Bertolli, G. Menacagli, and M. Vanneschi, "Adaptivity in risk and emergency management applications on pervasive grids.," *Proceeding of International Symposium on Pervasive Systems, Algorithms, and Networks (ISPAN), 2009.*, pp. 40–62, 2009.
- [75] M. Parashar and J.-M. Pierson, "Pervasive grids: Challenges and opportunities.," *Handbook of Research on Scalable Computing Technologies*, vol. IGI Global., pp. 14–30, 2010.
- [76] Q. Wu, M. Zhu, and N. S. Rao, "Integration of sensing and computing in an intelligent decision support system for homeland security defense.," *Pervasive and Mobile Computing*, vol. 5, pp. 182–200, Apr. 2009.
- [77] I. M. Shaluf, F.-R. Ahmadun, and S. Mustapha, "Technological disaster response criteria and models.," *Disaster Prevention and Management*, vol. 12, pp. 305–311, 2003.
- [78] S. Zlatanova and J. Li, "Geospatial information technology for emergency response.," *Leiden. The Netherlands: Taylor and Francis*, 2008.
- [79] C. Fortuna and M. Mohorcic, "Trends in the development of communication networks: Cognitive networks.," *Computer Networks*, vol. 53, pp. 1354–1376, June 2009.
- [80] B. S. Manoj, R. R. Rao, and M. Zorzi, "Cognet: a cognitive complete knowledge network system.," *IEEE Wireless Communications*, vol. 15, pp. 81–88, Dec. 2008.
- [81] M. Conti, S. Giordano, M. May, and A. Passarella, "From opportunistic networks to opportunistic computing.," *IEEE Wireless Communications Magazine.*, vol. 48, pp. 129–139, Sept. 2010.
- [82] M. Vanneschi and L. Veraldi, "Dynamicity in distributed applications: issues, problems and the assist approach.," *Parallel Computing*, vol. 33, pp. 822–845, Dec. 2007.
- [83] R. Fantacci, D. Tarchi, and A. Tassi, "Wireless communication protocols for distributed computing environments.," *In M. Khatib, Advanced Trends in Wireless Communications.*, pp. 399–420, 2011.

- [84] S. Dobson, S. Denazis, A. Fernandez, D. Gaiti, E. Gelenbe, and et al. Mas-sacci, F., “A survey of autonomic communications,” *ACM Transactions on Autonomous and Adaptive Systems.*, vol. 1, pp. 223–259, Dec. 2006.
- [85] J. O. Kephart and D. M. Chess, “The vision of autonomic computing,” *Computer*, vol. 36, pp. 41–50, Jan. 2003.
- [86] *Technical Specification Group-System; System Overview*, 2005.
- [87] M. A. Razzaque, S. Dobson, and P. Nixon, “Cross-layer architectures for autonomic communications,” *Journal of Network and Systems Management*, vol. 15, pp. 13–27, Mar. 2007.
- [88] A. De La Oliva, A. Banchs, I. Soto, T. Melia, and A. Vidal, “An overview of ieee 802.21: media-independent handover services,” *IEEE Wireless Commu-nications.*, vol. 15, pp. 96–103, Aug. 2008.
- [89] I Macaluso, T.K. Forde, L. DaSilva, and L Doyle, “Impact of cognitive ra-dio: Recognition and informed exploitation of grey spectrum opportunities,” *Vehicular Technology Magazine.*, vol. 7, pp. 85–90, June 2012.
- [90] S. Kandeepan, L. De Nardis, M.-G. Di Benedetto, A. Guidotti, and G.E. Corazza, “Cognitive satellite terrestrial radios,” in *Trans. of IEEE GLOBE-COM 2010*, Miami, FL, USA, Dec. 2010.
- [91] Y.-C. Ko, M.-S. Alouini, and M. K. Simon, “Outage probability of diversity systems over generalized fading channels,” vol. 48, no. 11, pp. 1783–1787, Nov. 2000.
- [92] A. Guidotti, M. Di Renzo, G. E. Corazza, and F. Santucci, “Simplified ex-pression of the average rate of cellular networks using stochastic geometry,” in *Proc. of IEEE ICC’12*, 2012.
- [93] Steven Weber and Moshe Kam, “Computational complexity of outage prob-ability simulations in mobile ad-hoc networks,” in *Proc. of 39th CISS*, Balti-more, MD, USA, March 2005.
- [94] European Commission Information Society and Radio Spectrum Committee Media Directorate-General, *Opinion of the RSC pursuant to Article 4.2 of Radio Spectrum Decision 676 2002 EC, RSCOM08-06final*, 2008.

- [95] European Parliament and of the Council, *Directive 2009/114/EC amending Council Directive 87/372/EEC on the frequency bands to be reserved for the coordinated introduction of public pan-European cellular digital land-based mobile communications in the Community*, 2009.
- [96] Y Akhtman and L. Hanzo, “Power versus bandwidth efficiency in wireless communications: from economic sustainability to green radio,” *China Communications*, vol. 7, no. 2, pp. 6–15, 2010.
- [97] B. Barbiroli, C. Carciofi, P. Grazioso, D. Guiducci, and C. Zaniboni, “Analysis of macrocellular and microcellular coverage with attention to exposure levels,” *PIMRC*, 2008.
- [98] M. Barbiroli, C. Carciofi, V. Degli Esposti, and G. Falciasecca, “Evaluation of exposure levels generated by cellular systems: methodology and results,” *IEEE Transactions on Vehicular Technology*, vol. 51, no. 6, 2002.
- [99] V. Degli Esposti, D. Guiducci, A. De Marsi, P. Azzi, and F. Fuschini, “An advanced field prediction model including diffuse scattering,” *IEEE Transactions on Antennas and Propagation*, vol. 52, no. 7, pp. 1717–1728, 2004.
- [100] F. Fuschini, H. El Sallabi, V. Degli Esposti, L. Vuokko, D. Guiducci, and Vainikainen P., “Analysis of multipath propagation in urban environment through multidimensional measurements and advanced ray tracing simulation,” *IEEE Transactions on Antennas and Propagation*, vol. 56, pp. 848–957, 2008.
- [101] M. Papaleo, V. Petrini, R. Firrincieli, A. Vanelli-Coralli, and G.E. Corazza, “Optimizing cross layer coding redundancy in slow fading channel,” *Advanced satellite multimedia systems conference (asmsa) and the 11th signal processing for space communications workshop (spsc), 2010*, September 2010.

Acknowledgements

The achievement of this important goal of my professional career has been possible also thank to the support and to the help of some people that directly or indirectly have contributed to this thesis.

The first thank goes to my supervisors Professor Giovanni E. Corazza and Ing. Guido Riva for welcoming me in their research groups and for following me in my professional growth in these three years.

I want to thank my colleagues Franco, Marina, Claudia, Doriana and Vittorio because it is always a pleasure to work with them. Thank to them I had the opportunity to improve a lot my scientific knowledge and to work with a very stimulating team.

I am truly indebted and thankful to Maria. Her collaboration and help in the last months of my PhD were precious.

I thank Fernando Velez for hosting me in Covilha, for his collaboration and for being always available to share scientific ideas.

I would like to show my gratitude to all the people I met in Ofcom. In particular, my supervisor Professor Reza Karimi for his supervision and his availability even when he was very busy. Many thanks also to Steve Leach for giving me the opportunity of working within Ofcom for six months. About my English colleagues, a warm thank goes to Andrew for the laughter and advices.

I would also like to acknowledge my international reviewers, Professor Narcis Cardona and Dr. Alexandre Kholod, for their greatly appreciated comments and suggestions.

Another important thank goes to my friend and 'little colleague' Flavia for sharing with me all good and bad moments during my PhD. Our deep understanding and her constant presence has been very useful and often truly comforting.

A special thank to Manuel and Andrea to be as they are. Thanks for your technical support but most of all for making me laugh in the toughest times.

My gratitude goes also to all Digicomm colleagues for sharing with them not only business moments but also enjoyable times. A particular thank to Lina for her important advices.

The last but not the least thank goes to my family that have supported my choices and believed in my capabilities.